1964

Spectra, magnetic susceptibilities and structure of some halogen complexes of niobium (IV) and tantalum (IV)

Bruce Alan Torp
Iowa State University

TORP, Bruce Alan, 1937–
SPECTRA, MAGNETIC SUSCEPTIBILITIES AND STRUCTURE OF SOME HALOGEN COMPLEXES OF NIOBIUM(IV) AND TANTALUM(IV).

Iowa State University of Science and Technology
Ph.D., 1964
Chemistry, inorganic

SPECTRA, MAGNETIC SUSCEPTIBILITIES AND STRUCTURE OF SOME HALOGEN COMPLEXES OF NIOBIUM(IV) AND TANTALUM(IV)

by

Bruce Alan Torp

A Dissertation Submitted to the

Graduate Faculty in Partial Fulfillment of

The Requirements for the Degree of

DOCTOR OF PHILOSOPHY

Major Subject: Inorganic Chemistry

Approved:

Signature was redacted for privacy.

In Charge of Major Work

Signature was redacted for privacy.

Head of Major Department

Signature was redacted for privacy.

Dean of Graduate College

Iowa State University
Of Science and Technology
Ames, Iowa

1964

TABLE OF CONTENTS

INTRODUCTION

In contrast to the abundance of literature pertaining to the chemistry and compounds of the heavy (4d and 5d) transition metals of groups IV, V and VI in their maximum oxidation states is the relatively small volume of information which describes and elucidates the chemistry of these elements in lower valences. In particular, very little work on the coordination and solution chemistry of lower valent halide compounds of these metals has been reported. The latter situation is in large measure a result of the very limited conditions under which stable solutions of these highly acidic compounds can be obtained in aqueous or hydroxylic media.

Recently, however, several lower valent metal halide complexes of these elements have been synthesized by carrying out all reactions in nonaqueous solvents under inert atmospheres or *in vacuo* (1-14). The unusual electronic spectra and magnetic behavior of these complexes could not be entirely explained on the basis of valence bond or ligand (crystal) field theory which was adequate for most 3d transition metal complexes. This is due to the rather large differences which exist between $3d^n$ transition metal complexes and those containing $4d^n$ and $5d^n$ electrons. These differences exist because the 4d and 5d electrons are less tightly bonded to the metal atom than are the 3d electrons. As a result, molecular orbital formation occurs more readily, 10 Dq usually is increased, and the "charge-transfer" states have lower energies than most "crystal field" states (15). In addition, spin-orbit coupling, usually omitted in calculations involving the 3d transition elements, becomes much more important, e.g. the one electron spin-orbit coupling constant (ζ_{nl}) varies as $\zeta_{5d} \sim 2\,\zeta_{4d} \sim 5\,\zeta_{3d}$ (16).

The most satisfactory explanation of the properties of these $4d^n$ and $5d^n$ transition metal complexes has come from the application of molecular orbital theory. Such a treatment considers not only the electrons utilized in σ-bonding but also gives an account of the other orbitals present, of which some are available for π-bonding (17). Indeed, recent investigations of the complex oxo-cations of the types MO^{+n} and MO_2^{+n} have shown that the remarkable stability of these ions can be directly attributed to the π character of the M-O bond (18, 19).

In view of the foregoing facts, it seemed desirable to study a series of $4d^n$ and $5d^n$ complexes with the metal ion in a particular oxidation state. The alkali metal hexahaloniobate(IV) and hexahalotantalate(IV) complexes, A_2MX_6 (A = K, Rb, Cs; M = Nb, Ta; X = Cl, Br, I), were chosen for the following reasons: (1) A study of similar transition metal complexes in a particular group (V A) permits a direct comparison of 4d and 5d ions since other factors such as the charge on the central ion, cationic size, the number of d-electrons, etc. are held approximately constant. (2) The d^1 configuration of the Nb(IV) and Ta(IV) ions greatly simplifies theoretical considerations of their bonding, electronic spectra and magnetic properties. (3) The metal ions are surrounded by six equivalent halide ligands so that O_h symmetry could be assumed. (4) High purity niobium(IV) and tantalum(IV) halides, used as starting materials, were recently prepared in this laboratory (1, 2) and were readily available. In addition, the synthesis and properties of some tetrahalobis(acetonitrile)niobium(IV) complexes, $NbX_4(CH_3CN)_2$ (X = Cl, Br, I) were investigated to examine the differences in the spectral and magnetic properties of the Nb(IV) ion due to the nonequivalence of the ligand field.

REVIEW OF PREVIOUS WORK

The Preparation and Properties of Some Hexahalo Complexes of Group IV, V and VI Transition Metals

A large number of hexahalo complexes containing metal ions with valences of III, IV, and V are known. These include the halides AMX_6, A_2MX_6, and A_3MX_6, the first comprising the alkali, ammonium, and thallous salts of the ions $M^{V}X_6^-$ and alkaline-earth salts of $M^{IV}X_6^=$, and the second and third the monovalent cation salts of ions $M^{IV}X_6^=$ and $M^{III}X_6^{\equiv}$. The octahedral ions MX_6 are large, approximately spherical ions. Therefore the crystal structures of these salts are determined by the relative sizes and charges of the A and MX_6 ions, rather than by the chemical properties of the element M.

Wells (20) has shown that the structures of many of these compounds may be described in two ways: (1) Considering the A and MX_6 ions as structural units, the A_nMX_6 complexes may be described as being derived from simple ionic structures AX_n by replacing A or X by MX_6 ions. (2) Alternatively, the A and X atoms can be thought of as forming a close-packed assembly with M atoms occupying certain octahedral holes between six X atoms. For most purposes it is easier to use the former description.

The AMX_6 structures are generally of two types, either a NaCl or CsCl packing of A and MX_6 ions. However, comparatively few crystallize with the ideal cubic structure. Most salts of the larger cations crystallize with a distorted CsCl structure, e.g. $RbNbF_6$ and $RbTaF_6$, while a number of salts containing smaller cations have the cubic NaCl structure, e.g. $NaNbF_6$ and $NaTaF_6$.

Compounds of the type A_2MX_6 containing discrete $MX_6^{=}$ anions and one of the larger alkali metals, NH_4^+ or Tl^+, crystallize in one of three basic structures. These are the trigonal K_2GeF_6, the cubic K_2PtCl_6, or the hexagonal K_2MnF_6 structure, or slightly distorted modifications thereof. The close-packed structures discussed above arise by filling one-half of the available X_6 holes (or one-eighth of the total number of octahedral holes in the close-packed AX_3 assembly) with M ions. The K_2PtCl_6 (anti-fluorite) structure is the most common type of lattice adapted by A_2MX_6 compounds. In this structure the A^+ ions and octahedral $MX_6^{=}$ anions occupy respectively the F^- and Ca^{2+} positions of the fluorite lattice.

The cubic structure adopted by salts of the composition A_3MX_6 is closely related to that of K_2PtCl_6. In this type of lattice two-thirds of the A^+ ions and the $MX_6^{\equiv}$ ions occupy the positions of the K^+ and $PtCl_6^{=}$ ions in the anti-fluorite structure. In addition there are A^+ ions at the mid-points of the edges and the body-center of the unit cell. Again, slight distortions from ideal cubic symmetry are common.

Since this dissertation is concerned with the preparation and properties of $4d^1$ and $5d^1$ ions, the following discussion will be primarily devoted to hexahalo complexes with this type of electronic configuration. In addition, certain $3d^1$, $4d^2$, and $5d^2$ complexes will be mentioned.

Niobium(IV) and tantalum(IV) hexahalo complexes

At the present time no pure hexahalo complexes of niobium(IV) or tantalum(IV) have been isolated. The existence of A_2NbCl_6 (A = Na, K, Rb, Cs) compounds has been demonstrated by Korshunov, et al. (21, 22) from phase equilibria studies of niobium(IV) chloride-alkali metal chloride systems. These studies were carried out in sealed, argon filled, quartz vessels. The A_2NbCl_6 salts were found to be congruently melting compounds with high melting points. Unlike the other A_2NbCl_6 compounds containing the larger alkali metal cations, Na_2NbCl_6 shows polymorphism. The α modification of this compound was found to transform into the high temperature β form at 365°. A list of the melting points found for the A_2NbCl_6 compounds by these workers is given in Table 1.

Table 1. Melting points of some alkali metal hexachloroniobate(IV) compounds

Compound	Melting point, °C.
β-Na_2NbCl_6	582
K_2NbCl_6	782
Rb_2NbCl_6	802
Cs_2NbCl_6	822

Cozzi and Vivarelli (23) have reported that the $NbCl_6^{=}$ ion is stable in 12N. HCl. This ion, which would necessarily have octahedral symmetry, has a single large absorption maximum in the visible region at 478 mμ (ε ~ 120).

Molybdenum(V) and tungsten(V) hexahalo complexes

Hargreaves and Peacock (13, 14) prepared the compounds $AMoF_6$ and AWF_6 (A = Na, K, Rb, Cs) by the reduction of MoF_6 or WF_6 with alkali metal iodide in liquid sulfur dioxide, Equation 1.

$$2MF_6 + 2AI \xrightarrow[SO_2]{liq.} I_2 + 2AMF_6 \qquad (1)$$

The reactions were carried out *in vacuo* or under an inert atmosphere since the AMF_6 products were unstable in the atmosphere. All of the compounds were found to crystallize in a slight tetragonal modification of the CsCl structure. These workers studied the magnetic properties of the compounds over the temperature range 90^o-300^oK. The variation of the molar magnetic susceptibility with temperature was found to obey the Curie-Weiss law ($\chi_M^{corr.} \propto 1/T+\theta$) with large positive values of θ. The magnetic moments (μ_{eff}) of all the compounds were calculated to be lower than the spin-only value (1.73 B.M.) at 300^oK. and were found to vary with temperature. For the tungsten compounds, Néel points in the temperature range 110^o-140^oK. were found. Thus strong antiferromagnetic lattice interactions must be at least partly responsible for the large values of θ observed.

Antiferromagnetic exchange interactions were also postulated for the molybdenum compounds to explain the deviations of their magnetic moments from the moment predicted by Kotani (24) for a d^1 ion with cubic symmetry. The electronic spectra of these hexafluoro compounds were not measured.

The molybdenum(V) compound $KMoCl_6$ has been characterized by Horner and Tyree (3). They prepared $KMoCl_6$ by the fusion of $MoCl_5$ and KCl at 800^o under a nitrogen atmosphere. The electronic spectrum of this dark green compound consisted of four peaks in the ultraviolet at 243, 275, 305, and 354 mμ, which were assigned to charge transfer transitions. A single peak at 415 mμ, in the visible region was assigned to the d-d transition $^2T_{2g} \rightarrow {}^2E_g$ for a cubic d^1 ion. Some asymmetry in the band at 415 mμ, centered roughly around 470 mμ, was postulated to be evidence of Jahn-Teller distortion in $MoCl_6^-$. Since the spectrum of this compound was obtained from a pellet of $KMoCl_6$ in KCl, extinction coefficients for the peaks could not be calculated. The magnetic moment of $KMoCl_6$ was found to be 1.68 B.M. at room temperature.

Molybdenum(IV) and tungsten(IV) hexahalo complexes

Peacock, et al. (4, 11) also have investigated the hexahalo complexes of molybdenum(IV) and tungsten(IV). The molybdenum compounds A_2MoCl_6 (A = K, Rb, Cs, Tl) were prepared by reacting $MoCl_5$ with ACl in the presence of ICl while the A_2MoBr_6 compounds (A = Rb, Cs) were prepared by the oxidation of $MoBr_3$ with IBr in the presence of ABr. The analogous tungsten(IV) hexahalo complexes A_2WX_6 (A = K, Rb, Cs; X = Cl, Br) were prepared by reacting WX_6 with AX at 130°, Equation 2.

$$WX_6 + 2AX \rightarrow X_2 + A_2WX_6 \tag{2}$$

Because the above compounds were found to react with the atmosphere, all preparations and manipulations were carried out *in vacuo* or under an inert atmosphere. All of the A_2MoX_6 and A_2WX_6 complexes were shown by x-ray analysis to have the cubic K_2PtCl_6 structure. The hexahalomolybdate(IV) complexes had temperature dependent magnetic moments which were lower than the spin-only value. These moments were generally in agreement with Kotani's theory for the magnetic behavior of a cubic $4d^2$ ion. The magnetic moments of the hexahalotungstate(IV) complexes showed the same general variation with temperature but the actual values of μ_{eff} at various temperatures were much lower than the spin-only value. However this behavior was postulated to be due to an antiferromagnetic exchange interaction, in addition to a variation of the moment as given by Kotani.

Fowles, Edwards and Allen (5) have also prepared the hexachloromolybdate(IV) compounds A_2MoCl_6 (A = Rb, Cs) by the reaction of $MoCl_5$ and ACl in liquid SO_2 under inert conditions. Measurements of the magnetic properties of these compounds were in good agreement with those of Peacock, discussed above. The visible spectra of these complexes contained two peaks which were assigned to d-d transitions.

Titanium(III) and zirconium(III) hexahalo complexes

Bedon, Horner, and Tyree (25) have investigated the electronic spectra and magnetic properties of the hexafluorotitanate(III) complexes $(NH_4)_3TiF_6$, Na_2KTiF_6, and NaK_2TiF_6. The ammonium salt was prepared by adding a water solution of $TiCl_3$ to a saturated, slightly acidic NH_4F solution. The mixed alkali metal salts were prepared by adding powdered titanium metal to a fused melt of $NaHF_2$ and KHF_2 in the appropriate ratio. The compounds were stable in air. The Ti^{III} ion was found to occupy an octahedral lattice site in the NaK_2TiF_6 salt. Ultraviolet and visible absorption spectra of these compounds were obtained in pellets of KCl and KBr. In each case two peaks were observed in the visible region at 530 mμ and 610 mμ while there was no absorption in the ultraviolet region down to 200 mμ. These workers presented a molecular orbital treatment of the bonding in $TiF_3^{\equiv}$. They were able to predict from energy level considerations all the features of the observed spectrum. It was necessary to consider π-bonding in the calculations. The two peaks in the spectrum were both assigned to the transition $t_{2g}^* \rightarrow e_g^*$ for a d^1 ion with cubic symmetry. These peaks, separated by ~3000 $cm.^{-1}$, were postulated to be caused by Jahn-Teller distortion of the ^2Eg excited state. The magnetic moments calculated from magnetic susceptibility data, assuming a Weiss constant of $0^oK.$, were close to the spin-only value.

There is very little information in the literature concerning hexahalo compounds of zirconium(III) or hafnium-(III). Nyholm and associates (6) have prepared the compound tetraphenylarsonium hexachlorozirconate(III), $(ph_4As)_3ZrCl_6$, by fusing a stoichiometric mixture of ph_4AsCl and $ZrCl_3$ under an argon atmosphere. The room temperature magnetic moment for this compound was found to be 0.9 B.M. The electronic spectrum of the hexachlorozirconate(III) complex was not measured.

The Preparation and Properties of Some Metal Halide Complexes with Organic Ligands

There is a complete lack of information in the literature concerning niobium(IV) or tantalum(IV) halide complexes with acetonitrile. As a result, the complexes cited below are those of acetonitrile with related metal halides or of niobium(IV) and tantalum(IV) halides with other organic ligands. Certain other metal halide complexes will also be discussed.

Niobium(IV) and tantalum(IV) halide complexes with organic ligands

McCarley, Torp and Boatman (1, 2) have prepared the following di-pyridine derivatives of some niobium(IV) and tantalum(IV) halides, $NbX_4(py)_2$ (X = Cl, Br, I) and $TaX_4(py)_2$ (X = Cl, Br), by the direct reaction of the appropriate metal tetrahalide with pyridine at room temperature, *in vacuo*. Conductance measurements in pyridine indicated that no ionic species were present. Visible spectra of pyridine solutions of the $NbX_4(py)_2$ complexes consisted of at least two peaks of relatively high intensity ($\varepsilon \geq 500$). These were attributed to charge-transfer transitions from the filled π-orbitals of pyridine to a nonbonding d-orbital on niobium. The magnetic susceptibilities of the tetrahalobis(pyridine)niobium(IV) and tantalum(IV) complexes were found to fit a simple Curie relationship over the temperature range -196 to 25°. The calculated magnetic moments of all the complexes were lower than the spin-only value with the tantalum complexes being much lower than their niobium analogs due to greater spin-orbit coupling effects. From the variations in the moments of a given series of pyridine complexes with halide ligand the following spectrochemical series was proposed: Cl < Br

< I < py.

A number of niobium(IV) complexes of the type $(BH)_2Nb(OR)Cl_5$ (RO^- = alkoxide; B = amine such as CH_3NH_2, pyridine or quinoline) have been investigated by Wentworth and Brubaker (7). These compounds were prepared by the electrolytic reduction of $NbCl_5$ in HCl-saturated alcohols followed by the addition of alcoholic solutions of BH^+ ions. The experiments were carried out under nitrogen. Magnetic susceptibilities of these complexes were measured as a function of temperature and found to obey the Curie-Weiss law. The calculated moments correspond to the spin-only value for a d^1 ion. The reflectance spectrum of $(CH_3NH_3)_2Nb(OEt)Cl_5$, measured in mineral oil, showed a single asymmetric peak in the visible region at 510 mμ such as might be expected for an octahedral d^1 complex.

Wentworth and Brubaker (8) also prepared two diamagnetic complexes of niobium(IV), $[NbCl(OEt)_3py]_2$ and $Nb(OEt)_4$. The former compound was synthesized by the addition of pyridine to niobium(IV) chloride solutions in ethyl alcohol. Tetraethoxoniobium(IV) was prepared by the reaction of NaOEt with $[NbCl(OEt)_3py]_2$ in ethyl alcohol. Both complexes react with the atmosphere. The diamagnetism of both compounds is explained in terms of direct metal-metal bonding between adjacent niobium ions.

Titanium(IV) and zirconium(IV) halide complexes with acetonitrile

Emeléus and Rao (26) have synthesized acetonitrile (methyl cyanide) adducts of the following tetrahalides: TiX_4 and ZrX_4 (X = F, Cl, Br, I). These complexes were prepared *in vacuo* by the reaction of the appropriate tetrahalide with an excess of dry acetonitrile. Removal of excess solvent and analysis of the solid products showed them to have the composition MX_4(acetonitrile)$_2$. These complexes hydrolyzed readily in the atmosphere. Dissociation pressures of the MX_4(acetonitrile)$_2$ complexes were measured with an isoteniscope in which a small mercury manometer was used as a null instrument. The acetonitrile adducts of both metal tetrahalides had dissociation pressures that varied in the order F > I > Br > Cl and for a given halogen the titanium(IV) complexes were more stable.

The infrared spectrum of the $TiCl_4$(acetonitrile)$_2$ complex has been obtained by Gerrard *et al.* (27). The compound was prepared as described above. They found an increase in the nitrile stretching frequency from 2248 cm.$^{-1}$ to 2303 cm.$^{-1}$

showed an increase in the nitrile stretching frequency of 35 cm^{-1} (similar to the Ti(IV) complexes discussed above). The complex was found to be a nonelectrolyte in acetonitrile. Reflectance and solution spectra of the acetonitrile adduct were identical having two peaks at 17,000 cm^{-1} (ϵ = 22) and 14,700 cm^{-1} (ϵ = 13). The distortion of the ^2Eg state is then 2,400 cm^{-1}, and the splitting of the ground ($^2T_{2g}$) state was estimated to be ca. 600 cm^{-1} from the magnetic data. From 10 Dq values obtained from the visible spectra of these complexes and from data in the literature the authors obtained the following spectrochemical series: acetonitrile > H_2O > acetone > dioxane > tetrahydrofuran > chloride.

Fowles and Hoodless (9) have prepared trimethylamine complexes of titanium(III) chloride and bromide by the direct reaction of trihalide with amine under inert conditions. Visible spectra of the $TiX_3(NMe_3)_3$ complexes contained a single asymmetric peak in each case (Br, 13,280 cm^{-1}; Cl, 14,900 cm^{-1}). These peaks were assigned to the $^2T_{2g} \rightarrow {}^2Eg$ transition for a d^1 complex of near octahedral symmetry. Magnetic susceptibilities of the complexes were measured over the temperature range 90-291°K. and found to fit the Curie-Weiss law ($\theta \sim 30°$). The calculated moments were close to the spin-only value.

upon complexing. This effect has been explained in terms of an increase in the carbon-nitrogen bond order. Brown and Kubota (28) have arrived at the same conclusion after studying the infrared spectrum of $SnCl_4$(acetonitrile)$_2$.

Muetterties (29) has studied the configuration of a large number of MF_4(acetonitrile)$_2$ complexes (M = Ti, Zr, Si, Ge, Sn, Te, Mo) by nuclear magnetic resonance spectroscopy. He found that the F^{19} NMR spectra of all the complexes gave conclusive evidence of octahedral coordination and a _cis_ configuration for the acetonitrile ligands in the compounds.

Titanium(III) halide complexes with organic ligands

The titanium(III) complexes $TiCl_3(L)_3$, where L = acetonitrile, tetrahydrofuran, acetone, or dioxane, have been investigated by Nyholm, _et al_. (10). These compounds were prepared by refluxing the appropriate ligand with $TiCl_3$ in a nitrogen atmosphere, followed by removal of the excess ligand _in vacuo_. Measurements of the visible spectra of these complexes indicated that the molecules are considerably distorted from O_h symmetry. The magnetic moments of the complexes were close to the spin-only value.

The $TiCl_3$(acetonitrile)$_3$ complex was obtained as a blue crystalline compound. The infrared spectrum of the complex

EXPERIMENTAL

Since all of the niobium(IV) and tantalum(IV) halides and their derivatives were extremely susceptible to hydrolysis and oxidation by the air, sealed and evacuated glass vessels or inert atmospheres were used in all preparations and experiments. In addition, all materials used in the preparations were rigorously dried and stored in evacuated containers. Whenever this was not possible, as in the case of solid or gaseous materials, these were purified immediately before use. Storage and handling of all solid materials were done in a dry-box under an argon atmosphere. This dry-box was maintained at a dew point of *ca.* -75°C by a semi-constant flow of argon (dried over Linde 4A Molecular Sieves) through the box. An adequate supply of exposed anhydrous magnesium perchlorate was also maintained in the dry-box to remove any remaining moisture.

Materials

Niobium and tantalum

High purity niobium and tantalum metal were used in all preparations of their respective tetrahalides. The niobium was obtained from the Pigments Department, E. I. Du Pont Company. This material was very low in tantalum. Tantalum

(99.9% pure) was obtained from the National Research Corporation, Metals Division.

Halogens

Chlorine was obtained from the Mathison Company, Incorporated, in lecture size cylinders. The chlorine was used directly in preparations by condensing the gas in a side arm of the glass apparatus at -78^{o} (provided by a Dry Ice-acetone bath). The liquid chlorine was outgassed on the vacuum line before beginning a reaction.

Bromine (J. T. Baker Analyzed Reagent) was first dried for several days, in vacuo, over well outgassed phosphorus(V) oxide. The dry bromine was vacuum distilled into a clean flask, fitted with a stopcock, for use in experiments as needed.

Iodine (J. T. Baker Analyzed Reagent) was purified by outgassing the solid at ca. 10^{-5} Torr directly in the glass reaction vessel.

Organic reagents

Acetonitrile and all other organic solvents used in this work were spectro-grade reagents obtained from the Eastman Company. The liquids were thoroughly dried before use by successively placing them over well outgassed Molecular Sieves and calcium hydride. The reagent and drying material were then frozen and the flask was completely outgassed at 10^{-5} Torr. The liquids were vacuum distilled into clean, freshly outgassed flasks for storage. Acetonitrile dried in this manner had a specific conductance of <u>ca</u>. 10^{-6} ohm^{-1} $cm.^{-1}$ at 20^{o} (literature value (30), 7 x 10^{-6} ohm^{-1} $cm.^{-1}$ at 20^{o}) and its infrared spectrum checked closely with that reported in the literature.

<u>Alkali metal halides</u>

The alkali metal halides, used in preparations of the hexahalo complexes, were obtained from two sources. The potassium salts were J. T. Baker Analyzed Reagent grade materials. The rubidium and cesium salts (99.9% purity) were obtained from Penn Rare Metals, Incorporated. All of the alkali metal halides were outgassed at 10^{-5} Torr and 200^{o} before use.

Analytical Procedures

The method of analysis varied with the type of compound being analyzed. These compounds fell into two categories, niobium(IV) or tantalum(IV) halides and acetonitrile complexes. Since the hexahalo complexes (A_2MX_6) were prepared from stoichiometric mixtures of AX and MX_4 in sealed tubes, their purity was best determined by x-ray diffraction analysis. The determination of small amounts ($\sim 10^{-5}$ mole) of niobium from solutions used in the spectroscopy experiments will be discussed under that section.

Niobium(IV) and tantalum(IV) halides

The niobium(IV) and tantalum(IV) halide starting materials were hydrolyzed in dilute aqueous ammonia and heated to assure complete hydrolysis. The solution was cooled, the hydrated metal oxide filtered off, and the filtrate diluted to 250 ml. in a volumetric flask.

For metal analysis, the filter paper containing the hydrated niobium(V) or tantalum(V) oxide was placed in a tared porcelain crucible. After igniting the sample to M_2O_5 at 800^o and reweighing the crucible, the per cent metal was calculated in the usual manner. Alternately, as a check on the above procedure, the metal content of a solid compound was determined by direct ignition to M_2O_5.

The amount of halide in a sample, hydrolyzed as described above, was determined by the standard Volhard method. Aliquots of the filtrate were acidified with 1:1 nitric acid and the usual procedure followed thereafter.

Acetonitrile complexes

Because it was desirable to determine the nitrogen content of the tetrahalobis(acetonitrile)niobium(IV) compounds, a modification of the method of Jonassen, Cantor and Tarsey (31) was used to decompose the chloride and bromide complexes.

In this procedure, a known amount of sample was heated in concentrated sulfuric acid for about six hours. The hydrogen halide evolved during the decomposition was transported in a stream of nitrogen to a 10% sodium hydroxide solution. The sodium hydroxide solutions were transferred to a 250 ml. volumetric flask and aliquots were taken for chloride or bromide analysis (Volhard) as described above.

In the case of samples containing bromide, some free bromine was always liberated in the course of the decomposition due to the oxidative nature of sulfuric acid. This bromine was quantitatively trapped in the NaOH solution (as NaOBr) and was reduced to Br^- with SO_2.

The concentrated sulfuric acid solution, containing niobium(V) and ammonium ions, was transferred to another 250 ml. volumetric flask, diluted to the mark with con. H_2SO_4, and a 100 ml. aliquot taken for the metal analysis. Acetonitrile and halogens were removed by adding several drops of 30% hydrogen peroxide to the hot sulfuric acid solution and then fuming the solution to dryness. The above process was repeated several times. The niobium content of the sample was subsequently determined spectrophotometrically[1] (32).

The remaining 150 ml. of sulfuric acid solution were analyzed directly for nitrogen by the Kjeldahl method[1].

For the tetraiodobis(acetonitrile)niobium(IV) complex an analytical procedure similar to that described for the niobium(IV) or tantalum(IV) halides was used. The sulfuric acid decomposition could not be used since free iodine liberated during the course of the reaction could not be quantitatively recovered. In this procedure a weighed amount of iodine complex was hydrolyzed in dilute sodium hydroxide. The solution was first evaporated to dryness to remove acetonitrile. The residue was taken up in distilled water and the metal tetrahalide procedure followed thereafter. The acetonitrile was removed because it was found to interfere with the halide analysis. The acetonitrile was determined by difference.

---

[1]The Kjeldahl nitrogen and spectrophotometric niobium analyses were kindly performed by the Analytical Service Group of the Ames Laboratory.

Physical Measurements

X-ray diffraction

X-ray diffraction data were obtained with an 114.59 mm. Debye-Scherrer camera. Powdered samples that had passed through a 200 mesh screen were used. These were packed in 0.2 mm. Lindeman capillaries in the dry-box and sealed immediately on removal. The filled capillaries were exposed to Ni-filtered CuK_{α} radiation for periods of 16 to 30 hours. Conversion from θ values to interplanar distances was obtained from NBS tables (33).

Whenever it was possible to index the powder patterns of a compound prepared in the course of this work, specifically the alkali metal hexahaloniobate(IV) and hexahalotantalate(IV) complexes, the resulting lattice parameters for each line were extrapolated against the Nelson-Riley function (34).

$$\frac{\cos^2\theta}{\sin\theta} + \frac{\cos^2\theta}{\theta} \qquad (3)$$

This process reduced systematic errors due to absorption, off-centering of the specimen, incorrect camera radius or film shrinkage. The extrapolation was made using the least squares method to determine the best value for a given lattice parameter. The least squares analysis was carried out on the IBM 7074 computer using an appropriate computer program[1].

A detailed structural analysis of one of the hexahalo complexes (K_2NbCl_6) was undertaken in order to verify its postulated structure with O_h symmetry around the niobium(IV) ion. First graded intensity values were obtained for all the lines present in the powder pattern of the complex by the multiple film technique. The integrated intensities of the lines in the multiple films were estimated visually relative to a set of standard intensity spots.

It can be shown (35) that the relative intensity of a powder pattern line is dependent on a number of factors, Equation 4, including the arrangement and types of atoms in the lattice.

$$I = |F|^2 \, p \left[\frac{1 + \cos^2 2\theta}{\sin^2\theta \cos\theta}\right] \quad (4)$$

Where: I = relative integrated intensity (arbitrary units),

F = structure factor,

p = multiplicity factor,

θ = Bragg angle,

[1]This program, as well as those described on the following pages, was kindly provided by Mr. Donald M. Bailey of the Ames Laboratory.

$$\frac{1 + \cos^2 2\theta}{\sin^2\theta \cos \theta} = \text{Lorentz-polarization factor.}$$

The structure factor can be expressed by Equation 5.

$$F = \sum_{1}^{N} f_n e^{2\pi i(hu_n + kv_n + \ell w_n)} \tag{5}$$

Where: f_n = atomic scattering factor for atom n,

$hk\ell$ = Miller indices for the reflection,

$u_n v_n w_n$ = atom positions for atom n.

The integrated intensity values from the multiple film analysis were corrected by applying the Lorentz-polarization and multiplicity factors as indicated in Equation 4. Absorption and temperature factor corrections were not made since these factors are hard to estimate and, to a first approximation, cancel each other (35, p. 130). These corrections were made on the IBM 7074 computer.

The corrected intensities for the lines in the powder pattern of K_2NbCl_6 cannot be used to calculate atom positions since solution of Equation 4 yields only the absolute value of the structure factor $|F|$, i.e. only the relative amplitude of each reflection but not the phase. Atom positions, therefore, can be determined only by trial and error. A set of atom positions is assumed, the intensities corresponding to these positions are calculated, and the calculated intensities are compared with the observed values. This process is repeated until a satisfactory agreement between the calculated and observed intensities is obtained.

The K_2NbCl_6 complex was assumed to have the anti-fluorite (K_2PtCl_6) structure and a structure factor was calculated for each reflection using atomic scattering factors obtained from the International Tables, Vol. III (36). The resulting calculated intensities were compared with the observed values, as described above, using a least squares program, on the IBM 7074 computer. The results of this study are found in the results and discussion section.

Magnetic susceptibility

Magnetic susceptibility measurements were made from -196^{o} to room temperature by Mr. J. D. Greiner using the Faraday method.

Powdered samples were put through a 100-mesh sieve and incapsulated in cylindrical Pyrex bulbs ca. 2 cm. long and 1 cm. in diameter. These bulbs were connected to the vacuum system through a narrow piece of Pyrex tubing ca. 1 mm. in diameter. This small constriction allowed sealing off of the sample without decomposition. A diagram of the apparatus is given in Figure 1. The bulbs were filled in the dry-box,

Figure 1. Glass apparatus used in the determination of magnetic susceptibilities of niobium(IV) and tantalum(IV) halide complexes

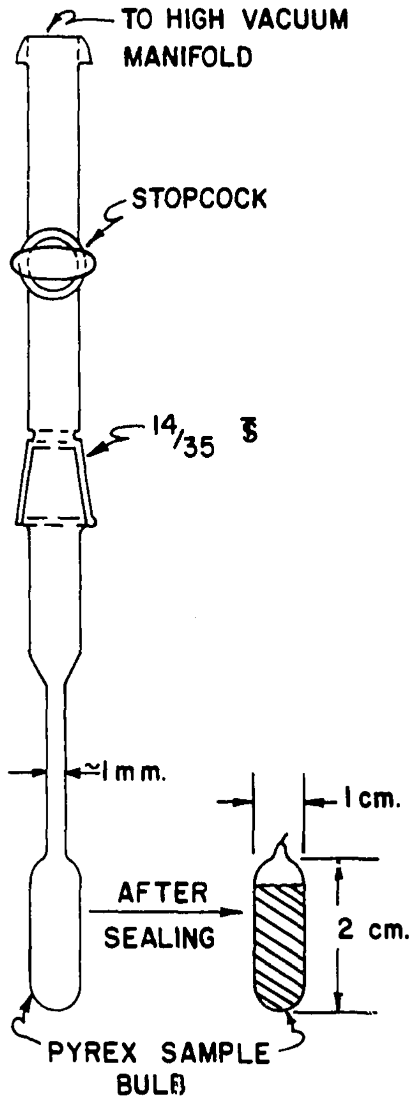
TO HIGH VACUUM MANIFOLD
STOPCOCK
14/35 $
≃1 mm.
1 cm.
AFTER SEALING
2 cm.
PYREX SAMPLE BULB

outgassed on the vacuum line at 10^{-5} Torr, and sealed off before measurement. The weight of the sample was obtained by weighing the bulbs containing argon before and after filling with sample. Corrections for the diamagnetism of the Pyrex glass bulbs were made for all measurements.

Diffuse reflectance spectra

The diffuse reflectance spectra of the solid complexes were measured from 200 to 1200 mμ on a Beckman DU spectrophotometer equipped with the Beckman 2580 reflectance attachment.

The samples were powdered and homogeneously diluted *ca.* 10:1 with dry magnesium carbonate or alkali metal halide in the dry-box. It was found that better resolution of the spectra was obtained when the alkali metal halides were used as diluting agents. The halogens of the complex and the diluting agent were matched in this case.

The diluted samples were compacted inside a stainless steel cell (Figure 2) and sealed from the atmosphere by a circular quartz disk, 1 mm. thick, which extended over both the sample well and the rubber O-ring. The cell cover, which was countersunk to accommodate the quartz disk, was aligned on the cell with short dowel pins and secured with four

Figure 2. Apparatus used in the determination of the diffuse reflectance spectra of niobium(IV) and tantalum(IV) halide complexes

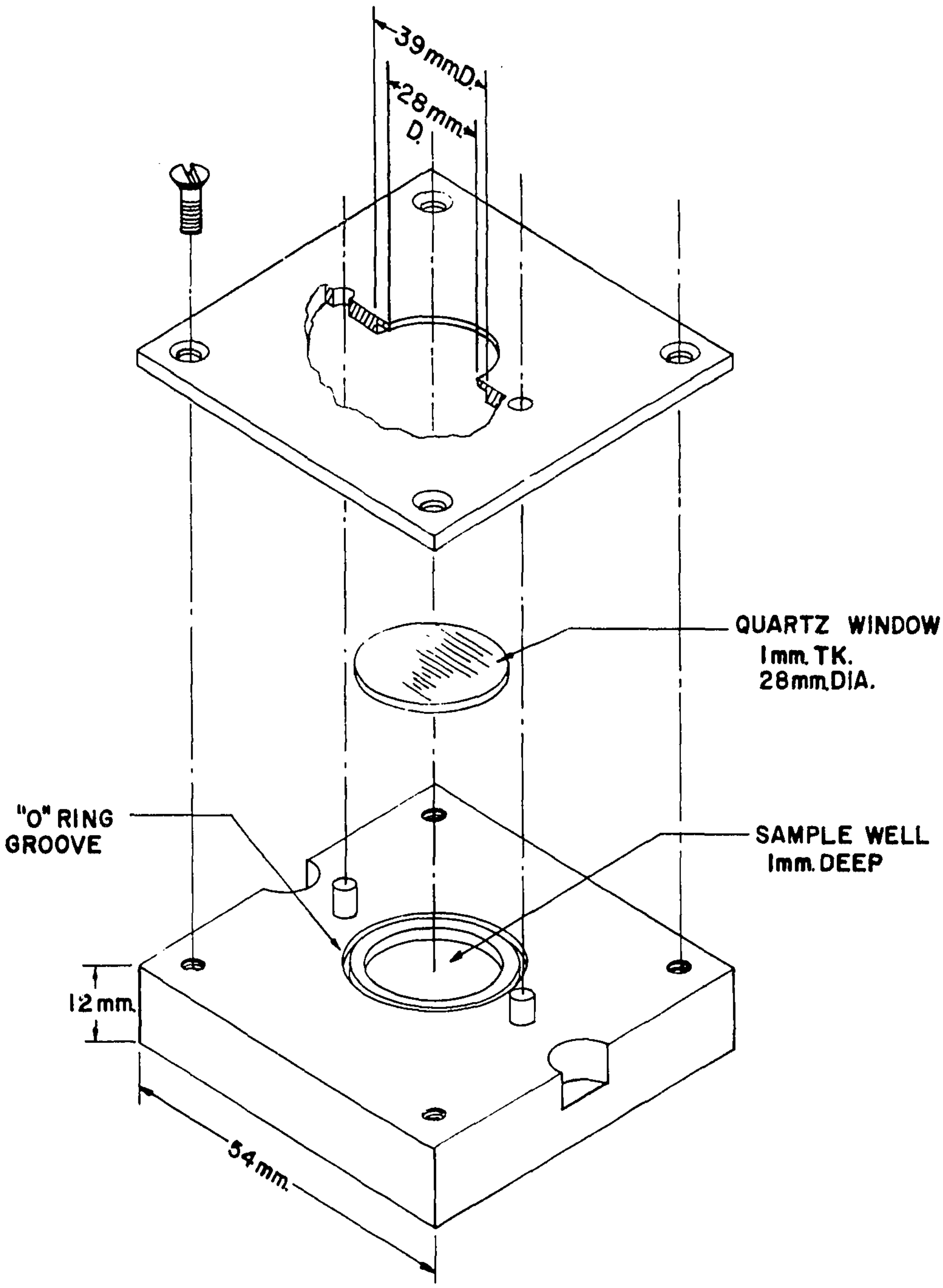
39mm D.
28mm. D.
QUARTZ WINDOW
1mm. TK.
28mm.DIA.
"O" RING
GROOVE
SAMPLE WELL
1mm. DEEP
12mm.
54mm.

screws. The dimensions of the cell were such that it fit into the sample compartment of the Beckman reflectance attachment. No hydrolysis of reactive samples contained in the cell was observed to take place after several days exposure to the atmosphere.

The spectra were measured in reference to the diluting agent used, either a block of magnesium carbonate or finely ground (<100-mesh) alkali metal halide.

Ultraviolet, visible, and near-infrared absorption spectra

The absorption spectra of the tetrahalobis(acetonitrile)-niobium(IV) complexes were determined in the region 210 to 2200 mμ using a Cary 14 recording spectrophotometer.

The glass apparatus, Figure 3, used in this study was constructed so that concentration changes could be made without opening the vessel and destroying the complex. The vessel consisted of a Pyrex mixing chamber sealed to a cylindrical quartz cell (1-cm. light path) through a fine porosity fritted disk. A second arm from the mixing chamber was connected to a high vacuum manifold.

The sealed apparatus was designed to fit into the cell compartment of the Cary spectrophotometer. A solution was prepared in the mixing chamber by distilling solvent onto the samples and sealing off the vessel from the vacuum system.

Figure 3. Glass apparatus used in the determination of the absorption spectra of the tetrahalobis(acetonitrile)niobium(IV) complexes

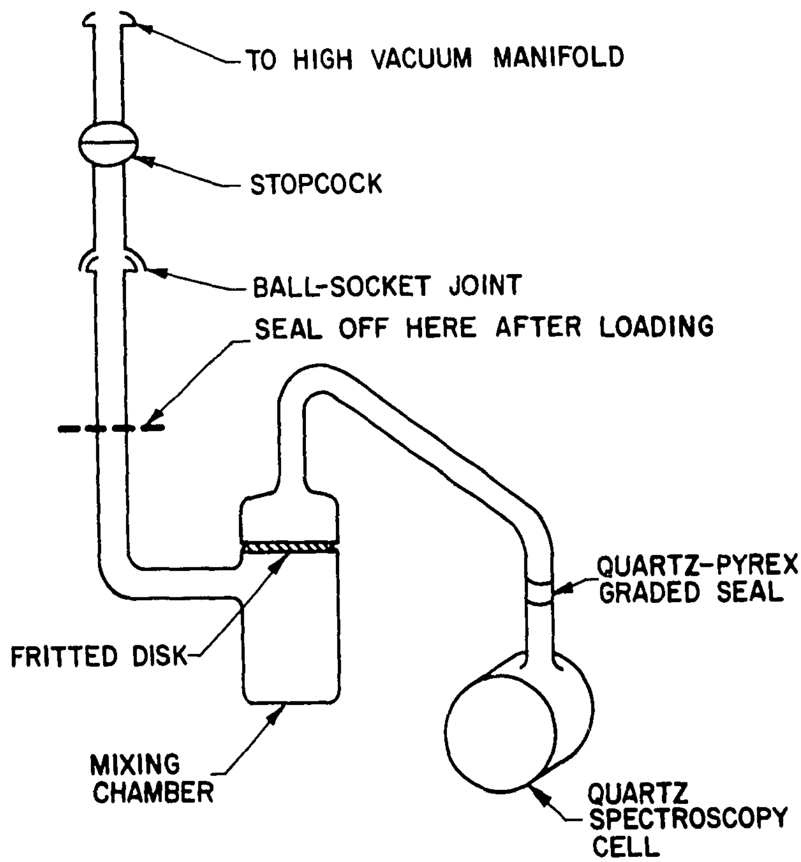
TO HIGH VACUUM MANIFOLD
STOPCOCK
BALL-SOCKET JOINT
SEAL OFF HERE AFTER LOADING
QUARTZ-PYREX
GRADED SEAL
FRITTED DISK
MIXING
CHAMBER
QUARTZ
SPECTROSCOPY
CELL

By alternately filtering and distilling the solution between the mixing chamber and the cell, a concentration was obtained which gave peaks of suitable intensity. The spectra of the solutions were determined using pure solvent as a reference.

During the process of studying the reflectance spectra of the hexahaloniobate(IV) complexes, the need for accurate intensity data became apparent. In this regard the visible spectrum of the $NbCl_6^=$ ion was measured in molten pyridinium chloride (pyHCl). The preparation and characterization of the resulting $(pyH)_2NbCl_6$ complex are described in the synthesis portion of the experimental section.

The spectrum was obtained on a Cary 12 recording spectrophotometer which had been modified for high temperature measurements[1]. This instrument had a heated cell compartment capable of maintaining a constant temperature from 30 to 500°.

The glass apparatus used for this experiment, Figure 4, consisted of a rectangular quartz spectroscopy cell (1-cm. light path) sealed to a mixing chamber through a fine porosity fritted disk. An extention of the mixing chamber was used for filling the apparatus and for connection to a high

---

[1]The high temperature spectrophotometer was designed and built by Richard D. Barnes of this laboratory, who graciously consented to its use by the author.

Figure 4. Glass apparatus used in the determination of the absorption spectrum of niobium(IV) chloride in molten pyridinium chloride

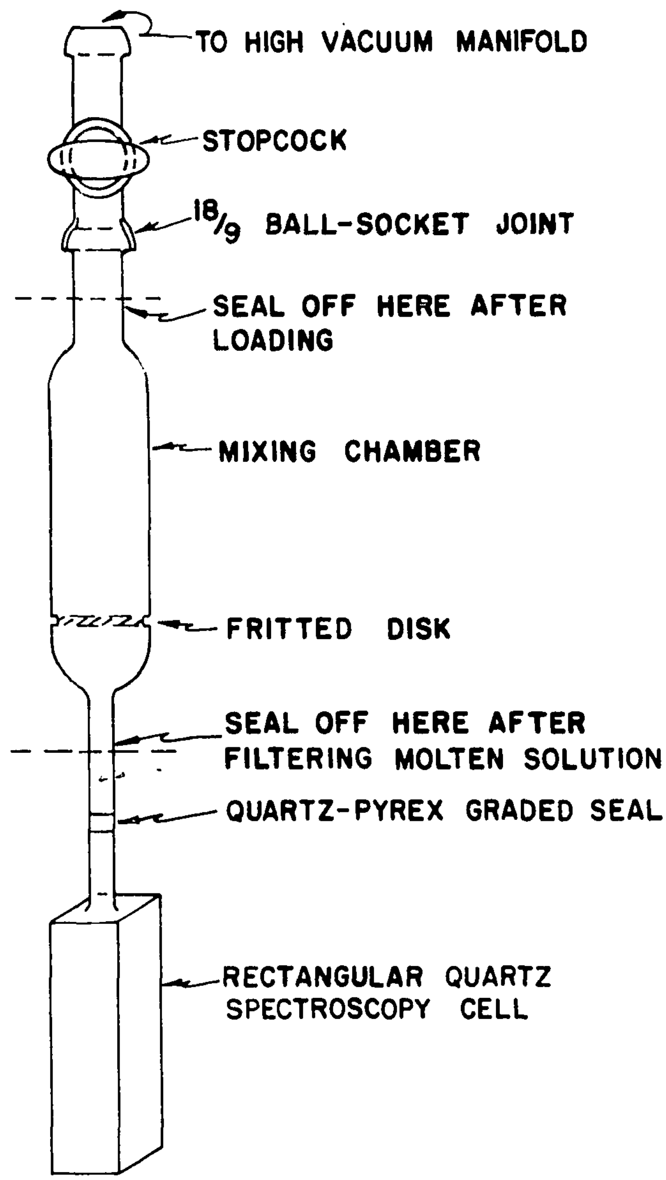

TO HIGH VACUUM MANIFOLD
STOPCOCK
18/9 BALL-SOCKET JOINT
SEAL OFF HERE AFTER LOADING
MIXING CHAMBER
FRITTED DISK
SEAL OFF HERE AFTER FILTERING MOLTEN SOLUTION
QUARTZ-PYREX GRADED SEAL
RECTANGULAR QUARTZ SPECTROSCOPY CELL

vacuum manifold.

A solution of $NbCl_6^{=}$ in pyHCl was prepared by fusing a mixture of $NbCl_4$ and pyHCl in the mixing chamber of the sealed evacuated vessel at 150°. When the melt became colored, the molten solution was filtered into the rectangular cell. After allowing the solution to cool, the cell was sealed off from the mixing chamber.

The spectrum of $NbCl_6^{=}$ was scanned, against air, from 1000 mμ to the pyridinium ion cutoff (350 mμ) at temperature intervals of 150°, 162.5°, and 175°. The spectrum of anhydrous pyHCl was also obtained over the same temperature range. The shoulders due to $NbCl_6^{=}$ in the pyHCl solution were resolved into peaks by graphically subtracting the pure pyHCl absorption.

Molar extinction coefficients for the spectrum of an acetonitrile complex were obtained from Equation 6 after analyzing a known volume of solution in the spectroscopy cell for niobium.

$$\epsilon = A(1/C\ell) \qquad (6)$$

Where: ϵ = molar extinction coefficient,

A = absorbance of the peak,

C = concentration of the solution in moles/liter,

ℓ = thickness of the absorbing solution in cm.

The concentration of niobium was determined spectrophotometrically (32) after opening the cell, pouring the solution into a beaker, and removing organic products and the halides by successive evaporations with ammonia and sulfuric acid. The niobium(V) oxide that remained was treated with sulfuric acid and peroxide as described in the analytical section.

The procedure used in determining the concentration of niobium in the pyHCl solution was similar to that described above. The cell was opened, the solid pyHCl dissolved in distilled water, and the same analytical method followed thereafter. Molar extinction coefficients were calculated from Equation 6.

Infrared spectra

Infrared absorption spectra of the solid A_2MX_6 and NbX_4(acetonitrile)$_2$ complexes were measured by Miss Evelyn E. Conrad of the Ames Laboratory Spectrochemistry Group. The spectra were obtained from 4000 to 700 cm.$^{-1}$ on a Beckman IR-7 spectrophotometer.

Sample preparation, carried out in a dry-box, consisted of mixing the powdered complexes with finely ground (<100-mesh) dry alkali metal halide and loading the mixture in a pellet press between layers of pure alkali metal halide, then placing the filled pellet press in a polyethylene bag. In this manner the complexes could be removed from the dry-box and kept under argon until pressed, _in vacuo_, into a transparent pellet. The pellets were scanned immediately upon their removal from the press to minimize hydrolysis.

Conductivity

The electrolytic conductivities of the tetrahalobis(acetonitrile)niobium(IV) complexes were determined in acetonitrile. The conductance apparatus, Figure 5, consisted of an all glass cell connected to a mixing chamber through a fritted disk. Bright platinum electrodes were sealed into the cell in such a way that the cell was vacuum tight. These electrodes were square, 2 cm. on an edge and 5 mm. apart. The mixing chamber was connected to the vacuum system in the usual manner. A Leeds and Northrup AC conductance bridge, Model 4866-60, was used for all measurements. The conductance was measured at $20 \pm 0.1^{\circ}$ by placing the cell in a constant temperature bath.

The conductance vessel was thoroughly outgassed, loaded with a niobium(IV) halide, and evacuated to _ca_. 10^{-5} Torr. Acetonitrile was distilled directly into the electrode chamber and the apparatus was sealed off from the system.

Figure 5. Glass apparatus used in the determination of the electrolytic conductance of the niobium(IV) halides in acetonitrile

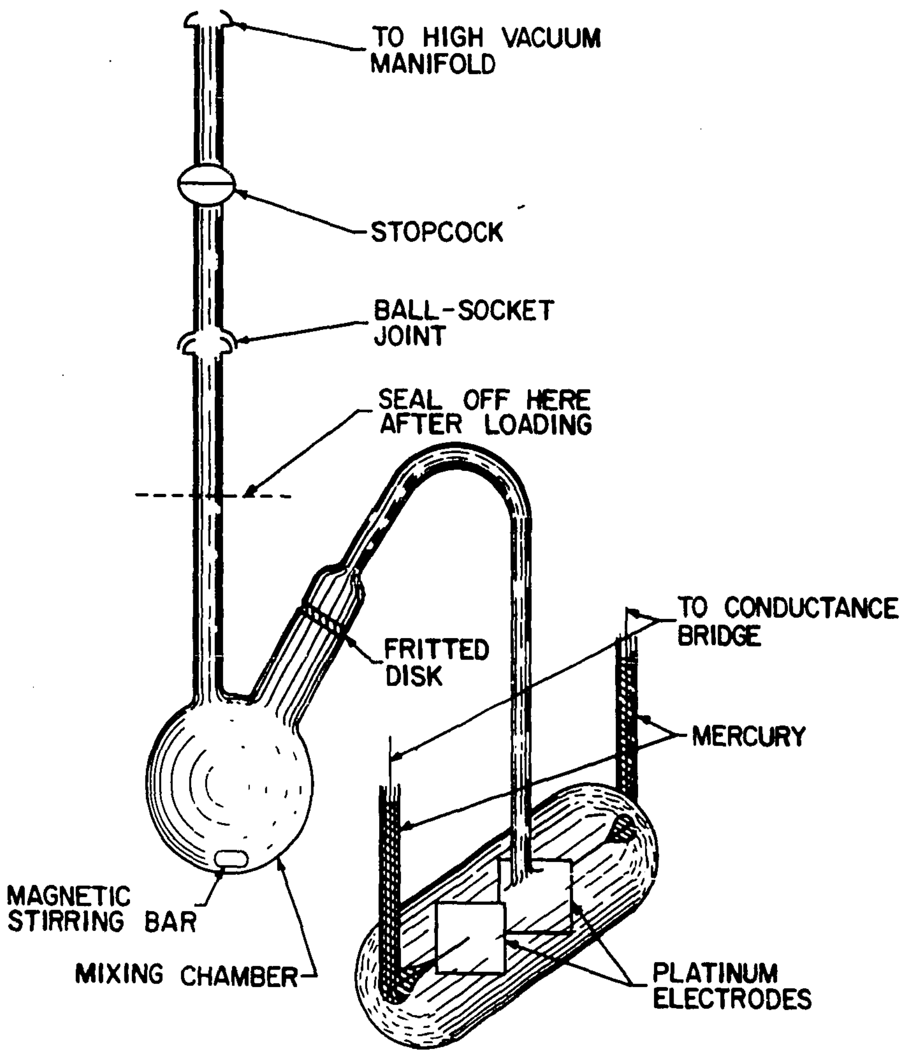
TO HIGH VACUUM MANIFOLD
STOPCOCK
BALL-SOCKET JOINT
SEAL OFF HERE AFTER LOADING
TO CONDUCTANCE BRIDGE
FRITTED DISK
MERCURY
MAGNETIC STIRRING BAR
MIXING CHAMBER
PLATINUM ELECTRODES

For use as a reference value and to check the purity of the solvent, the resistance of acetonitrile was determined at 20^{o} and its specific conductance was calculated from Equation 7.

$$K = k(1/R) \tag{7}$$

Where: K = specific conductance in ohm^{-1} cm.$^{-1}$,

k = cell constant in cm.$^{-1}$,

R = resistance of the solution in ohm.

The acetonitrile was then decanted onto the tetrahalide and the complexing reaction allowed to go to completion, with stirring. The saturated solution that resulted was filtered into the electrode chamber and its specific conductance was determined at 20^{o}.

The equivalent conductance of the solution was calculated from Equation 8.

$$\Lambda = 1000(K/C) \tag{8}$$

Where: Λ = equivalent conductance in cm.^{2} eq.$^{-1}$ ohm^{-1},

K = specific conductance in ohm^{-1} cm.$^{-1}$,

C = concentration of the solution in g. eq./ℓ.

<u>Molecular weights</u>

The apparent molecular weights of niobium(IV) chloride and niobium(IV) bromide were determined cryoscopically in acetonitrile. The apparent molecular weight of niobium(IV) iodide could not be measured in acetonitrile due to the insolubility of the resulting $NbI_4(acetonitrile)_2$ complex. The molecular weight apparatus is shown in Figure 6. The apparatus was submersed in a Dry Ice-acetone bath and the rate of cooling controlled by regulating the pressure in the outer jacket of the vessel. A uniform cooling rate in the solution was maintained through constant agitation with a magnetic stirring bar.

The temperature of solutions in the cell was determined with a Sargent Model S-81630 Thermometric Element in conjunction with a Sargent Model S-81600 Thermometric Bridge. The degree of bridge unbalance which resulted from temperature changes in the solution was plotted on a Bristol multirange recorder. Actual temperatures were not needed in this determination because of the calibration procedure described below.

The freezing point of pure acetonitrile was arbitrarily fixed on the recorder after several cooling curves had been obtained. Weighed amounts of napthalene, in pellet form, were added to the solvent and the resulting depressions in freezing point recorded. A calibration curve plotting recorder deflection vs. molality of the solution was constructed from the data. The molecular weight of a known

Figure 6. Apparatus used in the cryoscopic determination of the molecular weights of the niobium(IV) halides in acetonitrile

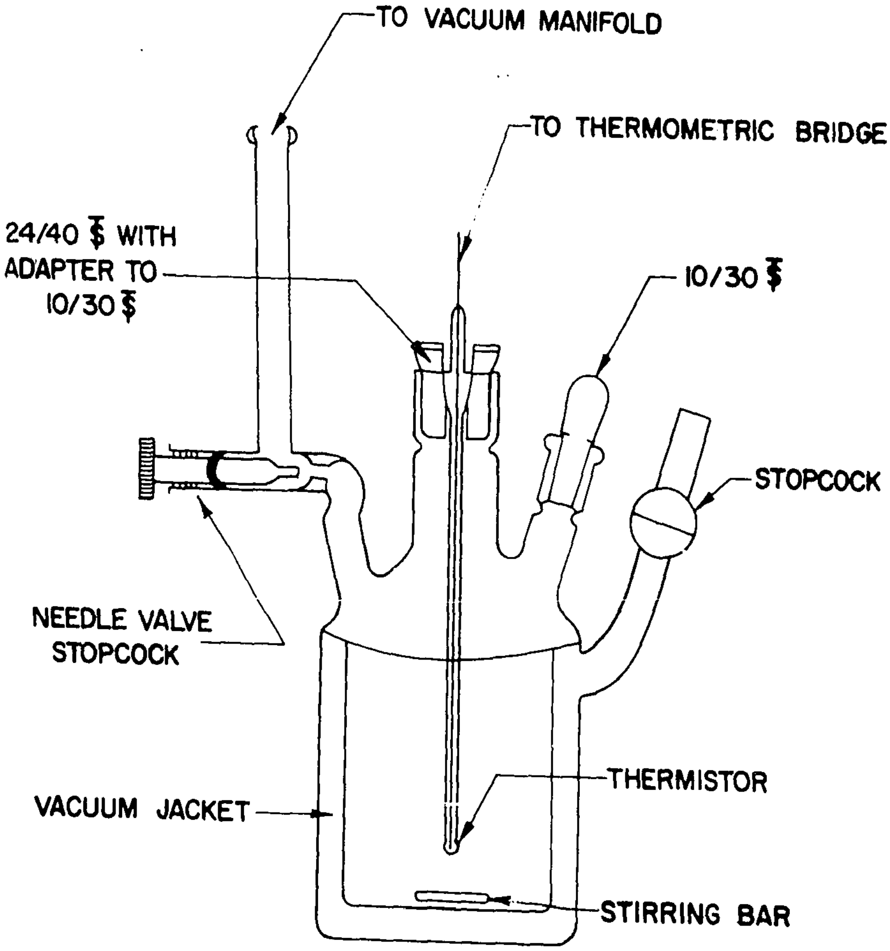
TO VACUUM MANIFOLD
TO THERMOMETRIC BRIDGE
24/40 $ WITH
ADAPTER TO
10/30 $
10/30 $
STOPCOCK
NEEDLE VALVE
STOPCOCK
THERMISTOR
VACUUM JACKET
STIRRING BAR

weight of solute in a known amount of acetonitrile could now be calculated after determining the freezing point of the solution and obtaining its corresponding molality from the graph.

Solutions of the niobium(IV) halides in acetonitrile were prepared in the following manner: A weighed amount of tetrahalide was placed in the molecular weight cell. The apparatus was outgassed and a weighed amount of dry acetonitrile distilled onto the compound. This solvent had previously been distilled into a weighing flask. The reaction of NbX_4 with CH_3CN was allowed to continue with stirring until all the tetrahalide had dissolved. Then several cooling curves were determined and the apparent molecular weight was calculated. The apparent molecular weights of the niobium(IV) halides are given with the analytical data for the NbX_4(acetonitrile)$_2$ complexes.

Dipole moment

As a first step in determining the dipole moment of a molecule, dielectric constants and indices of refraction of the species in a nonpolar solvent are obtained as a function of concentration. Plots of dielectric constant (ε) and refractive index (n) versus concentration (X) are made and the respective slopes $d\varepsilon/dX$ and dn/dX are computed. The orientation polarization of the solute is then calculated from Equation 9 (37).

$$P_o = \frac{3M}{D(\varepsilon_o+2)^2} \left[\frac{d\varepsilon}{dX} - 2(n_o)\frac{dn}{dX}\right] \tag{9}$$

Where: P_o = orientation polarization of the solute,

M = molecular weight of the solvent,

D = density of the solvent,

ε_o = dielectric constant of the solvent,

$d\varepsilon/dX$ = change in dielectric constant of the solution with concentration (X),

n_o = index of refraction of the solvent,

dn/dX = change in index of refraction of the solution with concentration (X).

Since $d\varepsilon/dX$ is much larger than dn/dX for a polar molecule (37, p. 85), Equation 9 may be simplified to

$$P_o = \frac{3M}{D(\varepsilon_o+2)^2} \left[\frac{d\varepsilon}{dX}\right] . \tag{10}$$

After obtaining the orientation polarization (P_o), the dipole moment of the solute may be calculated from Equation 11 (37).

$$\mu = \left[\frac{9kTP_o}{4\pi N}\right]^{\frac{1}{2}} \tag{11}$$

Where: μ = dipole moment in Debye's,

T = absolute temperature,

k = Boltzman constant,

N = Avogadro's number,

P_o= orientation polarization of the solute.

The dielectric constants of solutions of various concentrations of $NbBr_4$(acetonitrile)$_2$ in benzene were determined using a Sargent Model V Oscillometer. The Oscillometer cell was calibrated with pure dry benzene, toluene, dioxane, cyclohexane, and heptane[1].

The glass apparatus used to prepare solutions of $NbBr_4$-(acetonitrile)$_2$ in benzene and to transfer these solutions *in vacuo* into the Oscillometer cell is shown in Figure 7. The apparatus consisted of a mixing chamber connected to the Oscillometer cell through a series of Teflon needle valve stopcocks and ground glass joints. The stopcocks and joints were arranged so that the solution never came in contact with silicone lubricant on the joints. Addition of complex and solvent distillations into the mixing chamber were performed through other connections to a vacuum line.

---

[1]The author is indebted to Mr. D. G. Hendricker and Mr. T. J. Hutteman for the loan of the Oscillometer and cell and for performing the necessary calibrations.

Figure 7. Apparatus used to determine the dielectric constants of tetrabromobis(acetonitrile)niobium(IV)-benzene solutions

A,C,D. Needle valve stopcocks
B. Vacuum stopcock
E. Magnetic stirring bar
F. Oscillometer cell
G. 100 ml. round bottom flask

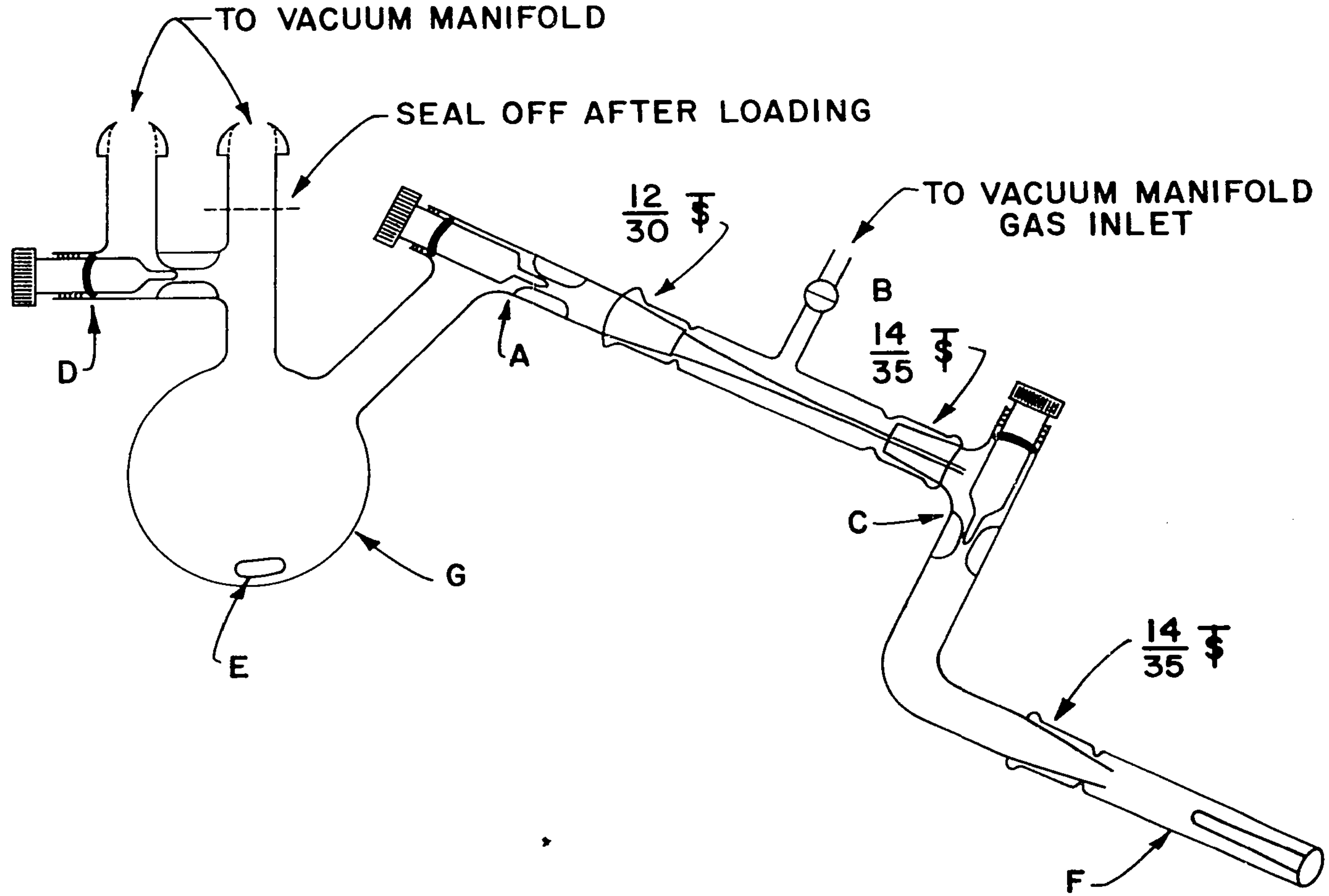
TO VACUUM MANIFOLD
SEAL OFF AFTER LOADING
12/30 $
TO VACUUM MANIFOLD
GAS INLET
B
14/35 $
A
D
C
G
E
14/35 $
F

The following procedure was used in order to obtain various known concentrations of complex in benzene, then transfer these solutions to the Oscillometer cell, and detach the filled cell from the mixing chamber without exposing the solution to the atmosphere: A known weight of $NbBr_4$-(acetonitrile)$_2$ complex was placed in the mixing chamber of the apparatus, the mixing chamber was subsequently evacuated and weighed, dry benzene was distilled onto the complex, and the flask reweighed to obtain the weight of the solvent. After solution of $NbBr_4$(acetonitrile)$_2$ had taken place, the Oscillometer cell was joined to the mixing chamber, as shown in Figure 7, and evacuated through stopcock B. The solution was poured into the cell after opening stopcock A. By closing stopcocks A and C, then opening stopcock B to the atmosphere, the Oscillometer cell could be removed from the mixing chamber without exposure of either of the solutions. By weighing the mixing chamber after removal of some solution, and after dilution with more solvent, it was possible to calculate the concentrations of the solutions used. The dielectric constants of these solutions were determined and the dipole moment of $NbBr_4$(acetonitrile)$_2$ was calculated as described above.

Synthesis

Niobium(IV) halides

Niobium(IV) chloride and bromide were prepared by the reduction of the appropriate niobium(V) halide with niobium metal as described by McCarley and Torp (1).

Anal. Calcd. for $NbCl_4$: Nb, 39.6; Cl, 60.4. Found: Nb, 39.7; Cl, 60.3. Calcd. for $NbBr_4$: Nb, 22.5; Br, 77.5. Found: Nb, 22.6; Br, 77.4.

Niobium(IV) iodide was prepared by the thermal decomposition of niobium(V) iodide as described by Corbett and Seabaugh (38).

Anal. Calcd. for NbI_4: Nb, 15.5; I, 84.5. Found: Nb, 15.6; I, 84.5.

Tantalum(IV) halides

The tantalum(IV) halides $TaCl_4$ and $TaBr_4$ were synthesized by reduction of TaX_5 with tantalum metal in sealed, evacuated vycor tubes. The procedure of McCarley and Boatman (2) was followed.

Anal. Calcd. for $TaCl_4$: Ta, 56.0; Cl, 44.0. Found: Ta, 56.2; Cl, 43.7. Calcd. for $TaBr_4$: Ta, 36.2; Br, 63.8. Found: Ta, 36.0; Br, 63.5.

Alkali metal hexahaloniobate(IV) and hexahalotantalate(IV) complexes

The A_2MX_6(A = K, Rb, Cs; M = Nb, Ta; X = Cl, Br, I) complexes were prepared by heating a stoichiometric mixture of AX and MX_4 in one end of an evacuated, sealed quartz tube which had been filled in the dry-box. The tube was held at the melting point of the alkali metal halide for 1-3 hours in a resistance furnace whose temperature was governed by a Brown proportionating controller. A temperature gradient was maintained along this quartz vessel, with the end containing material ca. 50^{o} cooler than the other end, to prevent sublimation of metal tetrahalide from the reaction zone.

On cooling, dark colored, sintered solids were found in the tubes (with the exception of K_2NbBr_6), providing evidence that the complexes have melting points above the reaction temperature.

The reactions between AX and MX_4 to form A_2MX_6 complexes were observed to go to completion under the above conditions. No unreacted metal tetrahalide could be sublimed from the reaction product and x-ray diffraction patterns (30 hour exposures) showed no lines which could be attributed to either starting material. The powder patterns also verified the presence of a single unique face centered compound in each case.

The hexahalo complexes were found to be sensitive to air and moisture and had to be handled by glove-box and vacuum techniques.

Pyridinium hexachloroniobate(IV) complex

Anhydrous pyridinium chloride used in the preparation of $(pyH)_2NbCl_6$ was synthesized since the compound could not be obtained commercially. The synthesis was carried out by bubbling dry HCl gas through an ether solution of spectro-grade pyridine. The ether was distilled off in vacuo and the white pyHCl dried at 50^o.

The preparation of $(pyH)_2NbCl_6$ was accomplished by the reaction of excess molten pyHCl with $NbCl_4$ at 150^o in an evacuated, sealed Pyrex tube. Niobium(IV) chloride was found to be very soluble in fused pyridinium chloride yielding a red solution and a dark red crystalline material after removal of excess pyHCl by sublimation.

This product was found to be isomorphous with $(pyH)_2PtCl_6$ by graphical comparison of their powder x-ray diffraction patterns. Therefore the red product of the reaction between pyHCl and $NbCl_4$ is most likely $(pyH)_2NbCl_6$ and the $NbCl_6^=$ ion is the predominant niobium species in pyHCl solution.

Tetrahalobis(acetonitrile)niobium(IV) complexes

The isolation of stoichiometric $NbX_4(Ac)_2$ (X = Cl, Br, I; Ac = acetonitrile) complexes was accomplished by the reaction of excess dry acetonitrile with the appropriate niobium(IV) halide, followed by removal of the excess solvent *in vacuo*. This reaction was most easily carried out in the soxlet extraction apparatus shown in Figure 8.

In a typical experiment, *ca*. 4-5 grams of niobium(IV) halide were placed on the fritted disk of the extraction vessel, in the dry-box. The apparatus was outgassed on the vacuum line at *ca*. 10^{-5} Torr, about 50 ml. of dry acetonitrile was vacuum distilled into the vessel at 0^{o}, and the vessel was sealed off from the rest of the system. Condensation of acetonitrile above the frit was accomplished by warming the solvent reservoir while directing a stream of cold air across the vessel above the frit. Complete extraction of the niobium(IV) halides usually required 3-4 days. The excess acetonitrile was removed from the flask, after evacuating and breaking the break seal, and the resulting solid complexes were dried at room temperature under a dynamic vacuum for 24 hours. The complexes were stored under argon in the dry-box

Figure 8. Soxlet extraction apparatus used to prepare the tetrahalobis(acetonitrile)niobium(IV) complexes

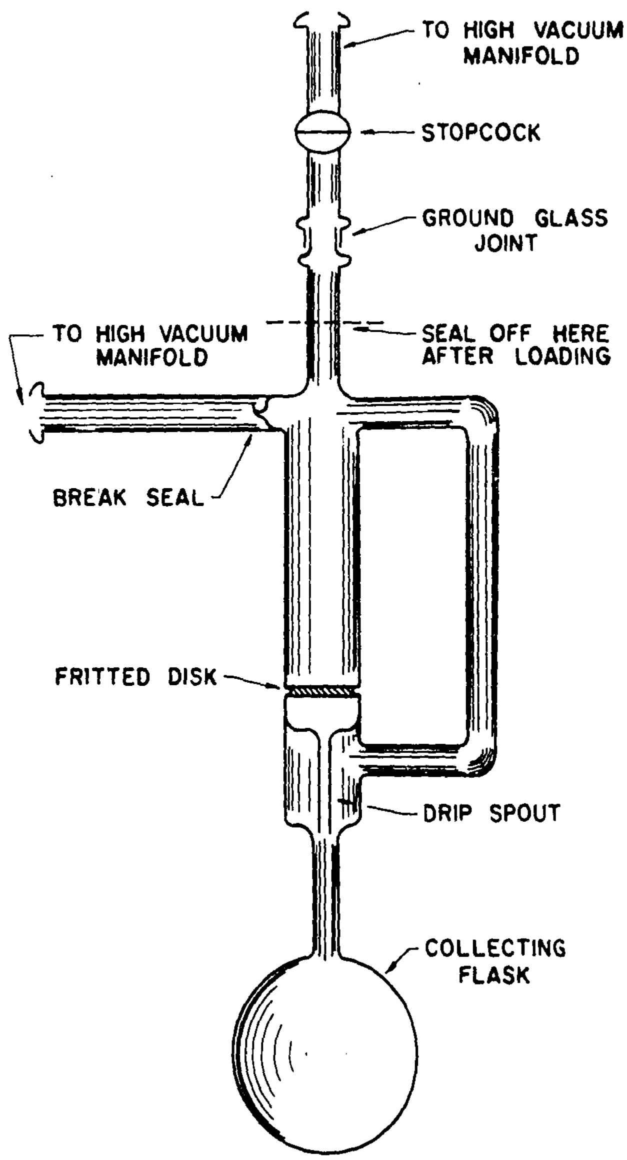
TO HIGH VACUUM
MANIFOLD
STOPCOCK
GROUND GLASS
JOINT
TO HIGH VACUUM
MANIFOLD
SEAL OFF HERE
AFTER LOADING
BREAK SEAL
FRITTED DISK
DRIP SPOUT
COLLECTING
FLASK

since they were found to decompose rapidly in the atmosphere.

In the reaction of niobium(IV) chloride with acetonitrile the solution gradually turned a yellow-orange color. During the removal of excess acetonitrile large ruby red crystals separated from the saturated solution. These crystals were unstable under a dynamic vacuum and decomposed at room temperature into a powdery orange solid. This solid was shown by analysis to have the composition $NbCl_4(Ac)_2$.

Anal. Calcd. for $NbCl_4(Ac)_2$: Nb, 29.3; Cl, 44.8; Ac, 25.9. Found: Nb, 28.9; Cl, 44.3; Ac, 24.5. Mol. wt. Calcd. for $NbCl_4$ in acetonitrile: 234.8. Found: 229 $\pm$ 30.

The extraction of niobium(IV) bromide with acetonitrile proceeded as described above with the solution in the reservoir gradually turning a dark red color. In contrast to the $NbCl_4$-acetonitrile system, the dark red crystals that were present during the removal of excess acetonitrile were stable under a dynamic vacuum. These crystals were dried at room temperature and were found to have the composition $NbBr_4(Ac)_2$.

Anal. Calcd. for $NbBr_4(Ac)_2$: Nb, 18.8; Br, 64.6; Ac, 16.6. Found: Nb, 19.4; Br, 64.2; Ac, 16.4. Mol. wt. Calcd. for $NbBr_4$ in acetonitrile: 412.6. Found: 435 $\pm$ 30.

The niobium(IV) iodide-acetonitrile reaction was very similar to that described for $NbBr_4$ with this ligand. A dark green solution formed in the solvent reservoir during the extraction and greenish-black crystals precipitated before any excess acetonitrile was removed. These crystals were found to be stable after removal of excess ligand and during the drying process. The solid also had the composition $NbI_4(Ac)_2$.

Anal. Calcd. for $NbI_4(Ac)_2$: Nb, 13.7; I, 74.1; Ac, 12.2. Found: Nb, 13.9; I, 73.5; Ac, 12.6.

When the solid complexes were heated to 50-60^{o} under a dynamic vacuum, decomposition of the di-adducts occurred. After one week under these conditions, Ac/NbX_4 ratios between 1.2 and 1.5 were found from weight loss experiments. X-ray diffraction analysis of the powdered residues showed that partial decomposition of the $NbX_4(Ac)_2$ complexes to the niobium(IV) halide had occurred in every case.

When the temperature of the complexes was raised above ca. 100^{o}, volatile products were observed to have sublimed to cooler portions of the vessels. In the $NbCl_4(Ac)_2$ decomposition reaction a yellow crystalline product was the predominant volatile species. Analysis of this yellow compound proved to be difficult due to the limited amount of material that could be obtained. The best results, given below, indicated that the material could be an acetonitrile adduct of niobium(V) chloride, $NbCl_5(Ac)$. The infrared spectrum of this compound verified the presence of coordinated acetonitrile.

Anal. Calcd. for $NbCl_5(Ac)$: Nb, 29.9; Cl, 56.9; Ac, 13.2. Found: Nb, 30.0; Cl, 54.0; Ac, 16.0 (by difference).

The postulated stoichiometry of the yellow product was verified after synthesizing the $NbCl_5(Ac)$ complex by the direct reaction of $NbCl_5$ with excess acetonitrile. The yellow crystalline solid that was formed and the yellow solid from the $NbCl_4(Ac)_2$ decomposition reaction had identical x-ray diffraction patterns.

The volatile products of the $NbBr_4(Ac)_2$ and $NbI_4(Ac)_2$ decomposition reactions were not characterized, but it is likely that similar $NbX_5(Ac)$ complexes are formed.

Pressure-Composition Studies of the Niobium(IV) Chloride-Acetonitrile System

In an effort to determine the composition of the ruby red crystals that were formed during the reaction of $NbCl_4$ with acetonitrile, the composition of this system was investigated as a function of the vapor pressure of acetonitrile over the system at constant temperature. A pressure-composition diagram was constructed from the data.

The glass apparatus used in this study, Figure 9, consisted of a 500 ml. round bottom flask (A) connected to one arm of a mercury U-tube null indicator (B). The other arm of the U-tube was joined to a mercury manometer (C) through a series of ballast bulbs (D). The ballast was also connected to the vacuum line and to a gas inlet (E). The mercury columns in the U-tube were balanced by partially evacuating that portion of the system and then slowly increasing the pressure, by adding gas, until the null-point was reached. Pressures from the manometer were measured with a Gaertner precision cathetometer having a sensitivity of 0.05 millimeter mercury.

A second arm from the round bottom vessel was connected to a series of gas collection traps (F) through a Teflon needle valve stopcock (G). These traps were used to collect small amounts of acetonitrile by freezing the vapor at -196^{o} and sealing off the trap. The composition of the material in the flask could be calculated after each increment of acetonitrile had been drawn off and weighed since the total weights of acetonitrile and $NbCl_4$ were known. The vapor pressure in the system was measured for a particular Ac/$NbCl_4$ mole ratio

Figure 9. Apparatus used to determine the pressure-composition diagram of the niobium(IV) chloride-acetonitrile system

A. 500 ml. round bottom flask
B. U-tube null indicator
C. Manometer
D. Ballast bulbs
E. Gas inlet
F. Collection traps
G. Teflon needle valve stopcock
H, I. Glass break-seals and breakers

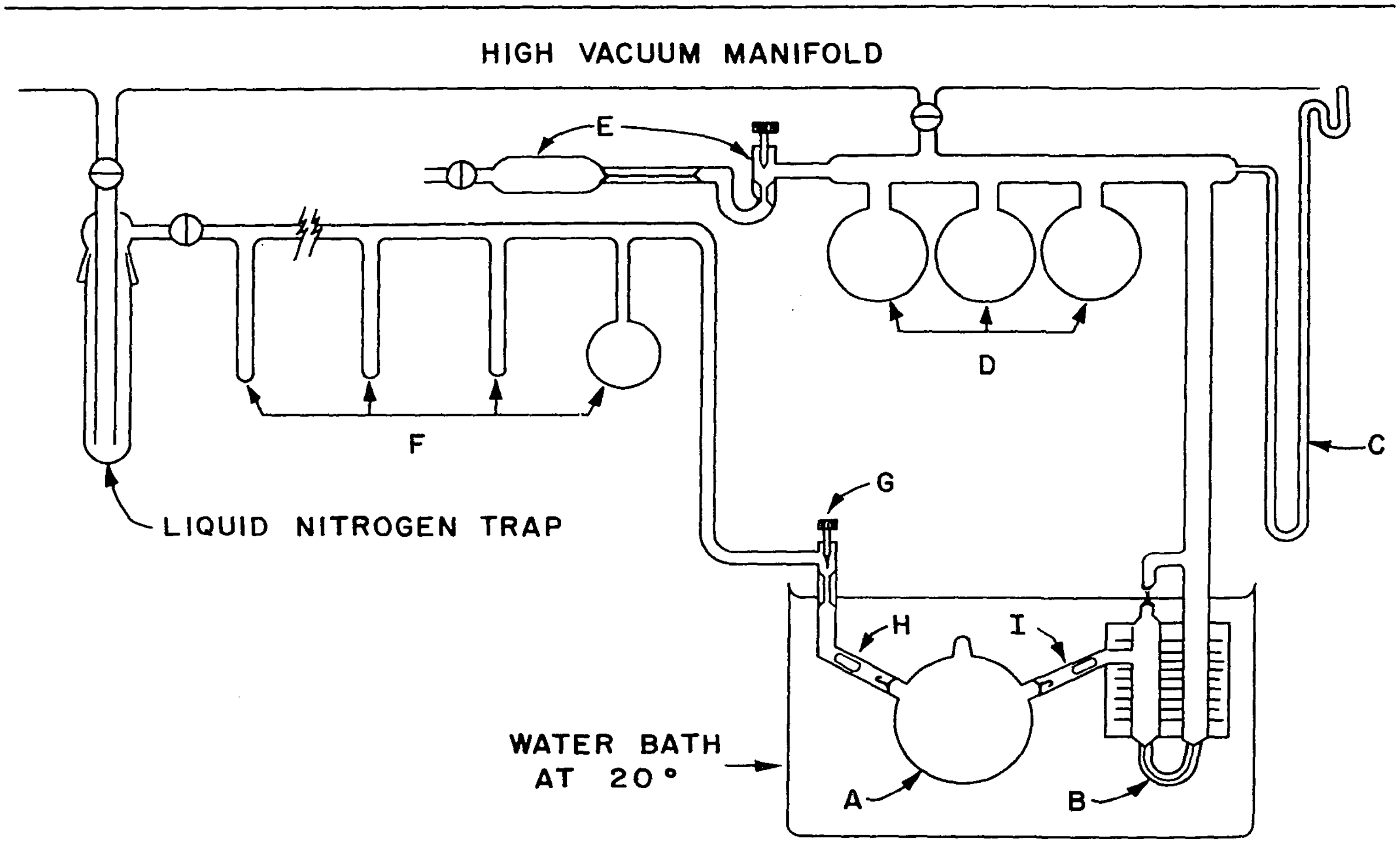

HIGH VACUUM MANIFOLD
E
D
C
F
G
LIQUID NITROGEN TRAP
H
I
WATER BATH
AT 20°
A
B

after equilibrium had been established (2-3 weeks).

The round bottom flask and U-tube were thermostated (as shown in Figure 9) at 20 ± 0.1^{o} in a water bath regulated by a Precision micro-thermoregulator.

The initial composition of the niobium(IV) chloride-acetonitrile solution was fixed by extracting a known weight of $NbCl_4$ into the round bottom flask with a known amount of acetonitrile. This flask was sealed off from the rest of the extraction apparatus and joined to the system as shown in Figure 9. Most of the acetonitrile was distilled into the large collection vessel at F, after evacuating that portion of the apparatus and breaking break-seal H. The pressure of the resulting saturated solution was determined after evacuating the rest of the system, sealing the U-tube null indicator, and breaking the other break-seal (I). Pressure-composition data were then obtained as described above.

The pressure-composition diagram for the $NbCl_4$-acetonitrile system at 20^{o} is shown in Figure 10. It is evident from this diagram that the ruby red crystals have the composition $NbCl_4(Ac)_3$. This compound is unstable at acetonitrile pressures below ca. 28 mm., decomposing to $NbCl_4(Ac)_2$. Decomposition of the $NbCl_4(Ac)_2$ complex was not observed.

Figure 10. Pressure-composition diagram for the niobium(IV) chloride-acetonitrile system

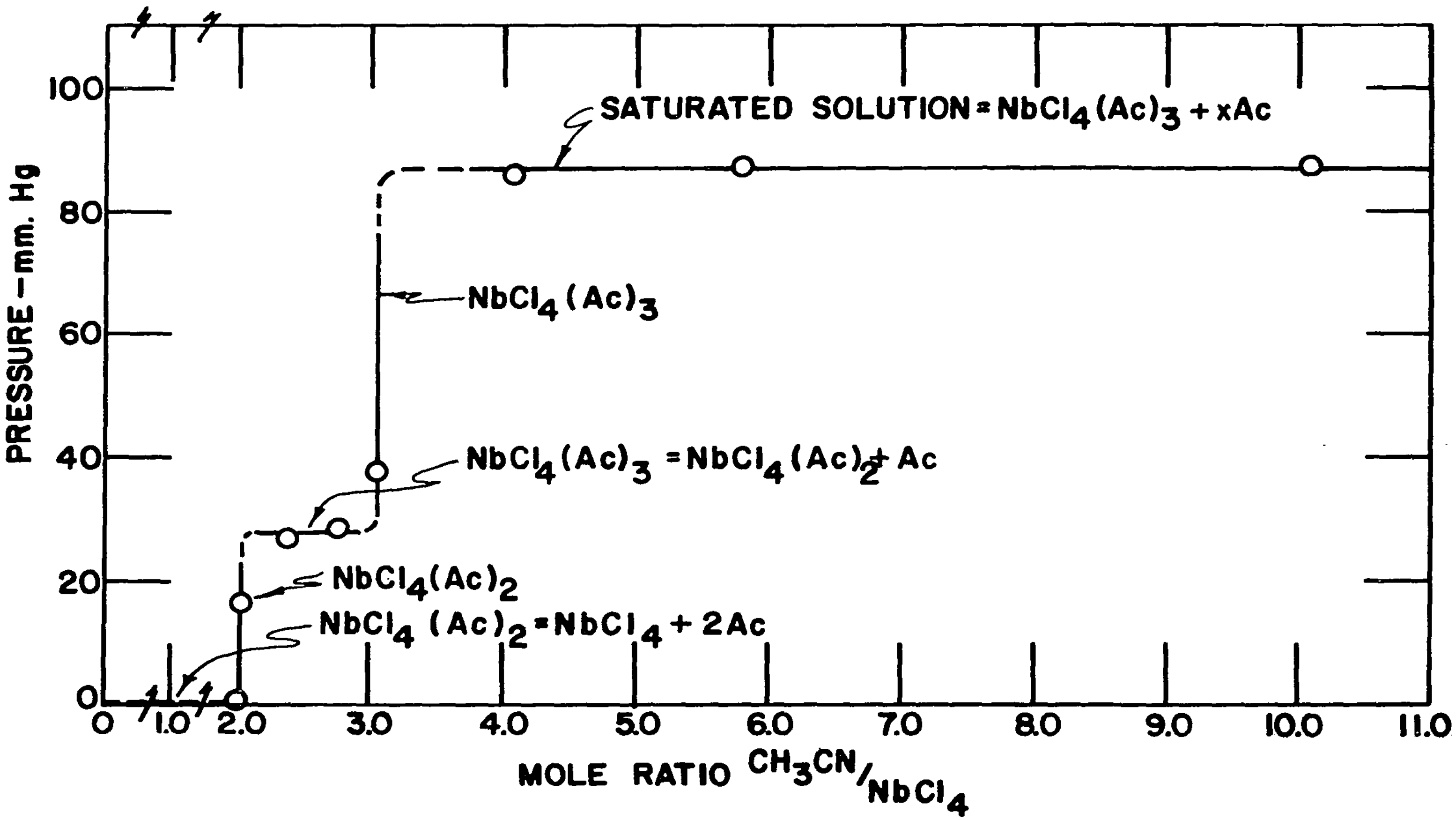
SATURATED SOLUTION = $NbCl_4(Ac)_3$ + xAc
$NbCl_4(Ac)_3$
$NbCl_4(Ac)_3 = NbCl_4(Ac)_2 + Ac$
$NbCl_4(Ac)_2$
$NbCl_4(Ac)_2 = NbCl_4 + 2Ac$
PRESSURE – mm. Hg
MOLE RATIO $CH_3CN/NbCl_4$
0
20
40
60
80
100
1.0
2.0
3.0
4.0
5.0
6.0
7.0
8.0
9.0
10.0
11.0

The vapor pressure of acetonitrile over this di-adduct was less than one millimeter after the system had equilibrated for five weeks.

In other experiments where the $NbCl_4(Ac)_2$ complex was placed in a dynamic vacuum at room temperature for ca. one week, some decomposition of the compound to $NbCl_4$ occurred. Therefore the $NbCl_4(Ac)$ complex is not stable under these conditions and decomposition of $NbCl_4(Ac)_2$ proceeds directly to $NbCl_4$.

RESULTS AND DISCUSSION

Hexahalo Complexes of Niobium(IV) and Tantalum(IV)

Pure crystalline alkali metal hexahaloniobate(IV) and hexahalotantalate(IV) complexes, A_2MX_6 (A = K, Rb, Cs; M = Nb, Ta; X = Cl, Br, I) were prepared as described in the experimental section. The reaction between a given alkali metal halide and niobium(IV) or tantalum(IV) halide, at the melting point of the alkali metal halide, was found to go to completion within one hour. In almost every case the melting point of the resulting hexahalo complex was above the reaction temperature. Also, in preparations where the starting materials were heated slowly to temperature and the reaction zone was kept ca. 50° hotter than the other portion of the sealed vessel, very little metal tetrahalide or pentahalide (from a disproportionation reaction[1]) was found on quenching. These observations indicate that the complexing reactions take place at relatively low temperatures according to Equation 12.

$$2AX_{(s)} + MX_{4(g)} = A_2MX_{6(s)} \qquad (12)$$

The driving force for this heterogeneous reaction at low

---

[1]The disproportionation of $NbCl_4(s)$ into $NbCl_3(s)$ and $NbCl_5(g)$ has been shown by Schäfer and Bayer (39) to proceed at low temperatures. The pressure of $NbCl_5(g)$ over this system is one atmosphere at 329°.

temperatures is most likely the high lattice energy of the resulting A_2MX_6 compound.

X-ray diffraction studies

Powder x-ray diffraction patterns were obtained for all of the hexahalo complexes to verify their purity and to investigate the structures of the solids. The complexing reactions were found to go to completion since all but one of the diffraction patterns contained no lines attributable to either starting material[1].

The x-ray patterns of all the hexahalo complexes could be indexed on the basis of a face centered unit cell. In addition, all of the compounds with the exception of K_2NbBr_6 were found to be face centered cubic. The potassium hexabromoniobate(IV) crystallized with a slightly distorted unit cell having tetragonal symmetry.

The fact that every line in the diffraction patterns of these complexes could be indexed on the basis of a face centered unit cell, i.e. only unmixed $hk\ell$ reflections are

[1]In the preparation of the K_2NbBr_6 complex, x-ray analysis showed some excess KBr to be present but no unreacted $NbBr_4$. This product was analyzed for niobium and bromine, as described in the experimental section, and found to contain 35.7% unreacted KBr. Corrections for the KBr impurity were made in subsequent magnetic studies of K_2NbBr_6.

present, indicates that the compounds do not possess an ordered sublattice. Such a superlattice could arise if disproportionation of MX_4 occurred and $M^{V}X_6^{-}$ and $M^{III}X_6^{\equiv}$ resulted. These ions would probably form an ordered sublattice because of their different charges.

Lattice parameters for the A_2MX_6 complexes, which were obtained from the x-ray data and refined as described in the experimental section, are given in Table 2. This table also presents some other physical properties of the compounds. Complete tables of x-ray diffraction data for the A_2MX_6 complexes are found in the Appendix.

Table 2. Physical properties of some hexahalo complexes of niobium(IV) and tantalum(IV)

Complex	Color	Melting point, ^{o}C	Bravais lattice	Refined lattice parameters, Å
K_2NbCl_6	purple	782	FCC	a_o = 9.97 ± 0.01
Rb_2NbCl_6	purple	802	FCC	a_o = 10.10 ± 0.01
K_2NbBr_6	green	<700	FCT[a]	a_o = 10.38 ± 0.01
				c_o = 10.86 ± 0.01
Rb_2NbBr_6	green	>700	FCC	a_o = 10.63 ± 0.01
Cs_2NbI_6	brown	>621	FCC	a_o = 11.54 ± 0.01
K_2TaCl_6	purple	>776	FCC	a_o = 9.96 ± 0.01
Rb_2TaCl_6	purple	>715	FCC	a_o = 10.11 ± 0.01
Rb_2TaBr_6	blue	>682	FCC	a_o = 10.62 ± 0.01

[a]Usually referred to as a body centered unit cell in the tetragonal system, a_o = 7.34 ± 0.01Å, c_o = 10.86 ± 0.01Å.

The similarity in the unit cell dimensions of corresponding hexahaloniobate(IV) and hexahalotantalate(IV) compounds can be seen from Table 2. Assuming that these complexes have the same structure, as will be discussed below, the covalent radii of Nb(IV) and Ta(IV) are then almost identical. This result is not unexpected in view of the lanthanide contraction experienced by elements in the third transition series.

In order to ascertain the exact ligand configuration around the niobium(IV) or tantalum(IV) ions in these complexes, a detailed structural analysis of K_2NbCl_6 was undertaken as described in the experimental section. The crystal lattice of K_2NbCl_6 was found to be isomorphous with K_2PtCl_6, space group Fm3m(O_h^5, No. 225), having four molecules per unit cell. The face centered cubic unit cell of the K_2NbCl_6 lattice is illustrated in Figure 11. The atoms in this unit cell are located at the following positions:

4Nb at $000,\frac{1}{2}\frac{1}{2}0,\frac{1}{2}0\frac{1}{2},0\frac{1}{2}\frac{1}{2}$,

8K at $\frac{1}{4}\frac{1}{4}\frac{1}{4}$,3/4 3/4 3/4,

24 Cl at $\pm$ X00,0X0,00X (X = 0.239 $\pm$ 0.008).

Observed intensity values and those calculated with atoms in the above positions are compared in Table 3. The agreement

Figure 11. Unit cell of the K_2NbCl_6 lattice

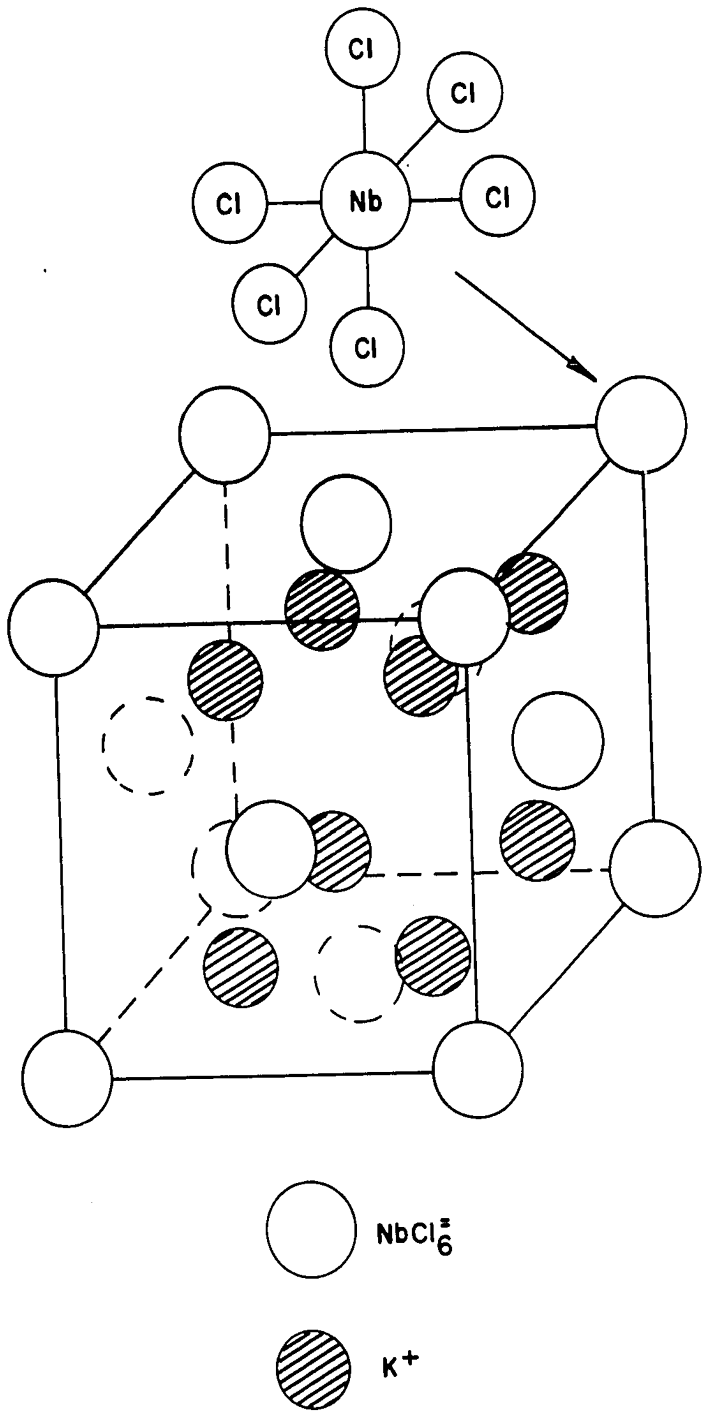
Cl
Cl
Cl
Nb
Cl
Cl
Cl
Cl
$NbCl_6^{=}$
K^+

Table 3. Observed and calculated intensity values for lines in the x-ray powder pattern of K_2NbCl_6

hkℓ	Observed integrated intensity[a]	Calculated integrated intensity
111	0.328	0.288
200	0.252	0.231
220	0.282	0.244
311	0.222	0.205
222	0.535	0.493
400	0.798	0.855
331	0.194	0.147
420	0.244	0.172
422	0.309	0.208
440	0.563	0.676
531	0.228	0.196
620	0.140	0.194
533	0.206	0.152
622	0.208	0.276
444	0.651	0.573
640	0.000	0.141
642	0.202	0.166

[a]Corrected for Lorentz-polarization and multiplicity effects.

between the calculated and observed intensities is expressed by the discrepancy factor in Equation 13.

$$R = \frac{\sum \left| (|F_o| - |F_c|) \right|}{\sum |F_o|} = 0.157 \qquad (13)$$

Where: R = discrepancy factor,

F_o = observed structure factor for a given reflection,

F_c = calculated structure factor for the same reflection.

The accuracy of this determination was limited by the errors involved in the visual estimation of integrated intensity values and by the failure to observe high-angle lines in the powder patterns.

Since all of the other alkali metal hexahalo complexes of niobium(IV) and tantalum(IV) have face centered unit cells approximately the same size as K_2NbCl_6, and their diffraction patterns show the same general variations in relative intensity for identical planes, they in all probability have the same structure.

From the cubic lattice parameter ($a_o = 9.97 \pm 0.01$ Å) for the unit cell of K_2NbCl_6 the following interatomic distances can be calculated:

$$\text{Nb-Cl} = 2.38 \pm 0.01 \text{ Å},$$
$$\text{Nb-K} = 4.32 \pm 0.01 \text{ Å},$$
$$\text{K-Cl} = 3.53 \pm 0.01 \text{ Å}.$$

Assuming a value of 0.99 Å for the covalent radius of chlorine (40), the octahedral radius of niobium in K_2NbCl_6 is computed to be 1.39 ± 0.01 Å. This covalent radius of Nb(IV) falls between values of 1.48 Å for Zr(IV) (41) and 1.32 Å for Mo(IV) (4). The trend in these values is in agreement with the expected contraction of the covalent radius with increasing atomic number for metal ions in the same oxidation state and period.

It is interesting to consider the stability of the various solid A_2MX_6 compounds as a function of the alkali metal cation in the lattice. Wells (20) has stated that the dominant factor influencing the stability of this type of compound is the size of the cation involved. Once the cation/anion radius ratio reached a critical value, anion-anion interactions (repulsions) are reduced sufficiently so that a more stable cubic close-packing of $MX_6^{=}$ anions results.

It is seen from Table 2 that K_2NbBr_6 has a distorted lattice (face centered tetragonal) and a lower melting point than the cubic Rb_2NbBr_6. The calculated radius ratio[1] (r_+/r_-) for the rubidium salt is 0.33 while that calculated for K_2NbBr_6 is 0.30. The minimum radius ratio for a tetrahedral packing of anions around a cation is 0.225. Also, in attempting to prepare stable A_2NbI_6 compounds it was found that the reaction between KI and NbI_4 did not yield a stable hexahalo complex whereas the Cs_2NbI_6 derivative forms quite

[1]In calculating radius ratios, r_+ is the ionic radius of the alkali metal cation (40); r_- is the sum of the covalent radius for Nb(IV), the covalent radius of the halide (40) and the Van der Waals radius of the halide (40).

readily. The calculated radius ratios[1] for K_2NbI_6 and Cs_2NbI_6 are, respectively, 0.27 and 0.34. These results are definitely in agreement with those predicted by Wells (20).

Absorption spectra

The absorption spectra of the niobium(IV) and tantalum(IV) hexahalo complexes were determined in the visible and ultraviolet regions as described in the experimental section. The experiments were initiated to study the spectral relationships between these isomorphous complexes as a function of the various ions in the lattice. The spectra of the alkali metal hexahaloniobate(IV) or hexahalotantalate(IV) complexes were only examined in the solid state (cf. Table 4 and Figures 12-14) since no solvent could be found which would dissolve the compounds without reaction. Solution spectra were also obtained for the $NbCl_6^{=}$ ion in molten pyHCl (cf. Table 4 and Figure 15).

As seen from Table 4 and Figures 12 and 13, the diffuse reflectance spectra of the A_2MX_6 (A = K, Rb; M = Nb, Ta; X =

---

[1]In calculating radius ratios, r_+ is the ionic radius of the alkali metal cation (40); r_- is the sum of the covalent radius for Nb(IV), the covalent radius of the halide (40) and the Van der Waals radius of the halide (40).

Table 4. Visible and ultraviolet absorption maxima of some hexahaloniobate(IV) and hexahalotantalate(IV) complexes

Compound[a]	Absorption maxima (λ_{max})[b], mμ						
	#1	#2	#3	#4	#5	#6	#7
K_2NbCl_6 (KCl)	---	*235(8)	265(9)	295(10)	*425(2)	545(6)	---
Rb_2NbCl_6 (RbCl)	---	*235(6)	265(9)	295(10)	*425(3)	535(5)	---
$NbCl_6^{=}$ (liq.pyHCl)	---	---	---	---	410(140)[c]	550(20)[c]	---
K_2NbBr_6 ($MgCO_3$)	*250(7)	*300(8)	*360(9)	410(10)	*520(1)	710(10)	---
Rb_2NbBr_6 (RbBr)	*250(7)	*305(8)	355(9)	405(10)	*530(1)	715(10)	---
Cs_2NbI_6 (CsI)	225(2)	*265(7)	315(8)	*425(1)	500(10)	665(10)	935(6)
K_2TaCl_6 ($MgCO_3$)	---	---	220(10)	250(10)	*375(1)	530(8)	---
Rb_2TaCl_6 (RbCl)	---	---	220(10)	250(10)	*400(3)	510(7)	---
Rb_2TaBr_6 (RbBr)	225(8)	275(10)	295(10)	340(10)	*460(1)	615(6)	---

[a]For diffuse reflectance measurements, the diluting agent and standard are given in parenthesis below the compound.

[b]Relative intensity values are given in parenthesis; these were estimated visually relative to a value of 10 for the most intense peak in a given spectrum. Peaks marked (*) appear as shoulders.

[c]ϵ_{max} values; $\epsilon_{\#5}$ is $\pm$ 25 $\ell mole^{-1}cm.^{-1}$, $\epsilon_{\#6}$ is $\pm$ 5 $\ell mole^{-1}cm.^{-1}$

Figure 12. Diffuse reflectance spectra of the rubidium hexachloroniobate(IV) and rubidium hexachlorotantalate(IV) complexes

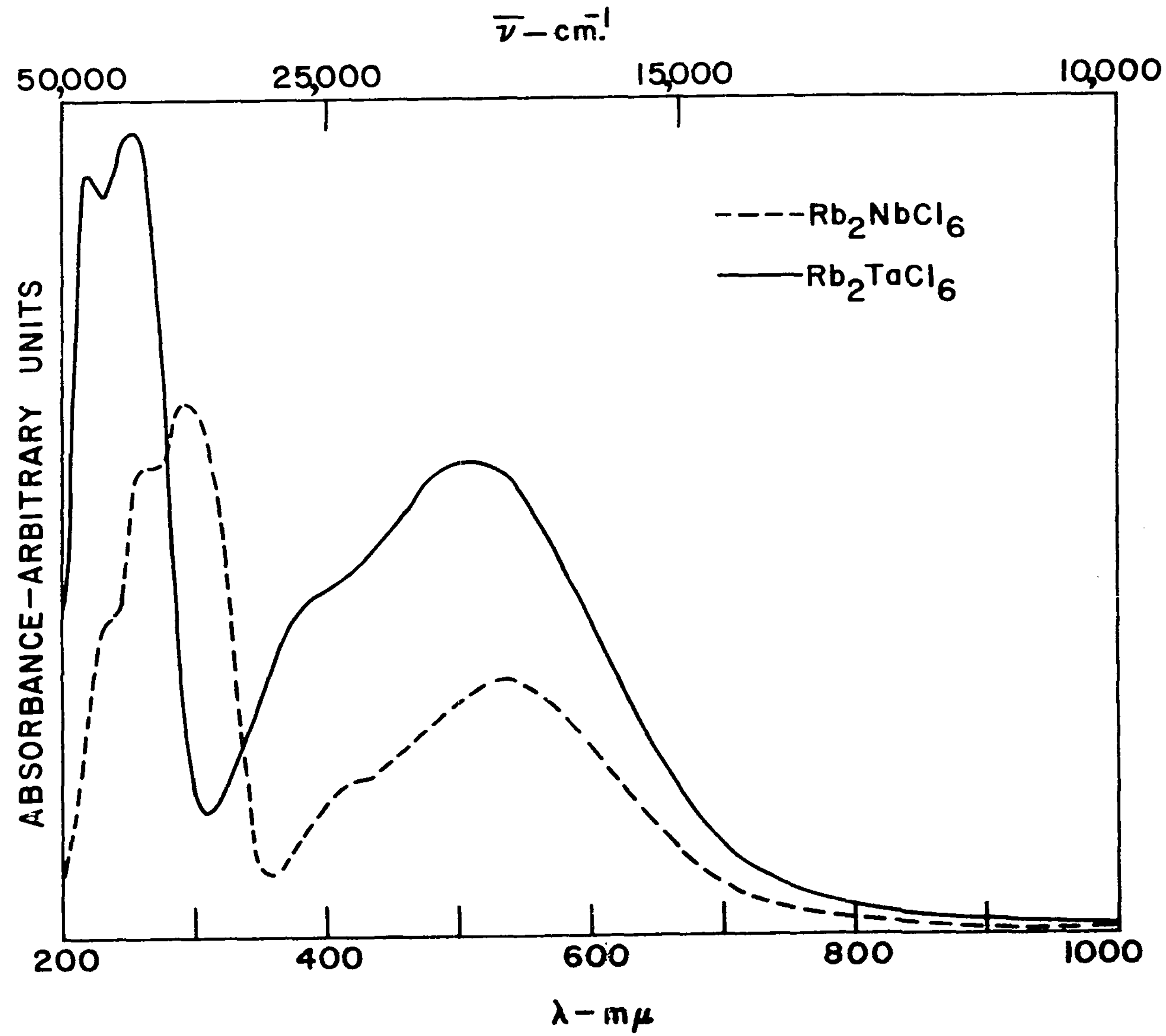

$\overline{\nu}$ — cm.$^{-1}$
50,000
25,000
15,000
10,000
----Rb_2NbCl_6
——Rb_2TaCl_6
ABSORBANCE—ARBITRARY UNITS
200
400
600
800
1000
λ — mμ

Figure 13. Diffuse reflectance spectra of the rubidium hexabromoniobate(IV) and rubidium hexabromotantalate(IV) complexes

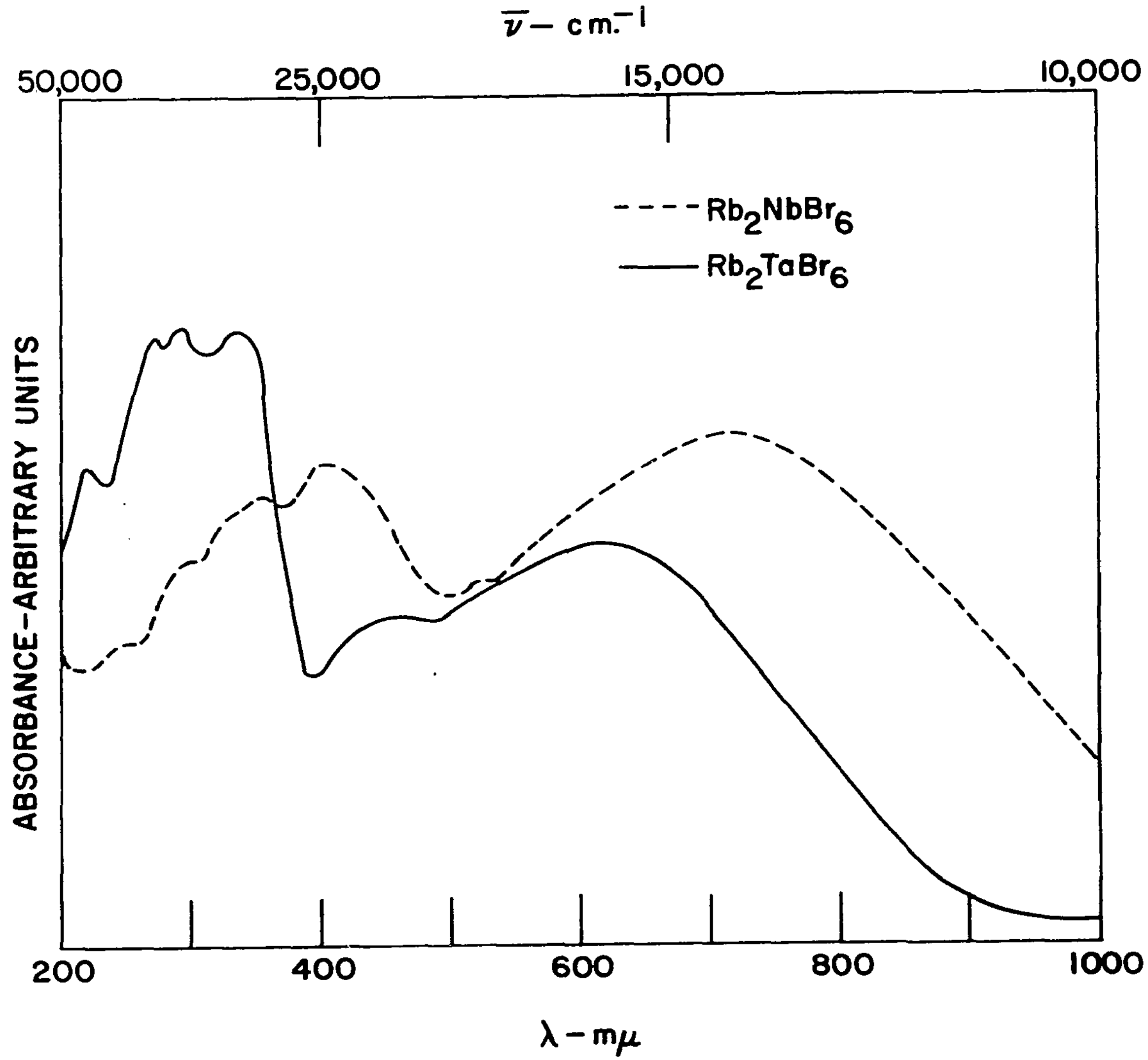
$\bar{\nu}$ – cm.$^{-1}$
50,000
25,000
15,000
10,000
- - - - Rb_2NbBr_6
—— Rb_2TaBr_6
ABSORBANCE-ARBITRARY UNITS
200
400
600
800
1000
λ – mμ

Figure 14. Diffuse reflectance spectrum of the cesium hexaiodoniobate(IV) complex

Figure 15. Absorption spectra of the hexachloroniobate(IV) ion in molten pyridinium chloride at 162.5°

(a) Spectrum obtained for a 7×10^{-3} molar solution

(b) Spectrum obtained for a 8×10^{-2} molar solution

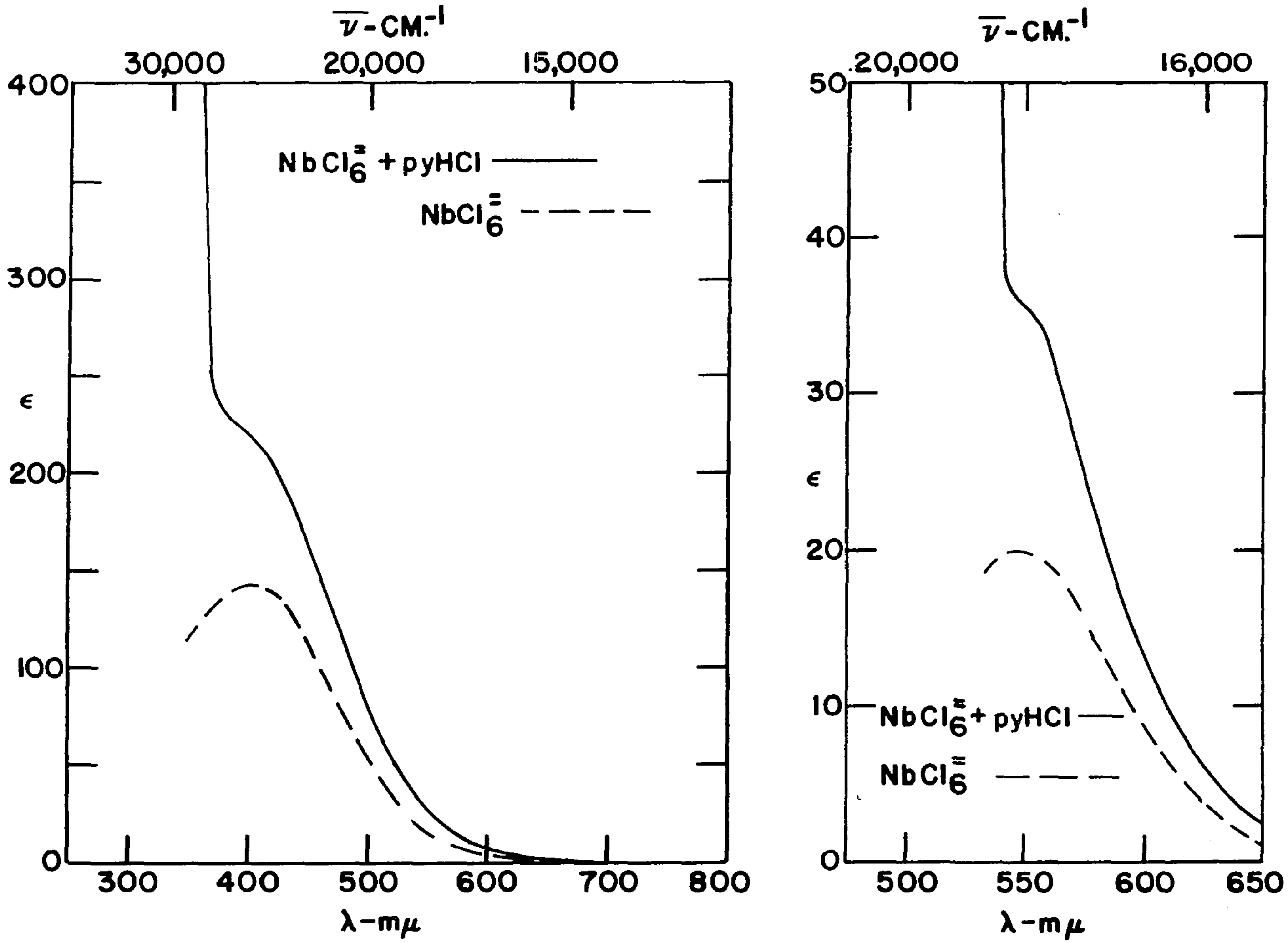

$\overline{\nu}$ - CM.$^{-1}$
30,000
20,000
15,000
400
300
200
100
0
ϵ
$NbCl_6^{=}$ + pyHCl
$NbCl_6^{=}$
300
400
500
600
700
800
λ - mμ
$\overline{\nu}$ - CM.$^{-1}$
20,000
16,000
50
40
30
20
10
0
ϵ
$NbCl_6^{=}$ + pyHCl
$NbCl_6^{=}$
500
550
600
650
λ - mμ

Cl, Br) complexes are very similar, containing two peaks (5, 6) at longer wavelengths and additional peaks (1-4) at higher energies (shorter wavelengths). The spectrum of Cs_2NbI_6 (Figure 14) contains broad absorption bands over the entire visible-ultraviolet region and will be discussed separately. It can be concluded from the data in Table 4 that the spectrum of a given $MX_6^{=}$ ion is not dependent on the alkali metal cation in the lattice. The spectra of A_2NbCl_6, A_2NbBr_6 or A_2TaCl_6 (A = K, Rb) complexes are all identical within experimental error.

There are several disadvantages to determining the absorption spectra of compounds by reflectance techniques: extensive broadening of the absorption bands occurs, making the exact assignment of band maxima difficult, and intensity data cannot be obtained since the concentrations of the mixtures are not known. However, these reflectance measurements permitted the resolution of low intensity peaks at long wavelengths. These peaks, arising from "Laporte-forbidden" d-d transitions ($\epsilon_{max} \sim 10\text{-}10^2$), are often covered by "Laporte-allowed" charge-transfer transitions ($\epsilon_{max} \sim 10^4$) in many transition metal complexes (42). During the course of this study it was found that the intensities of allowed transitions in the ultraviolet are decidedly lowered with respect to transitions in the visible region. This leveling effect is demonstrated by the spectrum of the $PtCl_6^{=}$ ion in the solid state and in solution, Table 5. The diffuse reflectance spectrum of this ion, as $(pyH)_2PtCl_6$, was determined to check the purity of the compound. The spectrum of $PtCl_6^{=}$ in solution has been measured by Jørgensen(43).

Table 5. Visible and ultraviolet absorption spectra of the hexachloroplatinate(IV) ion

Type of spectra	Peak 1 λ max (mμ)	Peak 2 λ max (mμ)	Peak 3 λ max (mμ)	$(A_2/A_1)^a$	$(A_3/A_1)^a$	$(A_3/A_2)^a$
Reflecance (in $(pyH)_2$-$PtCl_6$)	462	355	~280	3	5	2
Solution (in HCl)	453	353	262	10	400	40

[a]The ratio A_x/A_y refers to the ratio of the intensity of peak #x to peak #y in a given spectrum.

As seen from Table 5, the positions of the peaks for $PtCl_6^{=}$ from the reflectance measurement are in good agreement with those reported for this ion in solution. However, there is a rather striking difference between the relative intensities of the peaks in a given spectrum. The reflectance spectrum of $PtCl_6$ shows the intensity of peak 3 (a charge-transfer transition) to be only 5 times greater than peak 1 (a d-d transition). Actual measurements of the extinction coefficients of these peaks in solution shows peak 3 to be 400 times as intense as peak 1. This difference could be even more striking since the pyH^+ ion absorbs at 250-280 mμ and thus is contributing to the intensity of peak 3 in the reflectance measurement.

The solution spectrum of $NbCl_6^=$ in fused pyHCl was obtained to check the accuracy of the reflectance measurements and to provide extinction coefficient data. Unfortunately, due to the intense absorption of the pyridinium ion, only the visible region could be investigated. The two peaks found for $NbCl_6^=$ at 410 mμ(ϵ = 140) and 550 mμ(ϵ = 20) are in good agreement with the reflectance spectrum of this ion as K_2NbCl_6 or Rb_2NbCl_6. It should be noted that the leveling effect of the reflectance measurements actually causes the more intense peak at ~425 mμ to become a slight shoulder on the 550 mμ peak. Because of the leveling effect on the high energy (low wavelength) peaks, these transitions (peaks 2-4) in $NbCl_6^=$ most likely have extinction coefficients between 10^3 and 10^4. Since the spectra of the other $MX_6^=$ (M = Nb, Ta; X = Cl, Br) ions are similar to $NbCl_6^{=}$, the same conclusions can be drawn, i.e. peaks 1-4 have $\varepsilon \sim 10^3$-10^4 while peaks 5-6 have $\varepsilon \sim 10^1$-10^2.

There are four major theoretical approaches which can be used to discuss the structure, magnetic properties and spectra of transition metal compounds. These are valence bond theory, crystal field theory, ligand field theory and molecular orbital theory. In the following sections a short description of these theories will be presented and reasons will be given for choosing the molecular orbital theory to describe the spectra of the A_2MX_6 complexes. A qualitative discussion of M.O. theory as it applies to d^1 complexes with O_h symmetry will also be presented.

The valence bond approach advanced by Pauling (44) describes the bonding in octahedral complexes, for example, as arising through the donation of electron pairs from the ligands to the metal ion. In order to accept these six electron pairs, the metal ion must have available six equivalent σ-orbitals with their lobes directed toward the apices of an octahedron. Such a set of orbitals may be constructed out of s, p and d atomic orbitals by hybridization. While this theory, in its usual form, can explain many of the physical properties of transition metal complexes, it pays no attention to excited states and offers no explanation at all for their spectra. In addition, it offers no possibility of explaining magnetic behavior other than predicting, sometimes inaccurately, the number of unpaired electrons in a complex (45).

In the crystal field theory proposed by Bethe (46), only ionic or electrostatic interactions between a transition metal ion and its ligands are considered. Essentially the theory states that the five d-orbitals of a transition metal, which are degenerate in an isolated, gaseous atom, are split into orbitals of different energy by the electrostatic fields created by the ligands. For an ion with an unfilled d-shell, transitions can occur between these levels of different energy. Normally only ligands directly attached to the metal ion are important in determining the structure of the energy-level scheme of the ion. Thus the general features of the spectrum of a complex ion in solution are similar to those of the same ion in a crystal (47). The degree of splitting of the d-orbitals is calculated from the quantum mechanical perturbation theory. Since the unperturbed wave functions generally are not known exactly and since the true value of the perturbing electric field is not known, only qualitative calculations can be made.

Ligand field theory is a modified form of crystal field theory in which the computational advantages of the latter are largely preserved. This approach can be thought of as a fusion of M.O. and C.F. theory. In order to calculate an energy level diagram and/or details of magnetic behavior in ligand field theory one proceeds in the same manner as in crystal field theory but allowances are made for interelectronic interactions (orbital overlap). The electrons which are concerned with σ-bonding supply the perturbation potential and are then ignored. The symmetry of this potential determines the symmetry of the molecular orbitals which can be formed from the remaining ligand and metal ion orbitals (42, 45).

The molecular orbital theory starts with the assumption that overlap of orbitals will occur whenever symmetry permits. It includes the electrostatic crystal field theory as one extreme, maximal overlapping of orbitals as the other extreme, and intermediate degrees of overlap (ligand field theory) in its scope. M.O. theory is more complete and more flexible than C.F. or L.F. theory in that it considers the behavior of all the ligand and metal orbitals in a compound. This is a decided advantage when π-bonding must be considered to explain spectra and/or magnetic properties. M.O. theory provides a good conceptual picture of how the arrangement of energy levels in a complex is determined by chemical bonding. The disadvantage of M.O. theory relative to the simpler C.F. or L.F. theories is that it does not provide a practical method for obtaining numerical values of these energies (17).

Molecular orbital theory was chosen to aid in the discussion of the spectra of the $MX_6^{=}$ ions for several reasons. The complicated spectra that were observed for these ions could not be explained entirely on the basis of C.F. or L.F. theory. In addition, it was evident from the positions of the peaks in these spectra that π-bonding, caused by overlap of the filled p_π orbitals on the halide ions with vacant d_π orbitals on the metal ion, must be considered.

Other workers have also recently found that π-bonding must be considered in interpreting the properties of transition metal halide complexes. Nakamura _et al_. (48) have shown from NMR studies of the K_2MCl_6 (M = Pt, Ir, Os) complexes that the π character of the M-Cl bond increases from Pt(IV) to Os(IV). The amount of π-bonding was found to be a function of the number of electrons in the t_{2g} metal orbitals, which have the proper symmetry for π-bond formation. Since the niobium(IV) and tantalum(IV) ions have only one electron in the t_{2g} orbitals, π-bond formation in their halide complexes should be expected. Tyree and associates (25) have calculated that F→Ti π-bonding in $TiF_6^{=}$ complexes decreases the 10Dq value from 34,200 $cm.^{-1}$ to the observed value of 17,500 $cm.^{-1}$

The methods used to construct a molecular orbital scheme for d^1 ions with octahedral symmetry have been discussed by a number of workers (15, 17, 25, 45, 49). The M.O. diagram shown in Figure 16 is representative of these and will be used in subsequent discussions of the spectra and bonding in A_2MX_6 complexes. It should be emphasized that this diagram is not based on fundamental calculation and can be regarded as at best semi-empirical. The following features of the M.O. diagram should be noted: Of the nine valence shell atomic orbitals of the metal ion which are available for bonding, six have lobes lying along the metal ligand bond directions and are utilized in σ-bonding. These are the (d_{z^2}, $d_{x^2-y^2}$), (s) and (p_x, p_y, p_z) orbitals forming respectively the e_g, a_{1g} and t_{1u} bonding M.O.'s by overlap with

Figure 16. Molecular orbital diagram for the hexahalo-niobate(IV) and hexahalotantalate(IV) ions

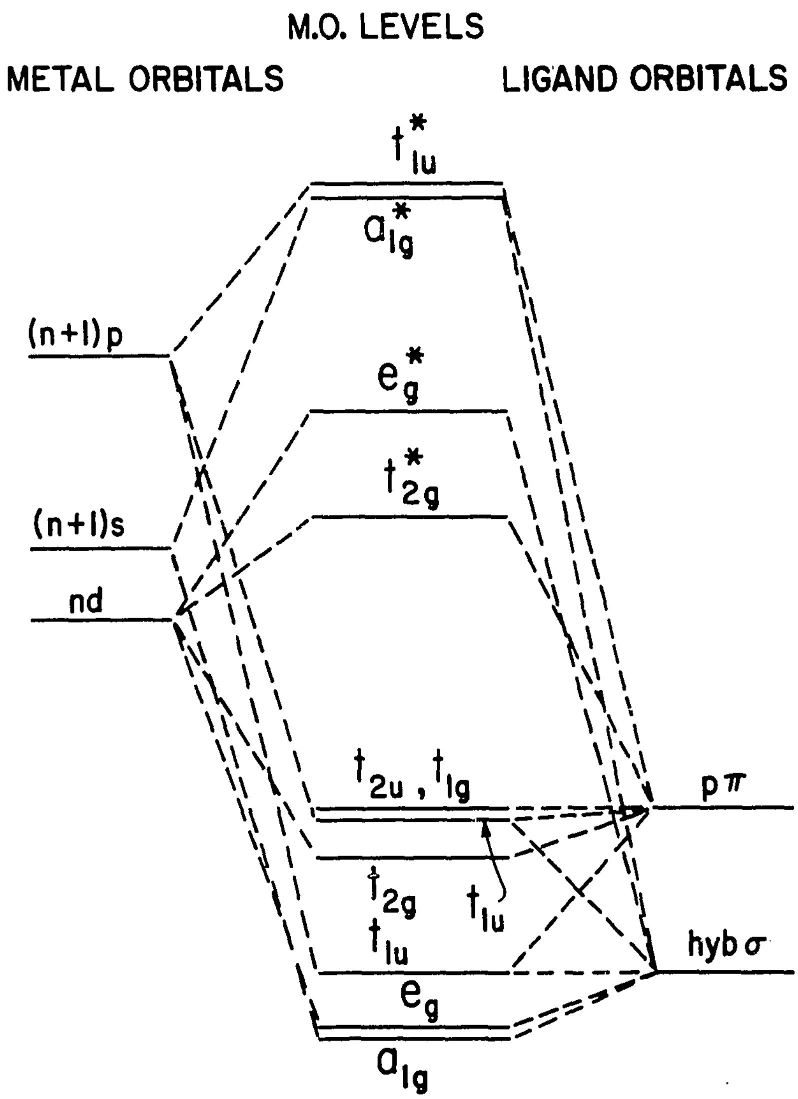
M.O. LEVELS
METAL ORBITALS
LIGAND ORBITALS
t_{1u}^*
a_{1g}^*
(n+1)p
e_g^*
t_{2g}^*
(n+1)s
nd
t_{2u} , t_{1g}
$p\pi$
t_{2g}
t_{1u}
t_{1u}
hyb σ
e_g
a_{1g}

halide hybrid σ-orbitals. The remaining d_{xy}, d_{xz} and d_{yz} metal orbitals have the proper symmetry (t_{2g}) to combine with suitable filled p_{π} orbitals on the halide ligands. The other nine ligand orbitals (t_{2u}, t_{1g}, t_{1u}) are regarded as essentially nonbonding. All of the bonding and nonbonding orbitals are filled in the $MX_6^{=}$ ions. In addition, there is a single electron in the t_{2g}^* orbitals. The halide → metal π-bonding in these complexes destabilizes the t_{2g}^* orbitals, which are regarded as nonbonding orbitals in C.F. theory, with respect to the e_g^* orbitals and thus diminishes the value of 10 Dq (the separation between these two levels).

There are two general types of electronic transitions which can take place in transition metal halide complexes. Charge-transfer spectra result from transitions in which an electron is removed from the ligand and transferred to the metal ion or, more correctly, transferred from a molecular orbital of predominantly ligand character to a molecular orbital which is largely concentrated on the metal. The relative positions of charge-transfer bands depend on the oxidizing power of the metal and the reducing power of the ligand. In this sense charge-transfer transitions are related to photochemical oxidation-reduction processes. As stated previously, these transitions are electronically allowed, with $\epsilon_{max} \sim 10^3\text{-}10^4$ (49). A second type of electronic transition involves transfer of an electron between orbitals of predominantly metal character. These d-d transitions are responsible for the usual colors associated with complex ions, since they often occur in the visible region of the spectrum. The intensities of bands occurring from d-d transitions are low ($\epsilon_{max} \sim 10^1\text{-}10^2$) (49).

From the above discussion, the spectra of the $MX_6^{=}$ ions would be expected to have a single low intensity peak corresponding to the d-d transition $^2T_{2g} \rightarrow {}^2E_g$ between the t_{2g}^* and e_g^* orbitals. In the complexes A_2MCl_6 and A_2MBr_6 there are in fact two low intensity peaks which can be distinguished at longer wavelengths. This type of spectrum has been found for other octahedral d^1 complexes (3, 25) and has been justified theoretically (42, 45). The two peaks result from a Jahn-Teller distortion of the excited ^2E_g state. The mean of the two transitions is then the 10 Dq value for the complex.

Therefore, the two low intensity peaks, 5 and 6, for the A_2MCl_6 and A_2MBr_6 complexes are assigned to the $^2T_{2g} \rightarrow {}^2E_g$ transition, the splitting being caused by the Jahn-Teller distortion. 10 Dq values and the magnitudes of the ^2E_g distortion for these complexes are given in Table 6. These values are only approximate since the reflectance spectra were quite broad and peak 5 appeared as a shoulder. The spectrum of $TiF_6^{=}$ is also included in Table 6 as a comparison (25).

Table 6. Spectral data derived from the $^2T_{2g} \rightarrow {}^2E_g$ transitions in the alkali metal hexahaloniobate(IV) and hexahalotantalate(IV) complexes

Complex	Position of absorption maxima[a] ($cm.^{-1}$) #5	#6	Mean 10 Dq for $^2T_{2g} \rightarrow {}^2E_g$ ($cm.^{-1}$)	Magnitude of ^2E_g splitting ($cm.^{-1}$)
A_2NbCl_6	23,500	18,700	21,100	4,800
$NbCl_6^{=}$ in liq. pyHCl	24,400	18,200	21,300	6,200
A_2NbBr_6	18,900	14,000	16,450	4,900
A_2TaCl_6	25,000	19,600	22,300	5,400
A_2TaBr_6	21,700	16,300	19,000	5,400
$TiF_6^{=}$	19,010	15,110	17,060	3,900

[a]Calculated from λ_{max} data given in Table 4.

It can be seen from Table 6 that both the niobium(IV) and tantalum(IV) hexahalo complexes agree with the expected trends in ligand field strength as predicted by the spectrochemical series Cl > Br > I (42, p. 266). For a given metal ion, the chloride complex has a greater 10 Dq value than the bromide complex. As Dunn (42) has indicated, this difference of ca. 4000 cm^{-1} in 10 Dq is really a compromise between the difference in σ-bond and π-bond strength, the former being the stronger interaction in this case.

The variation in 10 Dq with metal ion is also consistent with that expected for isoelectronic $4d^1$ and $5d^1$ ions, Ta(IV) > Nb(IV) (49, p. 45).

The magnitude of the Jahn-Teller distortion of the ^2E_g excited state cannot be readily explained. This distortion in the niobium and tantalum complexes is ca. 1000 cm^{-1} larger than splittings found in similar compounds (3, 25). It is doubtful that a crystallographic distortion, postulated by Tyree, et al. (25) in the $(NH_4)_3TiF_6$ complex, is responsible for this difference since the x-ray study of K_2NbCl_6 showed that the Nb(IV) ion occupies a lattice site of O_h symmetry.

Because of their high intensity ($\epsilon \sim 10^3$-10^4), peaks 1-4 in Table 4 for the A_2MCl_6 and A_2MBr_6 complexes are assigned to charge-transfer transitions. Due to the nature of the halide ligands and the high charge on the metal ions, the electron transfer most likely takes place from the nonbonding or filled π-orbitals (t_{1u}, t_{1g}, t_{2u}) localized mainly on the ligands to the predominantly metal t_{2g}^{*} orbitals. In the bromide complexes, the transition from these nonbonding orbitals on the ligand to the e_{g}^{*} orbitals could also occur above 200 mμ since peak 1 is ca. 16,000 $cm.^{-1}$ lower than peak 4. This added transition would account for the extra peak in their spectra.

The relative positions of the charge-transfer peaks are in agreement with the expected trends (49, p. 99). For a given halide complex, the $NbX_6^{=}$ charge-transfer transitions occur at higher wave lengths (lower energies) than $TaX_6^{=}$, in accord with the greater stability of the higher oxidation states of tantalum. In the spectra of both the A_2NbX_6 and A_2TaX_6 (X = Cl, Br) complexes, the charge-transfer peaks shift toward higher wavelengths when the chloride ligand is replaced by bromide. This is to be expected since the bromide ion is more easily oxidized than chloride.

The nature of the peaks in the absorption spectra of the Cs_2NbI_6 complex cannot be determined with any certainty. Due to the broadness and number of peaks in the reflectance spectrum of this complex, extinction coefficients cannot be estimated for any of the absorption maxima. If peaks 6 and 7 are assigned to the $^2T_{2g} \rightarrow {}^2E_g$ transition, 10 Dq equals 11,600

cm^{-1} and the splitting of the excited state is calculated to be 3,800 cm^{-1}. These values are not out of line with the chloride and bromide complexes. The data in Table 6 indicate that 10 Dq decreases from 21,100 cm^{-1} for A_2NbCl_6 to 16,450 cm^{-1} for A_2NbBr_6. However, there is also a distinct possibility that the peaks are due to charge-transfer transitions. Since iodide is the most oxidizable of the halide ligands, this type of transition for the $NbI_6^{=}$ ion could extend into the visible region.

Magnetic susceptibility studies

The alkali metal hexahaloniobate(IV) and hexahalotantalate(IV) complexes were found to be paramagnetic, as expected, with magnetic moments (μ) much lower than the spin-only value. Plots of the magnetic susceptibilities of the A_2NbX_6 complexes with reciprocal temperature were nonlinear, Figure 17, while within experimental error linear plots were obtained for the A_2TaX_6 complexes, Figure 18. Before attempting to discuss the origin and differences in the magnetic behavior of these compounds, a summary of pertinent magnetic theory will be presented.

The magnetic moment of a paramagnetic compound can be related to its magnetic susceptibility by the Van Vleck

Figure 17. Variation of the molar magnetic susceptibilities of some alkali metal hexahaloniobate(IV) complexes with reciprocal temperature

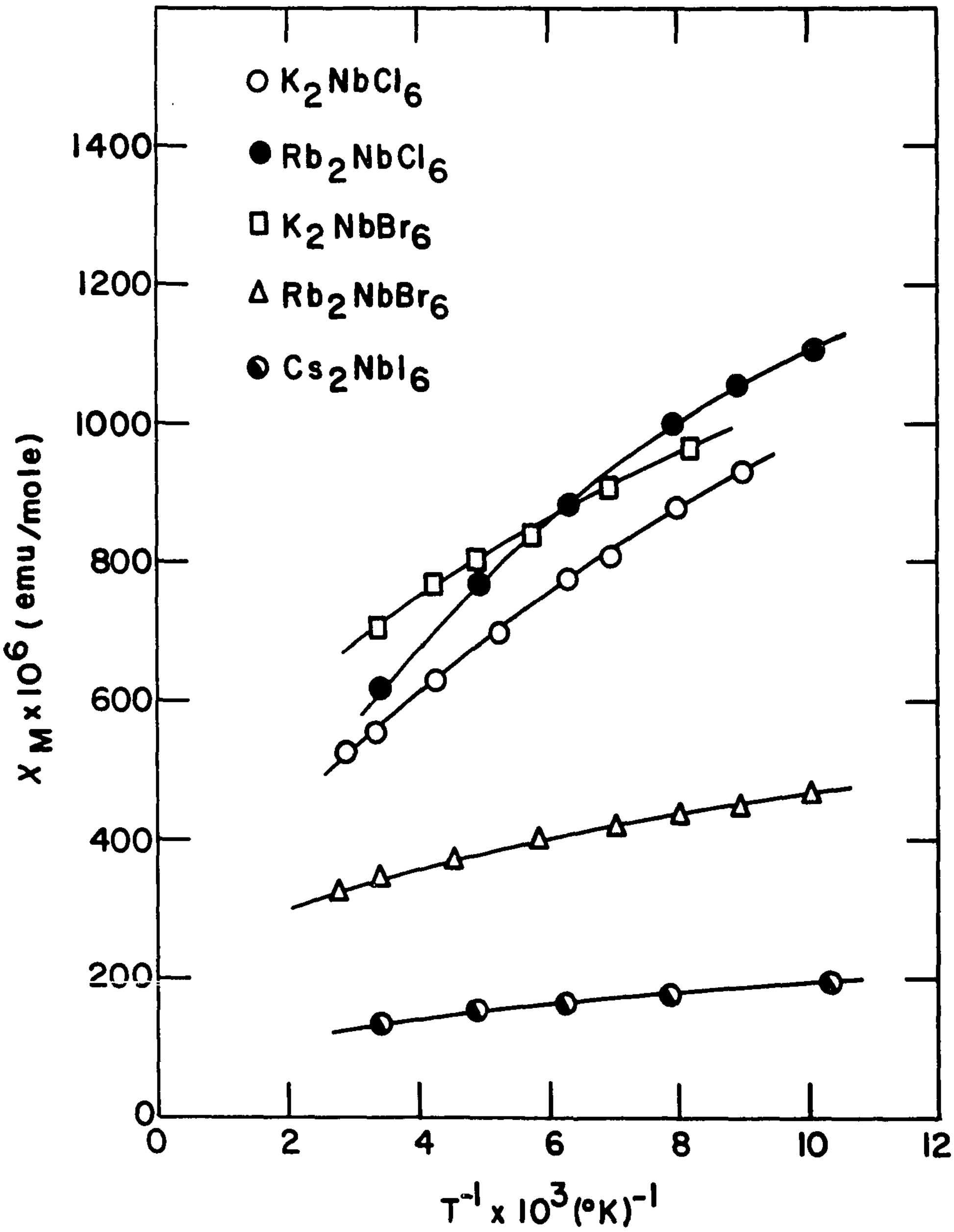

○ K_2NbCl_6
● Rb_2NbCl_6
□ K_2NbBr_6
△ Rb_2NbBr_6
◐ Cs_2NbI_6
$\chi_M \times 10^6$ (emu/mole)
1400
1200
1000
800
600
400
200
0
0
2
4
6
8
10
12
$T^{-1} \times 10^3 (°K)^{-1}$

Figure 18. Variation of the molar magnetic susceptibilities of some rubidium hexahalotantalate(IV) complexes with reciprocal temperature

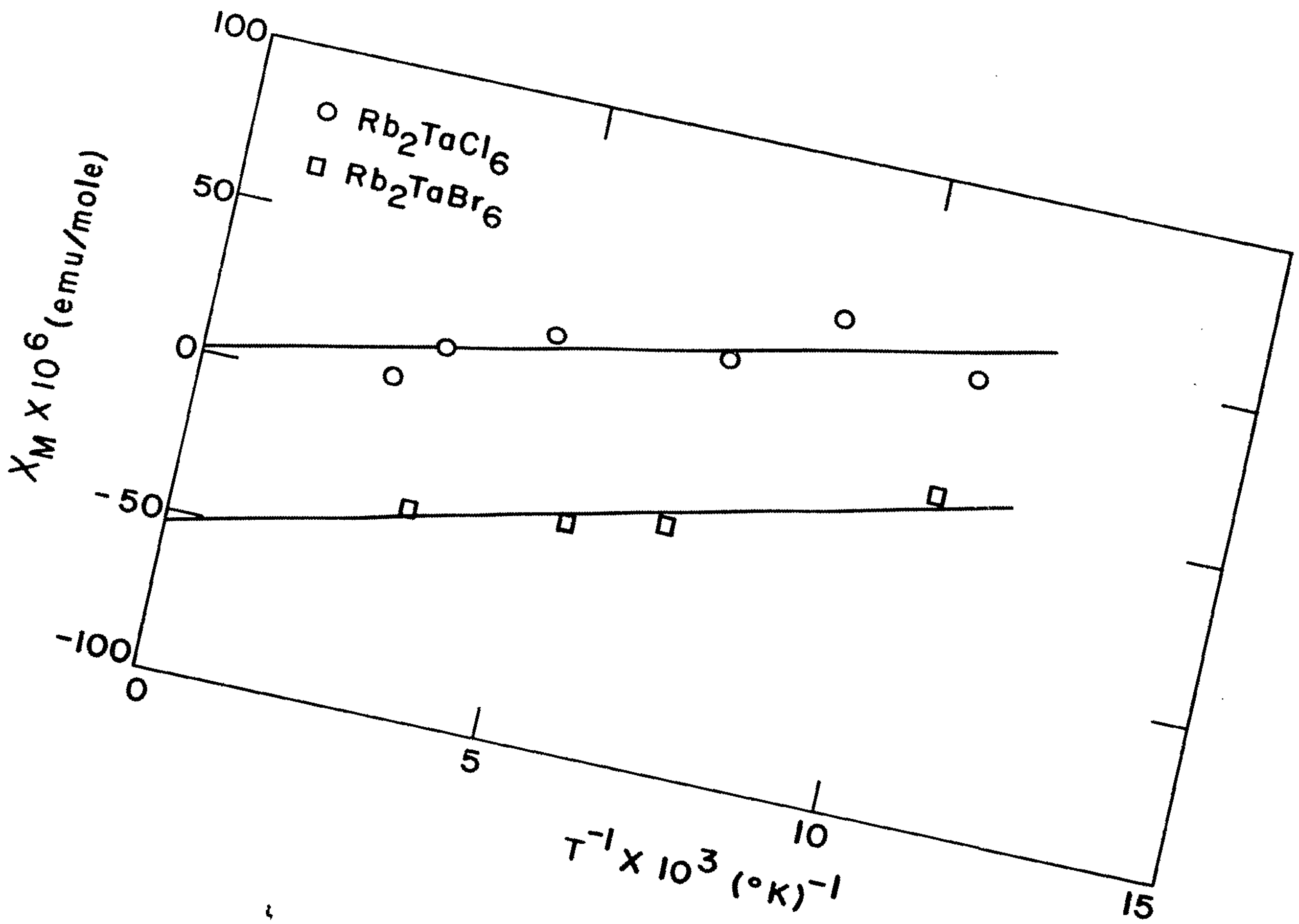

$\chi_M \times 10^6$ (emu/mole)
100
50
0
-50
-100
0
5
10
15
$T^{-1} \times 10^3$ (°K)$^{-1}$
○ Rb_2TaCl_6
□ Rb_2TaBr_6

expression, Equation 14 (41, p. 135).

$$\chi_M = N\beta^2\mu^2/3kT + N\alpha' \qquad (14)$$

where: χ_M = molar magnetic susceptibility, emu/mole,

N = Avogadro number,

β = magnitude of the Bohr magneton; erg gauss^{-1},

μ = paramagnetic moment, Bohr magnetons,

k = Boltzman constant,

T = absolute temperature,

α' = temperature independent contribution to the total susceptibility due to the diamagnetism of the paired electrons and Van Vleck paramagnetism.

Experimentally, a paramagnetic compound whose susceptibility varies linearly with reciprocal temperature is said to obey the Curie law. The magnetic moment of such a compound is obtained from the slope of a plot of χ_M versus $1/T$ by the application of Equation 14. The magnetic susceptibility of a great many paramagnetics deviates from the requirements of the Curie law in a way which may be described by a simple modification of this law, the Curie-Weiss law given in Equation 15.

$$\chi_M = C/T\text{-}\theta \qquad (15)$$

Where: χ_M = molar magnetic susceptibility,

C = Curie constant,

T = absolute temperature,

θ = constant.

Under some circumstances the origin and value of θ can be accounted for in terms of exchange interactions which tend to order the spins on neighboring paramagnetic ions, e.g. antiferromagnetism. However, for the majority of paramagnetic substances which exhibit Curie-Weiss behavior no particular significance can be attached to θ. θ is then an empirical quantity and is simply a measure of how far the origin of the paramagnetism in the system departs from the ideal basis on which a Curie law is derived (50).

For compounds whose plots of χ_M versus 1/T show curvature, but the deviation from linearity cannot be ascribed to a lattice interaction, the effective magnetic moment (μ_{eff}) can be calculated at a particular temperature by the application of Equation 16 (50).

$$\mu_{eff} = K[\chi_M^{corr.} \cdot T]^{\frac{1}{2}} \tag{16}$$

Where: μ_{eff} = effective magnetic moment, B.M.,

$\chi_M^{corr.}$ = molar magnetic susceptibility corrected for diamagnetism but not for temperature independent paramagnetism,

T = absolute temperature,

K = $[3k/N\beta^2]^{\frac{1}{2}}$, where these quantities have their usual significance.

The magnetic properties of the alkali metal hexahaloniobate(IV) or hexahalotantalate(IV) complexes and transition metal compounds in general are best described by ligand field theory since the magnetic behavior of these complexes arises primarily from the electrons in the d-shell of the transition metal ion. The energy level diagram for a single d-electron in an octahedral field as presented by Ballhausen (15, p. 119) and Dunn (42, p. 261) is given in Figure 19. From this diagram it can be seen that the degeneracy of the t_{2g} ground level in an octahedral ligand field is removed by spin-orbit coupling.

The spin-orbit coupling constant (ξ_{nl}) indicates the 'tightness' of coupling of the spin and orbital angular momenta vectors which give rise to paramagnetism. This constant may be regarded as a measure of the mean energy separation between successive possible values of the total angular momentum of the ground state. The strength of this coupling depends upon the intensity of the electric field which the

Figure 19. Energy level diagram for a d^1 ion in an octahedral field

(a) Field-free ion term energy
(b) Levels in a strong octahedral field
(c) Strong octahedral field + weak spin-orbit coupling
(d) Strong octahedral field + medium spin-orbit coupling

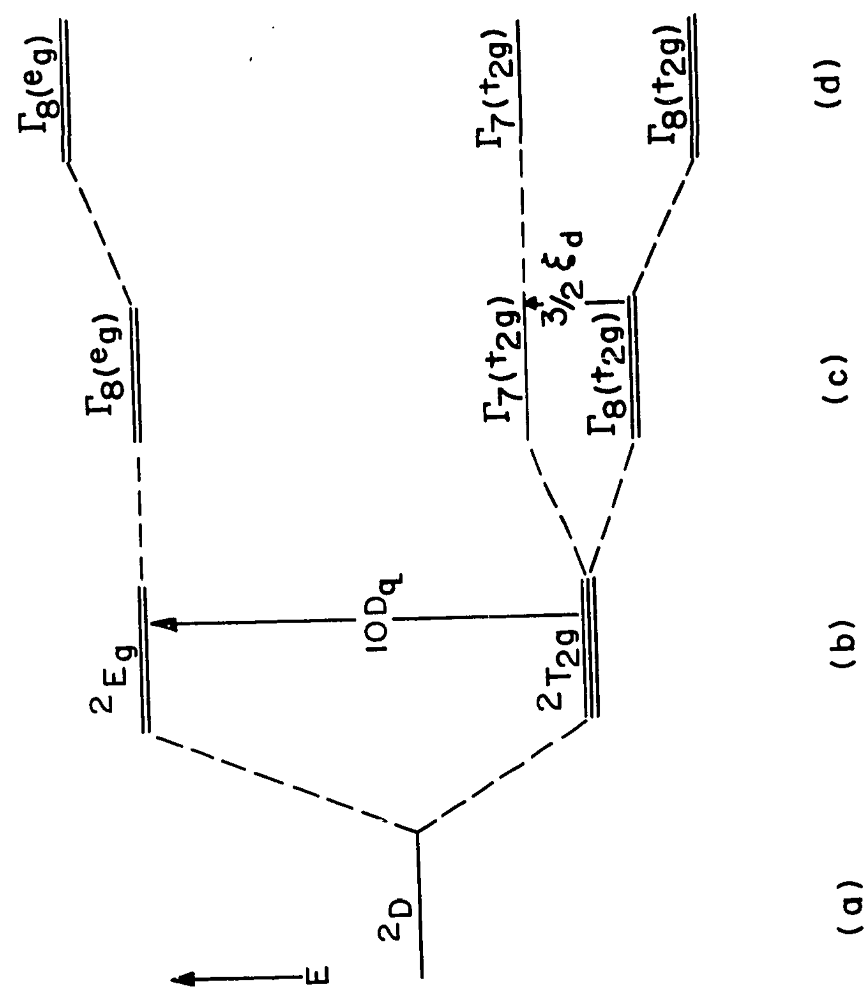

$\Gamma_8(e_g)$
$\Gamma_7(t_{2g})$
$\Gamma_8(t_{2g})$
(d)
$\Gamma_8(e_g)$
$\Gamma_7(t_{2g})$
$3/2\ \xi_d$
$\Gamma_8(t_{2g})$
(c)
^2E_g
$10D_q$
$^2T_{2g}$
(b)
^2D
(a)
E

electron experiences. This field increases in intensity as it approaches the nucleus. Thus the spin-orbit coupling constant increases with the charge Z on the nucleus and the extent to which the electron approaches the nucleus.

It is this spin-orbit coupling effect which causes the unusual magnetic behavior of $4d^1$ and $5d^1$ transition metal ions. The ground $\Gamma_{8(t_{2g})}$ state which results from the spin-orbit splitting of the t_{2g} level is nonmagnetic since the spin part and orbital part of the magnetism cancel each other. An electron residing in this state will have essentially no magnetic moment. Even in this case there will be a temperature independent paramagnetic contribution to the susceptibility arising from a quantum mechanical 'mixing' of higher states ($\Gamma_{7(t_{2g})}$, $\Gamma_{8(e_g)}$) with the ground state. At higher temperatures, when $\zeta_{nl} \approxeq kT$, population of the magnetic $\Gamma_{7(t_{2g})}$ state causes an increase in the magnetic moment (50).

Kotani (24) has applied ligand field theory to transition metal complexes and has deduced the variation in the effective magnetic moment with temperature and spin-orbit interaction for various d^n configurations. His theory predicts that in the case of a d^1 configuration, the moment will be markedly dependent on these variables. In deriving this relationship, Equation 17, Kotani assumed a perfect cubic field and no magnetic interaction between neighboring paramagnetic ions.

$$\mu^2_{eff} = \frac{8 + (3x - 8)e^{-3x/2}}{x(2 + e^{-3x/2})} \qquad (17)$$

Where: μ_{eff} = effective magnetic moment, in B.M., calculated from Equation 16,

X = ζ_{nd}/kT, where these quantities have their usual significance.

Kamimura, et al. (51) have shown that the Kotani theory does not hold explicitly for all $4d^n$ and $5d^n$ configurations since the coulomb repulsion effects (for $n > 1$) are often smaller than spin-orbit coupling effects. However, these authors state that for the nd^1 configuration, which has no coulombic repulsion, the Kotani theory should hold for even very large values of the spin-orbit coupling constant.

The energy level scheme in Figure 19c approximates that of a $4d^1$ transition metal ion in a strong octahedral ligand field where $\zeta_{4d} \approx kT << Dq$ at room temperature. Under these conditions the Kotani theory predicts that μ_{eff} should be strongly temperature dependent since the $\Gamma_7(t_{2g})$ state can be thermally populated. The energy level scheme for $5d^1$ ions is approximated by Figure 19d where now $\zeta_{5d} \approx Dq >> kT$.

Only the lowest level of the system, the $\Gamma_8(t_{2g})$ state, is occupied at available temperatures. Paramagnetism arises from the second-order Zeeman effect between this state and the $\Gamma_7(t_{2g})$ state and is of the temperature independent type. Under these conditions the Kotani theory predicts that μ_{eff} should be close to zero and should vary as $(T)^{\frac{1}{2}}$ (15, p. 144).

Moffitt, et al. (52) and Liehr (53) have used a different approach in deriving the magnetic susceptibility relationships for the $\xi_{5d} \cong Dq \gg kT$ case from quantum mechanical considerations. Mixing of the two Γ_8 states under spin-orbit coupling is now assumed to be the primary cause of the paramagnetism, with the $\Gamma_8(t_{2g})$ - $\Gamma_7(t_{2g})$ interactions yielding the high-frequency temperature independent term. They obtained the relationship given in Equation 18.

$$\chi_M^{corr.} = \frac{N\beta^2}{3kT}\left[\tfrac{1}{4}(1+\cos 2\varphi)(19-13\cos 2\varphi - 4\sqrt{6}\sin 2\varphi) + 3kT\alpha\right] \tag{18}$$

Where: $\tan 2\varphi = \dfrac{-\sqrt{6}\ \xi_{5d}}{10\ Dq + \frac{1}{2}\xi_{5d}}$,

α = temperature independent paramagnetism; all the other quantities have their usual significance.

As illustrated in Figure 17, plots of χ_M versus 1/T for the alkali metal hexahaloniobate(IV) complexes were nonlinear. A satisfactory value of θ could not be found for these compounds which would 'straighten out' the above curves. Plots of $1/\chi_M^{corr.}$ versus T have been used by Hargreaves and Peacock (13) to determine θ values for a series of $AMoF_6$ complexes. From Equation 19, a modification of Equation 16, it can be concluded that this type of treatment will only yield a constant slope when the magnetic moment (μ_{eff}) is constant.

$$1/\chi_M^{corr.} = \frac{KT}{\mu_{eff}^2} - \frac{K\theta}{\mu_{eff}^2} \qquad (19)$$

When plots of $1/\chi_M^{corr.}$ versus T were constructed for the A_2NbX_6 complexes nonlinear curves were always obtained. Therefore it is concluded that the magnetic moments of these compounds are varying with temperature as predicted by Kotani. However, it is not possible to rule out exchange interactions by the above treatment.

A number of workers (11, 13, 14) have postulated that antiferromagnetism is responsible for some of the magnetic properties of similar molybdenum and tungsten hexahalo complexes. Néel points above 100^oK were found by Hargreaves and Peacock (13) for AWF_6 (A = Na, K, Rb, Cs) complexes. This type of lattice interaction has been studied in detail by Westland and Bhiwandker (54) for K_2MCl_6 (M = Re, Os, Ir) complexes and by Busey and Sonder (55) for K_2ReCl_6 and

and K_2ReBr_6 complexes. Both groups have shown that magnetic superexchange causes a lowering of the effective magnetic moments of these compounds. This superexchange operates through d_π-p_π bonding orbitals which encompass the metal atom and its ligands and p_π-p_π overlap between ligands of the neighboring complex ions. The above compounds are isomorphous with A_2NbX_6 and A_2TaX_6.

The variation in μ_{eff} with T for the A_2NbX_6 complexes is compared with that predicted by Kotani in Figure 20. The experimental and theoretical effective magnetic moments were calculated from Equations 16 and 17 respectively. Complete tables of magnetic data for all the niobium and tantalum compounds are given in the Appendix.

Reference to Figure 20 shows that for all of the complexes the experimental results are in good agreement with the theory for spin-orbit coupling constants in the range 650-300 $cm.^{-1}$. Dunn (16) has assigned a value of 750 $cm.^{-1}$ for the niobium(IV) free ion spin-orbit coupling constant but Owen (56) has indicated that this constant can be considerably lower in the solid state due to the electron delocalization onto the ligands. The absorption spectra of the A_2NbX_6 complexes have indicated that considerable π-bonding takes

Figure 20. Variation of the effective magnetic moments of some alkali metal hexahaloniobate(IV) complexes with temperature

(a) Solid lines are curves calculated from experimental data

(b) Broken lines are theoretical curves calculated on the basis of those values of ξ as marked thereon

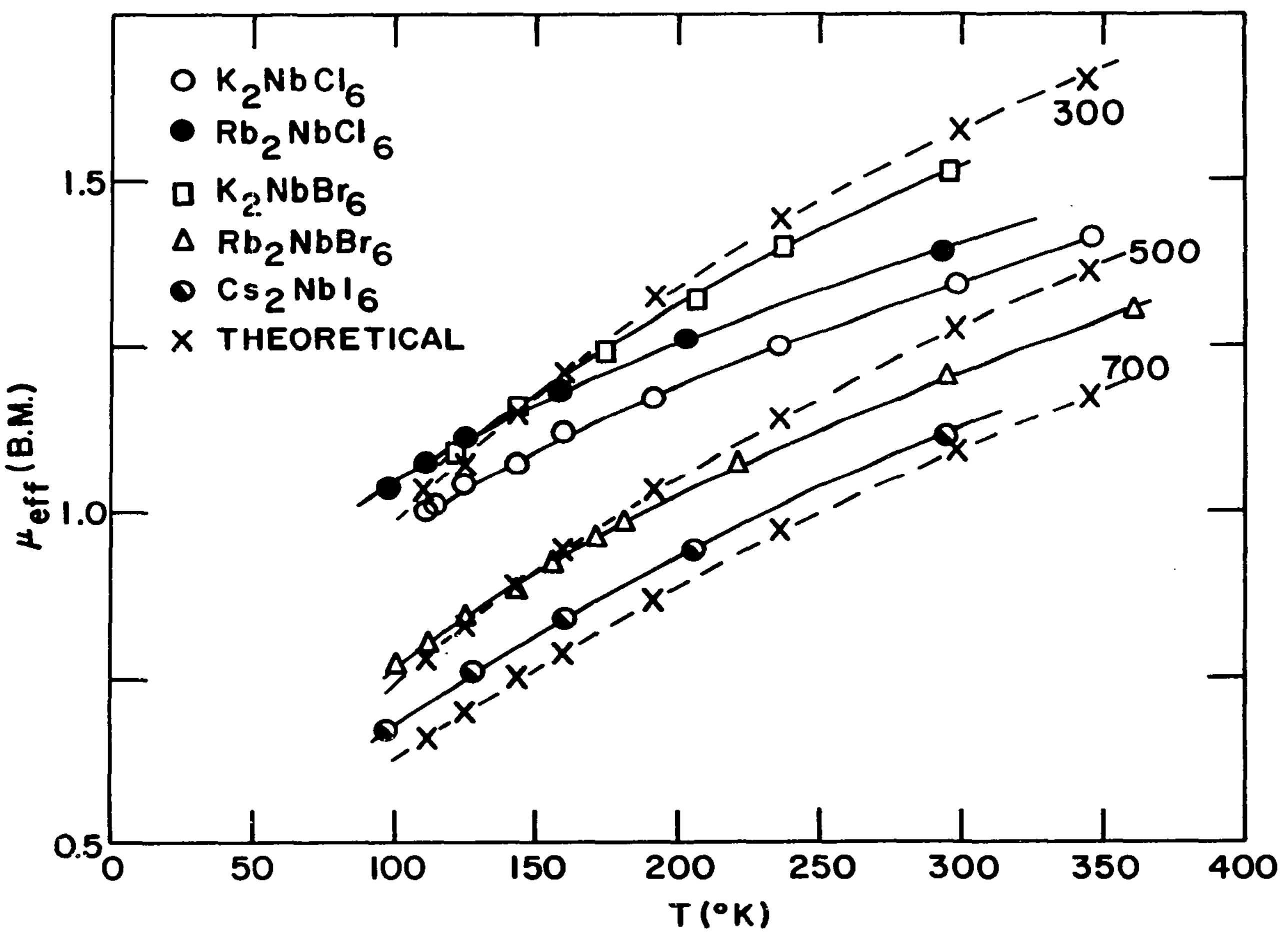

K2NbCl6
Rb2NbCl6
K2NbBr6
Rb2NbBr6
Cs2NbI6
THEORETICAL
300
500
700
μeff (B.M.)
1.5
1.0
0.5
0
50
100
150
200
250
300
350
400
T (°K)

place in these compounds; therefore $\xi_{Nb(IV)}$ values below $750\ cm^{-1}$ are to be expected.

It can be seen from Figure 20 that the effective moments for the A_2NbCl_6 and A_2NbBr_6 (A = K, Rb) complexes at a given temperature are markedly dependent on the cation in the lattice. The tetragonal K_2NbBr_6 complex has a moment proportionately higher than the cubic Rb_2NbBr_6 complex, while there is little difference between the slopes of their respective curves. These observations are consistent with those expected if antiferromagnetic interactions exist in the solid compounds. Figgis and Lewis (50, p. 440) have shown that such interactions, when of low magnitude, can lead to a constant lowering of the susceptibility and μ_{eff} below that predicted for paramagnetism. The tetragonal K_2NbBr_6 lattice would not be expected to cause much change in the moment if the distortion of the cubic unit cell results in little distortion of the octahedral symmetry at the metal ion. However, the tetragonal lattice could appreciably reduce the degree of antiferromagnetic interaction between neighboring $NbBr_6^{=}$ ions and increase the observed susceptibility. Of the two alkali metal hexachloroniobate(IV) complexes studied, the Rb_2NbCl_6 compound has a slightly higher moment at all temperatures.

Again, this behavior is consistent with an antiferromagnetic lattice interaction. The $NbCl_6^{=}$ ions are farther apart in the rubidium compound than in the potassium derivative; this should result in a decreased exchange interaction and a higher susceptibility, as observed. The antiferromagnetic interaction in these compounds is very likely the result of superexchange since the Nb-Nb distance (7.4 Å in K_2NbCl_6) is too large for any appreciable direct metal-metal overlap to occur.

Because of the nonlinearity of their χ_M versus 1/T plots, true magnetic moments (μ) and the temperature independent contributions ($N\alpha$) to the susceptibility of the A_2NbX_6 complexes could not be calculated. Table 7 lists the effective magnetic moments for the compounds at several temperatures and their approximate spin-orbit coupling constants obtained from Kotani's theory. These $\zeta_{Nb(IV)}$ values are not corrected for the effect of the antiferromagnetic interactions but were estimated from Figure 20.

It can be seen from Table 7 and Figure 20 that the spin-orbit coupling constants of the cubic hexahalo complexes decrease in the order $Cs_2NbI_6 > Rb_2NbBr_6 > Rb_2NbCl_6$. This comparison is made for the compounds containing the largest alkali metal ions in order to minimize the effects arising from exchange interactions. Because the 'magnetic' electron resides in the t_{2g}^* orbitals, the reduction of $\xi_{Nb(IV)}$ from the free ion value must result from delocalization of the electron onto the ligands via π-bonding. Hence in order to account for the above order of decrease of $\xi_{Nb(IV)}$ in these compounds the extent of π-bonding goes as $NbCl_6^{=} > NbBr_6^{=} > NbI_6^{=}$.

Table 7. Magnetic data for some alkali metal hexahaloniobate(IV) complexes

Compound	$\sim\xi_{Nb(IV)}{}^a$ (cm^{-1})	$\mu_{eff}{}^a$ (Bohr magnetons) 300°K	150°K
K_2NbCl_6	400	1.35	1.09
Rb_2NbCl_6	350	1.40	1.16
K_2NbBr_6	300	1.52	1.18
Rb_2NbBr_6	500	1.21	0.90
Cs_2NbI_6	650	1.13	0.81

[a]Estimated from Figure 20.

The rubidium hexahalotantalate(IV) complexes, Rb_2TaCl_6 and Rb_2TaBr_6, were found to have rather unusual magnetic properties. Plots of the experimental χ_M versus 1/T data were linear, with some susceptibility values actually being negative (Figure 18). Table 8 lists the true magnetic moments and temperature independent paramagnetic (TIP)

Table 8. Magnetic data for the Rb_2TaCl_6 and Rb_2TaBr_6 complexes

Magnetic property	Compound Rb_2TaCl_6	Rb_2TaBr_6
True magnetic moment[a] (μ)	0.19 ± 0.05 B.M.	0.20 ± 0.02 B.M.
Experimental TIP susceptibility[a] ($N\alpha$)	$212 \pm 20 \times 10^{-6}$ emu/mole	$216 \pm 10 \times 10^{-6}$ emu/mole
μ_{eff}[b] at 300°K	0.74 B.M.	0.75 B.M.
μ_{eff}[b] at 150°K	0.54 B.M.	0.55 B.M.
$\zeta_{Ta(IV)}$ from the Kotani theory[b]	~1,500 cm^{-1}	~1,500 cm^{-1}
μ calculated from Eq. 18[c]	0.31 B.M.	0.36 B.M.
$N\alpha$ calculated from Eq. 18[c]	185×10^{-6} emu/mole	182×10^{-6} emu/mole

[a]Calculated from the slopes or intercepts of the lines in Figure 18.

[b]Estimated from Figure 21.

[c]The true magnetic moments (μ) and the TIP terms ($N\alpha$) were calculated using $\zeta_{Ta(IV)} = 1,500$ cm^{-1} (from the Kotani theory) and 10 Dq values obtained from Table 6.

contributions to the susceptibilities of these compounds obtained from Figure 18. Other magnetic properties, calculated as described below, are also included in the table.

It can be seen from Table 8 that the true magnetic moments of both complexes are very low and equal within experimental error. The TIP terms are also of equal magnitude and constitute about 80-90% of the total paramagnetic susceptibility ($\chi_M^{corr.}$). These results are consistent with those proposed by Kotani for $5d^1$ ions where $\xi_{5d} \approx Dq \gg kT$. The low magnetic moments (μ) indicate that the $\Gamma_7(t_{2g})$ state is now far above the $\Gamma_8(t_{2g})$ ground state and thermal population of the former level does not occur to any appreciable extent. A nonzero magnetic moment is observed because of the mixing of the $\Gamma_8(e_g)$ wave function into the ground state wave function $\Gamma_8(t_{2g})$ under the spin-orbit interaction. The temperature independent contribution to the susceptibility arises from the high frequency elements between the $\Gamma_7(t_{2g})$ and $\Gamma_8(t_{2g})$ states.

The variation in μ_{eff} (which because of the method of calculation, contains a contribution from the TIP) with temperature for Rb_2TaCl_6 and Rb_2TaBr_6 is compared with the Kotani theory in Figure 21. The experimental results for

Figure 21. Variation of the effective magnetic moment of some rubidium hexahalotantalate(IV) complexes with temperature

(a) Solid lines are curves calculated from experimental data

(b) Broken lines are theoretical curves calculated on the basis of those values of ζ as marked thereon

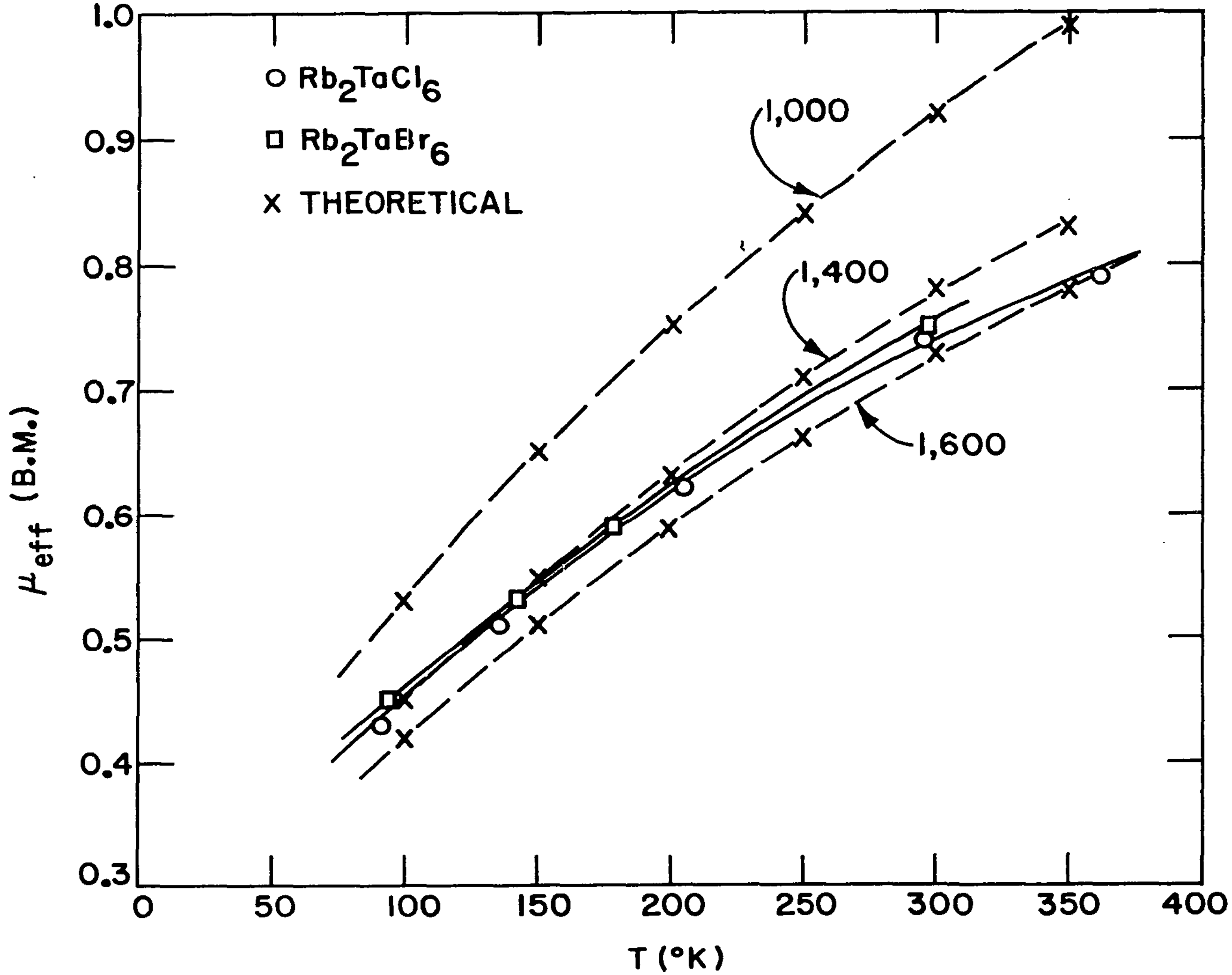

1.0
0.9
0.8
0.7
0.6
0.5
0.4
0.3
μ_{eff} (B.M.)
0
50
100
150
200
250
300
350
400
T (°K)
○ Rb_2TaCl_6
□ Rb_2TaBr_6
× THEORETICAL
1,000
1,400
1,600

both complexes are in very good agreement with theory for $\xi_{Ta(IV)} \approxeq 1,500$ cm.$^{-1}$. The experimental effective moments vary as $T^{\frac{1}{2}}$. Figgis and Lewis (50, p. 443) have shown that the Kotani theory (Equation 17) reduced to Equation 20 for large values of ξ.

$$\mu_{eff} = 2[\frac{kT}{\xi}]^{\frac{1}{2}} \qquad (20)$$

Using Equation 18, the spin-orbit coupling constant obtained from the Kotani theory, and 10 Dq values estimated from the absorption spectra, it is possible to calculate the true magnetic moments and TIP for the tantalum(IV) complexes. The results, given in Table 8, show that the calculated moments are much higher than the experimental values. If a spin-orbit coupling constant of ca. 1,000 $\pm$ 100 cm.$^{-1}$ is used in Equation 18, the calculated true moments agree with those obtained experimentally.

As discussed previously for the A_2NbX_6 complexes, a low magnitude antiferromagnetic lattice interaction could lead to a nearly constant lowering of μ_{eff} in the Rb_2TaX_6 compounds. The difference between the experimental curve for μ_{eff} and that calculated using $\xi_{Ta(IV)} = 1,000$ is shown in Fig. 21. This difference could result from the lowering of the susceptibility via the antiferromagnetic interactions.

However, Ballhausen (15, p. 145) has indicated that the Kotani theory yields low values for μ_{eff} (and therefore high values for ζ) for d^1 ions where $\zeta \cong Dq >> kT$. This is because Kotani did not take into account $\Gamma_8(t_{2g})$ - $\Gamma_8(e_g)$ 'mixing' which was shown by Moffitt (52) and Liehr (53) to yield a nonzero magnetic moment. Therefore at least part of the difference between the experimental true magnetic moment for Ta(IV) and that obtained by the treatment of Moffitt and Liehr, using Kotani's ζ , is due to this effect as well as an antiferromagnetic interaction. Hence a more accurate interpretation of the susceptibility data for the tantalum compounds is provided by the theory of Moffitt and Liehr and ζ = 1,000 $\pm$ 100 $cm.^{-1}$ is regarded as a better estimate of the spin-orbit coupling constant for tantalum(IV) in these complexes.

Although a free ion value for the spin-orbit coupling constant of tantalum(IV) has not been reported, the above value for $\zeta_{Ta(IV)}$ is ca. 50% lower than that estimated from the relationship $\zeta_{5d} \sim 2\,\zeta_{4d} \sim 5\,\zeta_{3d}$ (16). This difference is very likely due to π-bonding effects in the Rb_2TaX_6 complexes.

Infrared spectra

Infrared spectra of the alkali metal hexahaloniobate(IV) and hexahalotantalate(IV) complexes were determined as described in the experimental section. This investigation was carried out in an effort to determine the magnitude of the $\Gamma_8(t_{2g})$ - $\Gamma_7(t_{2g})$ splitting as a result of spin-orbit coupling. Electronic transitions between these two states should occur in the infrared region of the spectrum at ca. 500-700 $cm.^{-1}$ and 1,500-2,000 $cm.^{-1}$ for the niobium(IV) and tantalum(IV) complexes respectively. Although several measurements for each complex were carried out on pellets that were as concentrated as could be tolerated by the instrument, no peaks were ever found in these regions that could be assigned to this transition.

Most likely the intensity of the $\Gamma_8(t_{2g})$ - $\Gamma_7(t_{2g})$ transition is too low to be observed by the infrared method employed. This transition occurs entirely within the t_{2g} orbitals, and hence is expected to be of low intensity. Also, slight hydrolysis of the complexes always occurred during a measurement. Clouding of the pellet resulted which decreased the sensitivity of the instrument.

Niobium(IV) Halide Complexes with Acetonitrile

Formation of the tetrahalobis(acetonitrile)niobium(IV) complexes resulted from the reactions of the pure tetrahalides (chloride, bromide, iodide) with acetonitrile at room temperature as described in the experimental section. The vapor pressure of acetonitrile over the $NbCl_4(Ac)_2$ (Ac = acetonitrile) complex was less than one millimeter at 20°.

After exposure to a dynamic vacuum for extended periods of time or by heating to ca. 50°, all of the complexes were found to have undergone partial decomposition to their respective niobium(IV) halides. Duckworth, Fowles and Hoodless (57) have observed similar behavior for the $TiX_3(Ac)_3$ (X = Cl, Br) complexes. These compounds were found to decompose at ca. 40-50° into TiX_3 and CH_3CN. The $NbX_4(pyridine)_2$ (X = Cl, Br, I) complexes (1) appear to be considerably more stable than their acetonitrile analogs. Decomposition of these compounds was not observed after heating to 50-60° under a dynamic vacuum.

As indicated by the pressure-composition study (cf. p.66) in the reaction of niobium(IV) chloride with acetonitrile, a second complex, $NbCl_4(Ac)_3$, was found to be stable at acetonitrile pressures above 28 mm. Hg at 20°. Corresponding bromide and iodide complexes were not isolated. Without a detailed structural analysis of the $NbCl_4(Ac)_3$ complex it is not possible to determine if the niobium(IV) ion is actually seven coordinate or if the extra acetonitrile is accommodated between $NbCl_4(Ac)_2$ molecules in the lattice as solvent of crystallization. Spectral evidence, discussed below, strongly suggests that the niobium(IV) ion is octahedrally coordinated in acetonitrile solution, thus supporting the latter possibility.

Powder x-ray diffraction patterns of the $NbX_4(Ac)_2$ complexes contained a great number of lines. The complicated nature of these patterns indicated that the solids had lattices of low symmetry, therefore no attempt was made to index the films. No conclusions as to the similarity of the structures of the compounds could be arrived at from the x-ray data.

Infrared spectra

The infrared spectra of the solid tetrahalobis(acetonitrile)niobium(IV) complexes were studied in an effort to determine the extent and type of acetonitrile-niobium interaction. Since only the various acetonitrile vibrational frequencies are active in the region studied (700-4,000 $cm.^{-1}$) only indirect evidence for this bonding can be inferred by comparison of the observed spectra with that of pure acetonitrile. The C-N stretching frequency, which occurs at 2,248 $cm.^{-1}$ in liquid acetonitrile, should be a particularly sensitive indication of the type of N-M bonding. Shifts in the C-N stretch to higher energies have been cited by several workers (27, 28) as evidence that the carbon-nitrogen bond order is increasing. However, Fowles, et al. (57) have recently explained most of the 20-30 $cm.^{-1}$ increase in the nitrile stretching frequency in $TiX_3(Ac)_3$ (X = Cl, Br) complexes as arising through a coupling of the Ti-N and C-N vibrations.

The infrared spectra of all the $NbX_4(Ac)_2$ complexes were very similar to each other as well as being similar to noncoordinated acetonitrile. In all of the compounds the nitrile stretching frequency was shifted to higher frequencies relative to the noncomplexed ligand. These C-N stretching frequencies occurred at 2,300 $cm.^{-1}$ ($NbCl_4(Ac)_2$), 2,310 $cm.^{-1}$ ($NbBr_4(Ac)_2$), and 2,320 $cm.^{-1}$ ($NbI_4(Ac)_2$); an increase of 50-70 $cm.^{-1}$. This large shift in the nitrile stretching frequency to higher energies on complexing is evidence that little or no π-bonding takes place from nitrile to metal. Such an interaction would cause a shift to lower frequencies.

Conductance, molecular weight, and dipole moment studies

Conductance and molecular weight studies were carried out on acetonitrile solutions of the niobium(IV) halides in order to determine the type of coordination compound present in this solvent-ligand. In this connection, the dipole moment of $NbBr_4(Ac)_2$ was also measured in a nonpolar solvent. The procedures used in making these measurements are discussed in the experimental section.

The results of the conductance study are presented in Table 9.

Table 9. Conductance data for the niobium(IV) halides in acetonitrile at 20°

Solution	κ_{Ac}[a] ($ohm^{-1} cm.^{-1}$)	$\kappa_{soln.}$ ($ohm^{-1} cm.^{-1}$)	$\sim\Lambda$[b] ($cm.^2\ eq.^{-1}\ ohm^{-1}$)
$(C_2H_5)_4NBr$-Ac	---	---	159[c]
$NbCl_4$-Ac	(1) 3.3×10^{-6} (2) 4.8×10^{-7}	5.5×10^{-5}	1-5
$NbBr_4$-Ac	(1) 5.4×10^{-6} (2) 3.6×10^{-7}	10×10^{-5}	1-5
NbI_4-Ac	(1) 2.9×10^{-6} (2) 2.6×10^{-6}	23×10^{-5}	1-5

[a]The specific conductance of acetonitrile was determined: (1) before complexing, and (2) after being distilled from the complexes.

[b]The equivalent conductivities of the complexes were obtained from saturated solutions whose concentrations were greater than 10^{-2} g. eq. Nb/ℓ.

[c]Equivalent conductance of $(C_2H_5)_4NBr$ in acetonitrile ($\sim 10^{-3}$ molar solution) at room temperature (57).

As seen from Table 9, the products of the reactions of the niobium(IV) halides with acetonitrile are essentially nonelectrolytes in this solvent. The approximate equivalent conductivities of the solutions were much lower than that reported by Fowles et al. (57) for the univalent electrolyte $(C_2H_5)_4NBr$ in acetonitrile. Also, the experimental values of Λ (~1-5 $cm.^2$ $eq.^{-1}$ ohm^{-1}) are in good agreement with Fowles' results for an acetonitrile solution of nonionic $TiCl_3(Ac)_3$ ($\Lambda_{TiCl_3(Ac)_3}$ = 18 $cm.^2$ $eq.^{-1}$ ohm^{-1}). The small increase in the specific conductance of acetonitrile on complexing can be attributed to slight hydrolysis of the niobium complexes. This conclusion is substantiated by the fact that the specific conductivities of acetonitrile distilled off of the complexes were lower than the original values obtained for the solvent.

The apparent molecular weights of niobium(IV) chloride and niobium(IV) bromide in acetonitrile were found to be in good agreement with those calculated for monomeric NbX_4 in this solvent. Exact molecular weights of the NbX_4-Ac complexes can not be obtained in acetonitrile but spectral measurements, discussed below, indicate that the solid $NbX_4(Ac)_2$ complexes retain their coordination number of six in this solvent. The apparent molecular weight of NbI_4 could not be measured in acetonitrile due to the low solubility of the resulting $NbI_4(Ac)_2$. However spectroscopic data indicate that this compound is also a monomer. The results of the molecular weight study are given in the experimental section.

The dipole moment of tetrabromobis(acetonitrile)niobium(IV) was determined in benzene. Figure 22 shows the variation in the dielectric constant of the solution with mole fraction of solute. The linear relationship obtained from this plot indicates the expected behavior for a single species in the solutions over the observed concentration range. From the slope of this line ($d\varepsilon/dX = 93 \pm 10$), the orientation polarization was calculated from Equation 10 and found to be 1400 ± 150 cc. A dipole moment of 8.3 ± 0.6 Debye was calculated for the $NbBr_4(Ac)_2$ molecule by application of Equation 11.

The relatively large dipole moment of $NbBr_4(Ac)_2$ is consistent with a cis configuration for the molecule in benzene. The trans configuration would be expected to have a dipole moment close to zero since the ligand dipoles would cancel each other in an octahedral configuration. Muetterties (29) has also found that a large number of $MF_4(Ac)_2$ complexes have

Figure 22. Variation in the dielectric constant of benzene solutions of tetrabromobis(acetonitrile)niobium(IV) with mole fraction solute

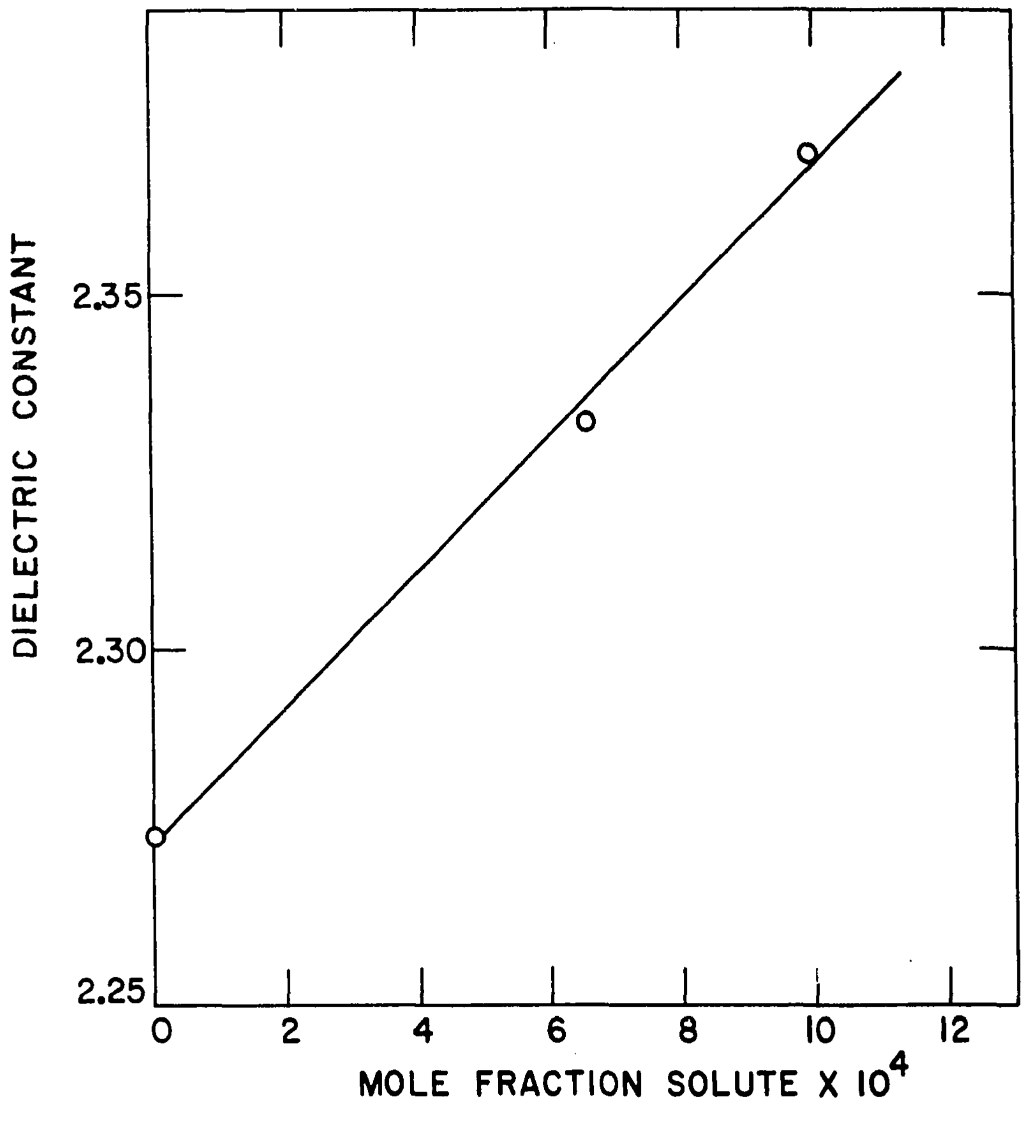
DIELECTRIC CONSTANT
2.35
2.30
2.25
0
2
4
6
8
10
12
MOLE FRACTION SOLUTE X 10^4

the _cis_-octahedral coordination indicated for $NbBr_4(Ac)_2$.

Ulich _et al_. (58) have found dipole moments of comparable magnitude for $TiCl_4(Ac)_2$ and $SnCl_4(Ac)_2$ complexes in benzene. However, these results were explained in terms of dissociation of the complexes into $MCl_4(Ac)$ and acetonitrile. Fowles and associates (57) have also explained the two-fold freezing point depression of $VCl_4(Ac)_2$ in benzene on this basis. It is difficult to understand why such a dissociation should take place in this noncoordinating solvent.

The absorption spectra of $NbBr_4(Ac)_2$ in benzene and $NbBr_4$ in acetonitrile are almost identical, strongly indicating that the same molecular species is present in both solvents. Therefore dissociation of this complex is not thought to take place in benzene. Dipole moments of the $NbCl_4(Ac)_2$ and $NbI_4(Ac)_2$ complexes were not measured, the former compound being too insoluble.

The information obtained from conductance, molecular weight and dipole moment studies indicates that the $NbX_4(Ac)_2$ complexes exist as nondissociated molecules in acetonitrile solution, with a _cis_-octahedral configuration of ligands about the niobium(IV) ion. Because of the nonionic behavior of these solutions and from the molecular weight data, any appreciable disproportionation or reduction of niobium(IV) in acetonitrile can be ruled out. The products of these reactions would necessarily be ionic and also would decrease the apparent molecular weight of the complexes below the observed value.

Ultraviolet, visible and near-infrared absorption spectra

The absorption spectra of the tetrahalobis(acetonitrile)-niobium(IV) complexes were determined from 200-2,500 mμ as described in the experimental section. These experiments were initiated to study the structural relationships between the compounds in the solid state and in solution as well as to determine the degree of distortion of the complexes from true octahedral symmetry. The results of these measurements in acetonitrile are shown in Figures 23-25 while diffuse reflectance spectra of the solid $NbX_4(Ac)_2$ complexes are shown in Figure 26. Spectral data for the compounds are tabulated in Table 10.

It can be seen from Figures 23-25 or Table 10 that the ultraviolet-visible spectra of the niobium(IV) halides in acetonitrile are quite similar, containing two peaks of low intensity at longer wavelengths and a number of high intensity peaks at shorter wavelengths. The spectrum of $NbBr_4(Ac)_2$

Table 10. Absorption spectra of the tetrahalobis(acetonitrile)niobium(IV) complexes in the solid state and in solution

Complex[a]	Absorption maxima (λ_{max}) in mμ (ϵ_{max} in parenthesis)							
	#1	#2	#3	#4	#5	#6	#7	#8
$NbCl_4(Ac)_2$ (Ac, solid)	235 (24000)	263 (~5000)	268 (16000)	307 (2400)	390 (88)[b]	440 (18)[b]	2150 (18)	----
$NbBr_4(Ac)_2$ (Ac, solid)	237 (1400)	254 (~1000)	263 (~1000)	270 (~2000)	285 (3100)	330 (2800)	403 (380)[b]	~525 (<20)[d]
$NbBr_4(Ac)_2$[c] (benzene)	----	----	----	----	285 (2000)	334 (1900)	405 (390)[b]	----
$NbI_4(Ac)_2$ (Ac, solid)	230 (~2000)	247 (8900)	293 (4400)	354 (2200)	478 (660)[b]	603 (150)[b]	----	----

[a]The type of measurement employed in determining the spectrum of a complex is given in parenthesis below the compound (Ac = acetonitrile solution; benzene = benzene solution; solid = reflectance measurement on the solid).

[b]Peaks resolved graphically by trial and error assuming a Gaussian shape for the absorption bands.

[c]The spectrum of $NbBr_4(Ac)_2$ in benzene could only be obtained to ca. 280 mμ (the benzene cutoff).

[d]Peak 8 was only observed in reflectance measurements. The extinction coefficient is estimated relative to the intensity of peak 7.

Figure 23. Absorption spectrum of niobium(IV) chloride in acetonitrile

(a) The extinction coefficient scale for curve A is given at the left of the figure

(b) The extinction coefficient scale for curve B is given at the right of the figure

(c) Dashed peaks 5 and 6 for curve B were graphically resolved by trial and error assuming à Gaussian shape for the absorption bands

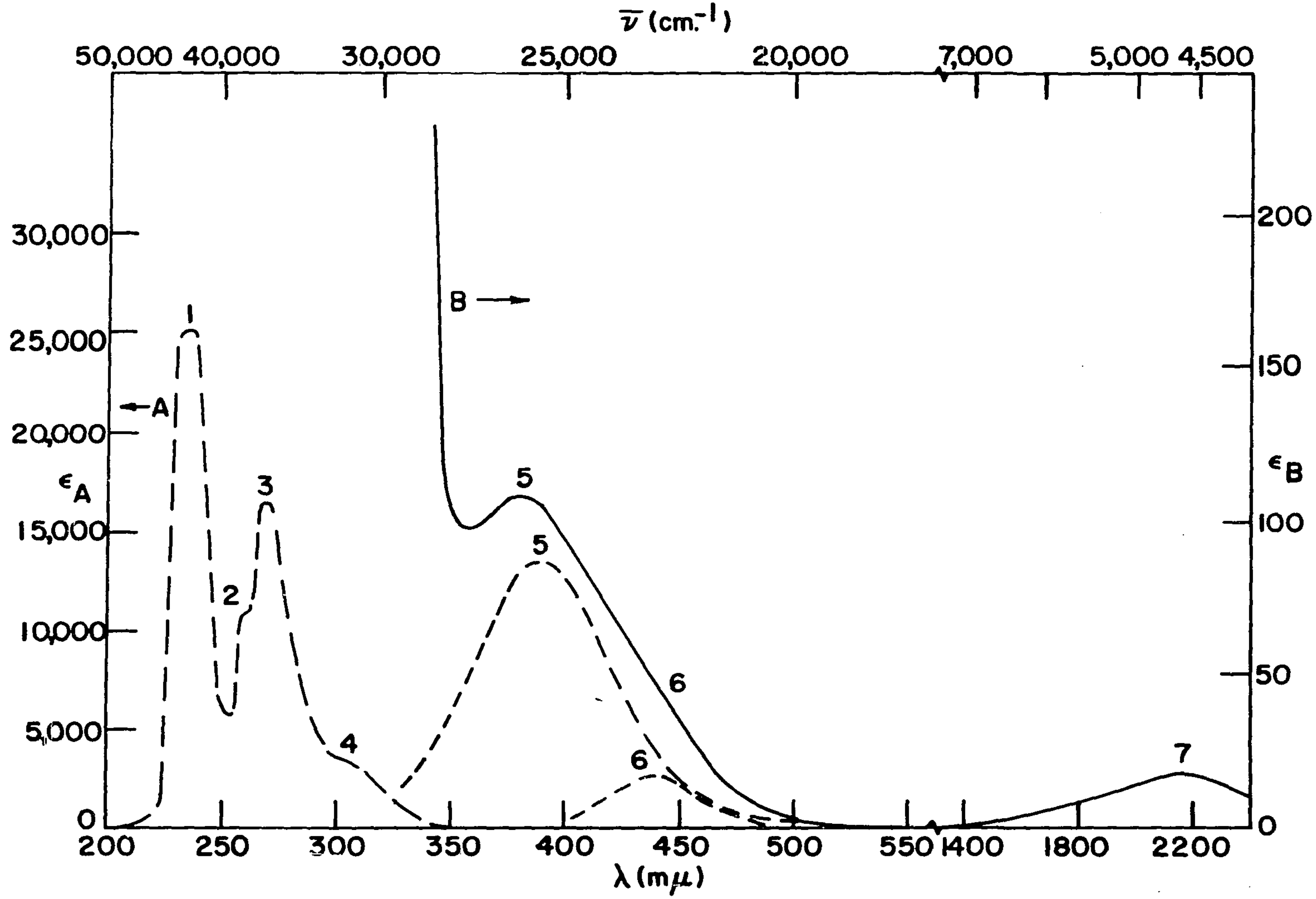

$\bar{\nu}$ (cm.$^{-1}$)
50,000 40,000 30,000 25,000 20,000 7,000 5,000 4,500
30,000
25,000
20,000
15,000
10,000
5,000
0
ϵ_A
A
B
200
150
100
50
0
ϵ_B
2
3
4
5
6
7
200 250 300 350 400 450 500 550 1400 1800 2200
λ (mμ)

Figure 24. Absorption spectrum of niobium(IV) bromide in acetonitrile

(a) The extinction coefficient scale for curve A is given at the left of the figure

(b) The extinction coefficient scale for curve B is given at the right of the figure

(c) Dashed peak 7 for curve B was graphically resolved by trial and error assuming a Gaussian shape for the absorption bands

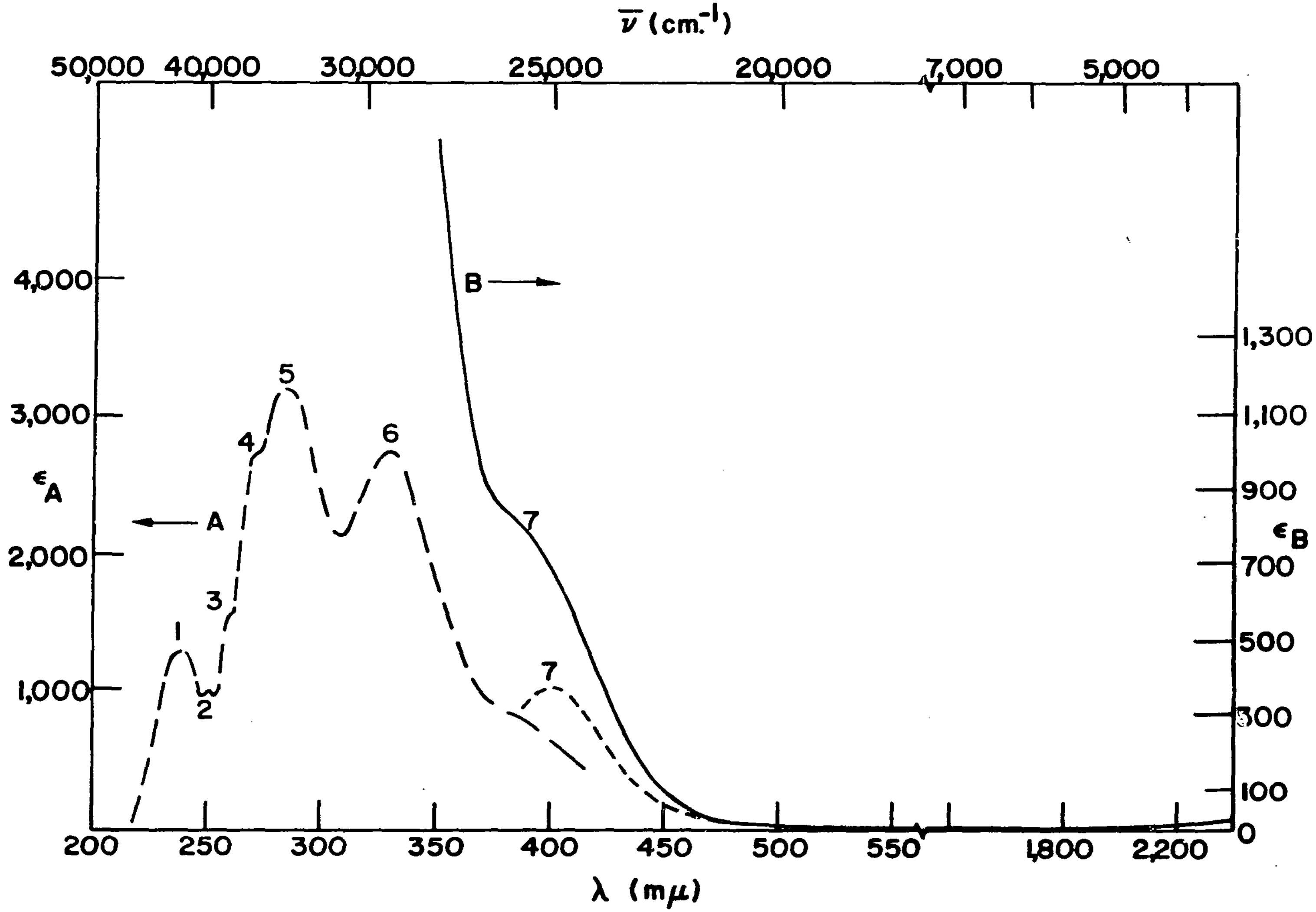

$\overline{\nu}$ (cm.$^{-1}$)
50,000
40,000
30,000
25,000
20,000
7,000
5,000
4,000
3,000
2,000
1,000
ϵ_A
A
B
1
2
3
4
5
6
7
7
1,300
1,100
900
700
500
300
100
0
ϵ_B
200
250
300
350
400
450
500
550
1,800
2,200
λ (mμ)

Figure 25. Absorption spectrum of niobium(IV) iodide in acetonitrile

(a) The extinction coefficient scale for curve A is given at the left of the figure

(b) The extinction coefficient scale for curve B is given at the right of the figure

(c) Dashed peaks 5 and 6 for curve B were graphically resolved by trial and error assuming a Gaussian shape for the absorption bands

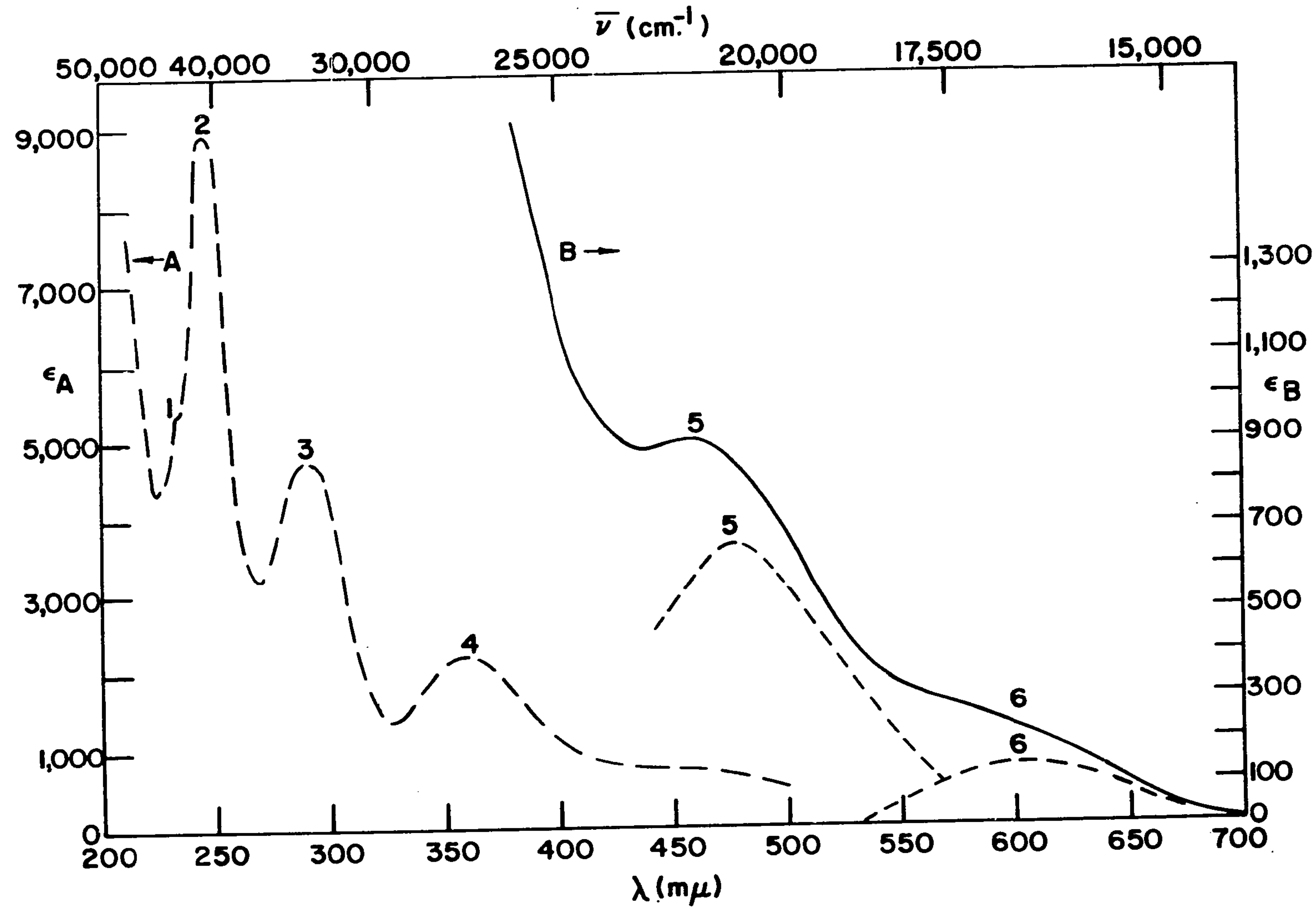

$\bar{\nu}$ (cm.$^{-1}$)
50,000
40,000
30,000
25000
20,000
17,500
15,000
9,000
7,000
5,000
3,000
1,000
0
ϵ_A
1,300
1,100
900
700
500
300
100
0
ϵ_B
A
B
1
2
3
4
5
5
6
6
200
250
300
350
400
450
500
550
600
650
700
λ (mμ)

Figure 26. Diffuse reflectance spectra of the tetrahalobis(acetonitrile)-niobium(IV) complexes

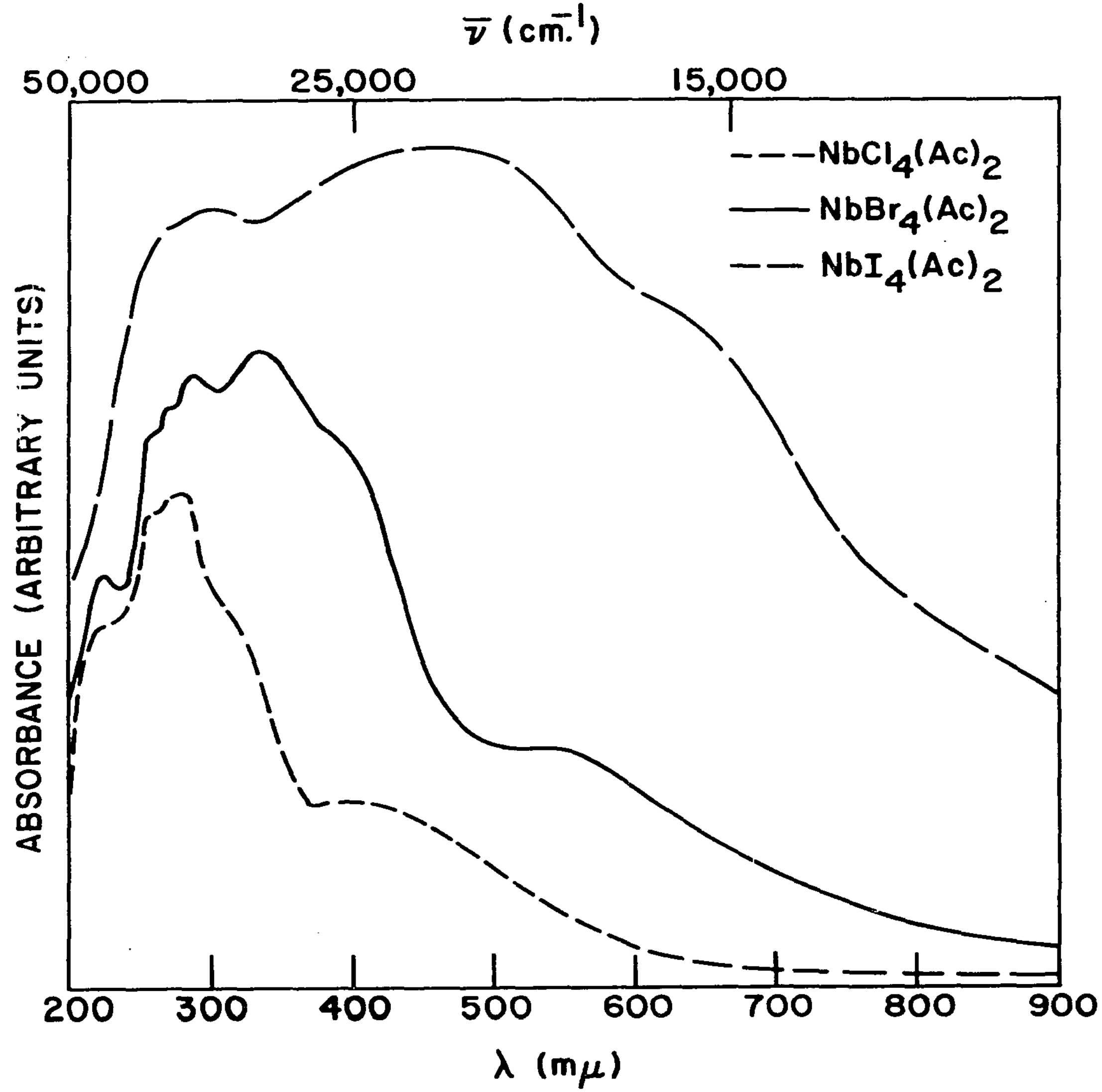

$\overline{\nu}$ (cm.$^{-1}$)
50,000
25,000
15,000
---NbCl$_4$(Ac)$_2$
—— NbBr$_4$(Ac)$_2$
— — NbI$_4$(Ac)$_2$
ABSORBANCE (ARBITRARY UNITS)
200
300
400
500
600
700
800
900
λ (mμ)

in benzene was found to be virtually identical with that obtained for $NbBr_4$ in acetonitrile. In addition, absorption spectra of the solid $NbX_4(Ac)_2$ complexes (Figure 26) are very similar to the solution spectra. This information coupled with that obtained from the conductance, molecular weight and dipole moment studies strongly suggests that all of the complexes have the same cis molecular configuration of ligands around the niobium(IV) ion in both the solid state and solution.

The leveling effect that reflectance measurements impose on the low wavelength peaks in the spectra of the $NbX_4(Ac)_2$ complexes can be readily seen by comparing Figures 23-25 (solution spectra) with Figure 26 (reflectance spectra). This effect in diffuse reflectance measurements of the spectrum of $NbBr_4(Ac)_2$ is responsible for the location of peak 8. The absorption band is of such low intensity ($\varepsilon < 20$) that it was completely covered by peak 7 ($\varepsilon = 380$) in solution spectra at high concentrations and did not show up in the spectra of more dilute solutions.

The electronic spectra and magnetic properties of the $NbX_4(Ac)_2$ complexes are best described by the molecular orbital theory since it was found experimentally that extensive p_π-d_π bonding was present in the compounds. Figure 27b shows the changes in the relative positions of M.O.'s for a d^1 complex with O_h symmetry (part a) when the symmetry of the complex is reduced to approximately D_{4h} (part b), and when π-bonding is present (part c). For simplicity, only molecular orbitals with some d-orbital character are presented in the diagram. These will be shown to account for the majority of spectral and magnetic properties of the complexes. It should be emphasized that the relative energies of the M.O.'s in Figure 27b are only approximate and that the diagram is not drawn to scale.

Ballhausen (15, p. 107) has shown that the deviation from octahedral symmetry in a complex of the type cis-MA_4B_2 can be treated as a tetragonal distortion (D_{4h}) even if formally the symmetry group of the complex is C_{2v}. Therefore, the lower symmetry of the cis-$NbX_4(Ac)_2$ complexes ($O_h \rightarrow D_{4h}$) causes a splitting of the cubic t_{2g} and e_g orbitals as shown in part b of Figure 27b, assuming that acetonitrile has a greater ligand field strength than the halide ligands (10) and that the ligands are oriented with respect to the coordinate axes shown in Figure 27a.

When p_π-d_π bonding from the halide ligands to the nio-

Figure 27a. Proposed structure of the tetrahalobis(acetonitrile)niobium(IV) complexes (X = Cl, Br, I; Ac = CH_3CN)

Figure 27b. Partial molecular orbital energy level diagram for a six coordinate d^1 complex, showing the results of an effective tetragonal distortion and π-bonding on M.O.'s having some metal d-orbital character (the single unpaired electron in the complex is shown on the diagram as a filled circle)

(a) M.O.'s in a strong octahedral field

(b) M.O.'s in a strong octahedral field plus a weak tetragonal distortion resulting from the ligand configuration shown in Figure 27a

(c) M.O. configuration resulting from π-bonding effects on the tetragonal field shown in (b)

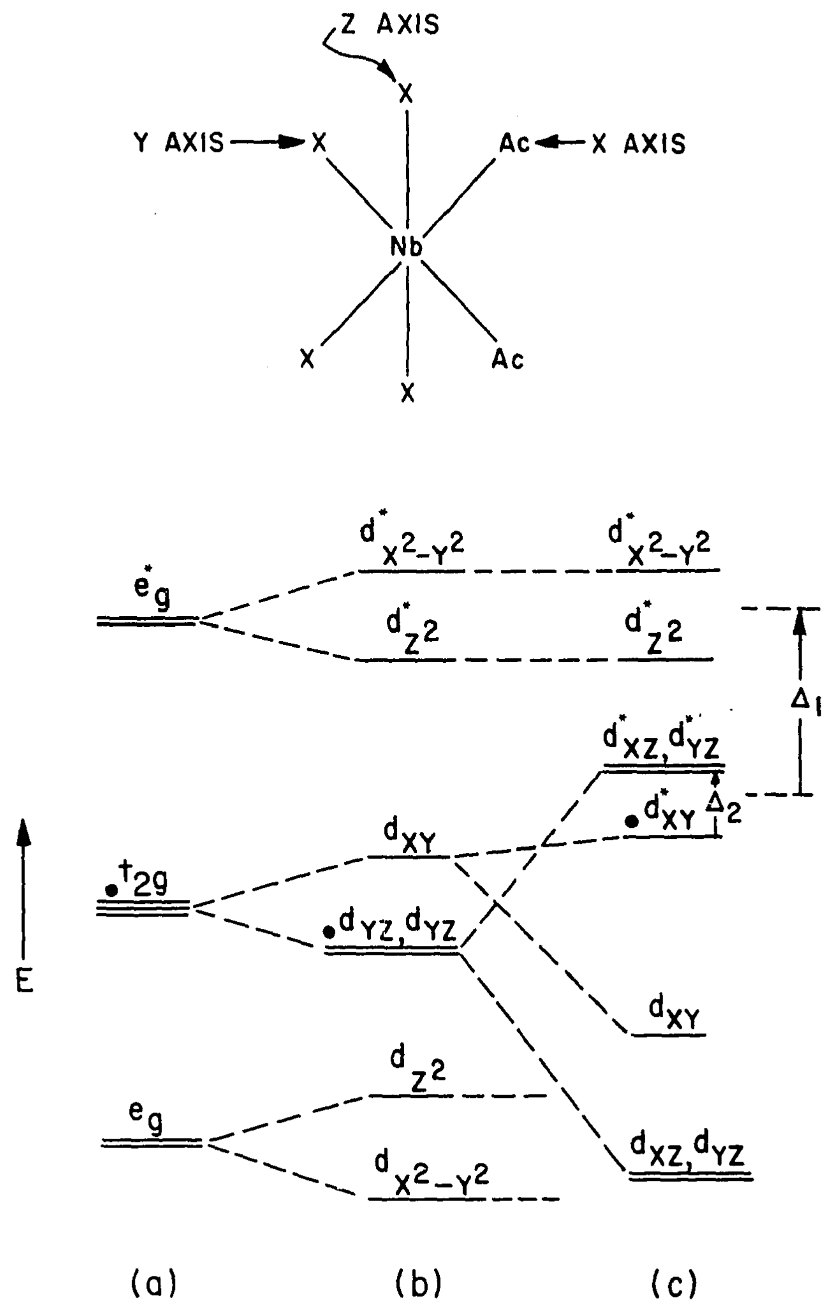

Z AXIS
X
Y AXIS
X
Ac
X AXIS
Nb
X
Ac
X
$d^*_{X^2-Y^2}$
$d^*_{X^2-Y^2}$
e^*_g
$d^*_{Z^2}$
$d^*_{Z^2}$
Δ_1
d^*_{XZ}, d^*_{YZ}
d^*_{XY}
Δ_2
d_{XY}
t_{2g}
E
d_{YZ}, d_{YZ}
d_{XY}
d_{Z^2}
e_g
$d_{X^2-Y^2}$
d_{XZ}, d_{YZ}
(a)
(b)
(c)

bium(IV) ion occurs, the nonbonding d_{xy} and d_{xz}, d_{yz} metal orbitals shown in part b break down into the two new sets of M.O.'s (a bonding and antibonding set) shown in part c of Figure 27b. Infrared spectra of the $NbX_4(Ac)_2$ complexes have indicated that the acetonitrile does not π-bond to any appreciable extent. Therefore the d_{xy} orbital, which is in the plane containing both of these ligands, should π-bond to a lesser extent than the d_{xz} or d_{yz} orbitals. The latter orbitals can π-bond to three halide ligands while the former orbital can π-bond to only two halides. The result of this difference in π interaction causes a reversal in the positions of the t_{2g} orbitals, with the singlet d^*_{xy} antibonding orbital now lying below the d^*_{xz}, d^*_{yz} orbitals. Magnetic susceptibility measurements, discussed below, verify the positions of these antibonding orbitals.

Dunn (42, p. 261) has shown that the d^*_{xz}, d^*_{yz} orbitals will be further split by spin-orbit coupling. However, magnetic data for the A_2NbX_6 complexes have indicated that this effect should be small in the $NbX_4(Ac)_2$ complexes, when compared to the splitting of the t^*_{2g} orbitals due to differences in π-bonding. Therefore the electronic spectra of these complexes will be discussed with reference to part c of Figure

27b.

The ground state of the $NbX_4(Ac)_2$ complexes with the M.O. configuration indicated in part c of Figure 27b would consist of the single unpaired electron in the d^*_{xy} orbital. Electronic d-d transitions from this orbital to the higher energy molecular orbitals should occur as low intensity peaks in the visible and near-infrared regions of the optical spectrum. Reference to Table 10 shows that all of the complexes have two low intensity peaks in the visible region. These are assigned to the transitions $(xy)^* \rightarrow (z^2)^*$ and $(xy)^* \rightarrow (x^2-y^2)^*$. In addition, the spectrum of $NbCl_4(Ac)_2$ contains one peak in the near-infrared region assigned to the transition $(xy)^* \rightarrow (xz, yz)^*$. The energies of these d-d transitions and other pertinent spectral data are presented in Table 11.

Fowles et al. (57) and Nyholm et al. (10) have found that the visible spectrum of the "tetragonal" $TiCl_3(Ac)_3$ complex contains two low intensity peaks at 14,700 $cm.^{-1}$ (ε = 15) and 17,200 $cm.^{-1}$ (ε = 31). In addition, Fowles found that the spectrum of $VCl_4(Ac)_2$ in benzene contained two peaks in the visible region at ~20,000 $cm.^{-1}$ and ~22,000 $cm.^{-1}$ with ε = 500. The peaks in both complexes were attributed to d-d transitions

Table 11. Spectral data obtained from the absorption spectra of the tetrahalobis(acetonitrile)niobium(IV) complexes

Complex	Energies of the indicated d-d transition[a] (cm^{-1})			Magnitude of e_g* splitting (cm^{-1})	$\Delta_1^{b}(cm^{-1})$
	$(xy)^* \rightarrow (z^2)^*$	$(xy)^* \rightarrow (x^2-y^2)^*$	$(xy)^* \rightarrow (xz,yz)^*$		
$NbCl_4(Ac)_2$	22,700	25,700	4,650	3,000	21,900
$NbBr_4(Ac)_2$	~19,100	24,700	<4,000[c]	~5,600	---
$NbI_4(Ac)_2$	16,600	20,900	<<4,000[c]	4,300	---

[a]Calculated from λ_{max} data given in Table 10.

[b]Calculated from the mean values of the e_g* and t_{2g}* splittings as indicated in Figure 27b.

[c]The peak corresponding to the $(xy)^* \rightarrow (xz, yz)^*$ transition occurred below the acetonitrile cutoff (4,000 cm^{-1}).

in accord with the assignments given above for the $NbX_4(Ac)_2$ complexes. These transitions in the titanium(III) and vanadium(IV) complexes occur at lower energies than in the niobium(IV) complexes. This result is expected since 10 Dq increases as Ti(III) < V(IV) < Nb(IV) for similar octahedral complexes (49, p. 45).

It can be concluded from Table 11 or Figure 26 that the spectra of the $NbX_4(Ac)_2$ complexes agree with the expected trends in ligand field strength as predicted by the spectrochemical series acetonitrile > Cl > Br > I. The magnitude of Δ_1 for the $NbCl_4(Ac)_2$ complex (21,900 cm^{-1}) is larger than the 10 Dq found for the A_2NbCl_6 complexes (21,100 cm^{-1}). Although Δ_1 values cannot be calculated for the bromide- and iodide-acetonitrile complexes because their $(xy)^* \rightarrow (xz, yz)^*$ transitions were not observed, it can be seen from Table 11 or Figure 26 that the d-d transitions shift to progressively lower energies in the order Cl > Br > I.

The magnitude of the splitting of the e_g^* state should also reflect the above trend. The data in Table 11 show that this splitting is smaller in $NbCl_4(Ac)_2$ than in $NbBr_4(Ac)_2$, as expected, since there is a greater difference in the bromide-acetonitrile ligand field strengths. The fact that the

e_g* splitting in $NbI_4(Ac)_2$ is less than that found for $NbBr_4$-$(Ac)_2$ cannot be readily explained by the argument presented above. Perhaps this discrepancy is due to the uncertainty in the position of peak 8 in the spectrum of $NbBr_4(Ac)_2$. This peak was only found as a broad band in the reflectance spectrum of the compound. There is also a possibility that peak 5 in the spectrum of $NbI_4(Ac)_2$ is due to a charge-transfer transition.

The magnitude of the e_g* splitting in the $NbX_4(Ac)_2$ complexes is quite small, approximately the same as that found in the A_2NbX_6 complexes due to Jahn-Teller effects. A small splitting is in accord with that predicted by Ballhausen (15, p. 107) for a cis complex. The analogous trans configuration for a $NbX_4(Ac)_2$ complex would be expected to cause approximately twice the splitting of the e_g* state.

An indication of the relative degree of π-bonding in the complexes can be obtained from noting the magnitude of their t_{2g}* splittings. This splitting, which is the energy of the $(xy)^* \rightarrow (xz, yz)^*$ transition, was found to be quite large (4,650 cm^{-1}) in $NbCl_4(Ac)_2$. This transition was not observed in the other halide complexes. However, the rising absorption in the spectrum of $NbBr_4(Ac)_2$ at the cutoff, see Figure

24, suggests that the $(xy)^* \rightarrow (xz, yz)^*$ transition does not lie too far below 4,000 cm^{-1} in this compound. No indication of this peak was ever found in the spectrum of $NbI_4(Ac)_2$ measured at the highest possible concentration. These results show that the degree of ligand to metal π-bonding in the complexes decreases in the order Cl > Br > I > acetonitrile.

As noted, there is some uncertainty in the assignment of peak 5 at 478 mμ in the spectrum of $NbI_4(Ac)_2$ to the $(xy)^* \rightarrow (x^2-y^2)^*$ transition. This peak is of sufficient intensity ($\varepsilon = 660$) to be in the realm of charge-transfer. Charge-transfer peaks in the spectrum of Cs_2NbI_6 were found to occur at 500 mμ and possibly as high as 665 mμ. However, Dunn (42, p. 266) has indicated that the intensities of d-d transitions can be increased in complexes where electron delocalization occurs. Moreover, the 'd' molecular orbitals needed to describe these compounds may have some 'p' character and partial breakdown of the Laporte selection rule occurs.

The high intensity peaks ($\varepsilon > 1000$) in the absorption spectra of the $NbX_4(Ac)_2$ (X = Cl, Br, I) complexes are assigned to charge-transfer transitions (see Table 10). Because of the high charge of the niobium(IV) ion and the nature of the ligands, the electron transfer most likely takes place from predominantly ligand M.O.'s to predominantly metal M.O.'s as described for the A_2MX_6 complexes. The uncertainty in the positions of the molecular orbitals in the acetonitrile complexes makes any exact assignment of these charge-transfer transitions impossible, but certain qualitative conclusions can be drawn.

The relative positions of the charge-transfer peaks in the $NbX_4(Ac)_2$ complexes are in agreement with the expected trends discussed previously. It can be seen from Table 10 that the positions of the two lowest energy C.T. transitions shift to lower energies in the order Cl > Br > I. This behavior is in accord with the expected shift in a given C. T. transition as the halide ligands become more oxidizable (49, p. 99).

Fowles et al. (57) have discussed the nature of the charge-transfer spectra in analogous $MCl_4(Ac)_2$ (M = Ti(IV), Zr(IV), V(IV)) complexes. They assigned the common peak at ca. 300-334 mμ ($\epsilon \sim 1000$) in the spectra of these compounds to the transitions AC(π) → M and peaks at lower wavelengths were assigned to Cl (π) → M transitions. While it is tempting to assign the peaks at 307 mμ($NbCl_4(Ac)_2$), 330 mμ($NbBr_4$-$(Ac)_2$) and 354 mμ($NbI_4(Ac)_2$) to the Ac(π) → Nb(π) transition, this assignment should be viewed with caution. Charge-transfer transitions, necessarily of the type X → Nb, in the spectra of the A_2NbX_6 complexes were observed in this region.

Magnetic susceptibility studies

The magnetic susceptibilities of the tetrahalobis(acetonitrile)niobium(IV) complexes were found to vary with reciprocal temperature as shown in Figure 28. As seen from this figure, $NbCl_4(Ac)_2$ shows a linear variation, while plots of χ_M versus 1/T for $NbBr_4(Ac)_2$ and $NbI_4(Ac)_2$ have progressively more curvature. It is also evident from Figure 28 that the magnetic moments (μ) of the complexes, which are proportional to the square root of the slopes of the curves (see Equation 14), are decreasing in the order $NbCl_4(Ac)_2$ > $NbBr_4(Ac)_2$ > $NbI_4(Ac)_2$. The true magnetic moment of $NbCl_4(Ac)_2$ was calculated to be 1.75 B.M. Because of the curvature of their χ_M plots, only effective magnetic moments (μ_{eff}) can be obtained for the other complexes. As discussed previously, it is not justifiable to straighten out these curves by applying a suitable value of θ (50). The effective magnetic moments of all the complexes are presented in Table 12 along with other pertinent magnetic data.

Spectral data for the $NbX_4(Ac)_2$ complexes have indicated

Figure 28. Variation of the molar magnetic susceptibilities of the tetrahalobis(acetonitrile)niobium(IV) complexes with reciprocal temperature

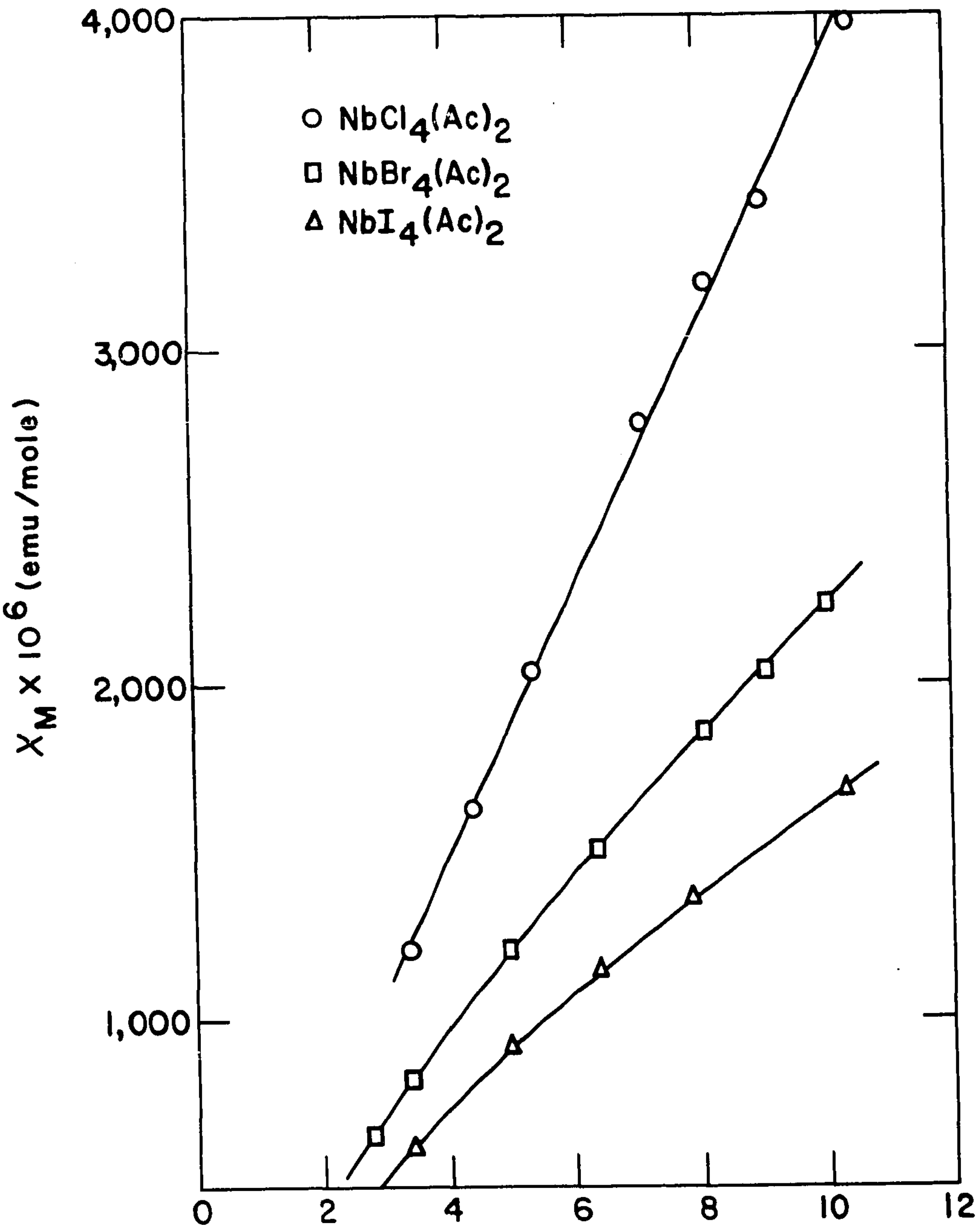

4,000
3,000
2,000
1,000
$\chi_M \times 10^6$ (emu/mole)
○ $NbCl_4(Ac)_2$
□ $NbBr_4(Ac)_2$
△ $NbI_4(Ac)_2$
0
2
4
6
8
10
12
$T^{-1} \times 10^3$ (°K)$^{-1}$

Table 12. Magnetic data for the tetrahalobis(acetonitrile)niobium(IV) complexes

Complex	Effective magnetic moment[a] (B.M.) 300°K	150°K	100°K	$\sim \Delta_2^b$ (cm^{-1})
$NbCl_4(Ac)_2$	1.83	1.82	1.81	4,000-5,000
$NbBr_4(Ac)_2$	1.57	1.47	1.40	1,000-2,000
$NbI_4(Ac)_2$	1.45	1.33	1.25	600-1,000

[a]Estimated from Figure 29.

[b]Calculated from the data of Figgis (59), assuming $\xi_{Nb(IV)}$ = 300-600 cm^{-1}.

that the magnitude of the t_{2g}* splitting (4,650 cm^{-1} in $NbCl_4(Ac)_2$) is much larger than the spin-orbit coupling constant for niobium(IV) ($\xi \sim 400$ cm^{-1}). Under these conditions, the generalization can be made that the moments of the complexes will be larger than those predicted by the Kotani theory (24) for octahedral d^1 complexes. This is because the asymmetric field causes a further quenching of the orbital angular momentum associated with the ground levels (50). Figgis (59) and Griffith (60) have further shown that as the magnitude of the asymmetric field component increases relative to ξ , the true magnetic moments will tend toward the spin-only value.

Figgis (59) has also studied the variation in the effective magnetic moments arising from the $^2T_{2g}$ term of a d^1 transition metal ion as a function of temperature, spin-orbit coupling, degree of asymmetry, and electron delocalization. Plots of μ_{eff} versus kT/ξ were constructed for various values of the ratio Δ_2/ξ . Δ_2 was defined as the separation between the orbital levels of $^2T_{2g}$ created by the asymmetric ligand field component, in the absence of spin-orbit coupling. As seen from Figure 27b, the splitting is into an orbital singlet and an orbital doublet. Δ_2 is positive if the singlet is lowest. For $\Delta_2(+)$, it was found that as the magnitude of Δ_2/ξ increased, i.e. the tetragonal ligand field component increased relative to the spin-orbit coupling, the effective moment departed from the cubic behavior and eventually tended toward the spin-only value at all temperatures ($\Delta_2/\xi = 10$). For smaller values of Δ_2/ξ, the effective moments were progressively lower than 1.73 B.M. and were found to decrease slowly with temperature. However for $\Delta_2(-)$, μ_{eff} was found to be considerably lower than the spin-only value and to decrease rapidly with temperature, for all values of Δ_2/ξ. The effect of t_{2g}* orbital delocalization (π-bonding) was found to cause the effective moment to tend towards the spin-only value.

Figure 29 shows the variation in the effective magnetic moments of the $NbX_4(Ac)_2$ complexes with temperature. Reference to this figure or to Table 12 indicates that the distortion from octahedral symmetry is greatest in the case of $NbCl_4(Ac)_2$ since the effective moment of this complex is nearest the spin-only value and does not vary appreciably with temperature. Similarly, the distortion is least in $NbI_4(Ac)_2$ with $NbBr_4(Ac)_2$ occupying an intermediate position. By comparing these plots with the data given by Figgis (59),

Figure 29. Variation of the effective magnetic moments of the tetrahalobis(acetonitrile)niobium(IV) complexes with temperature

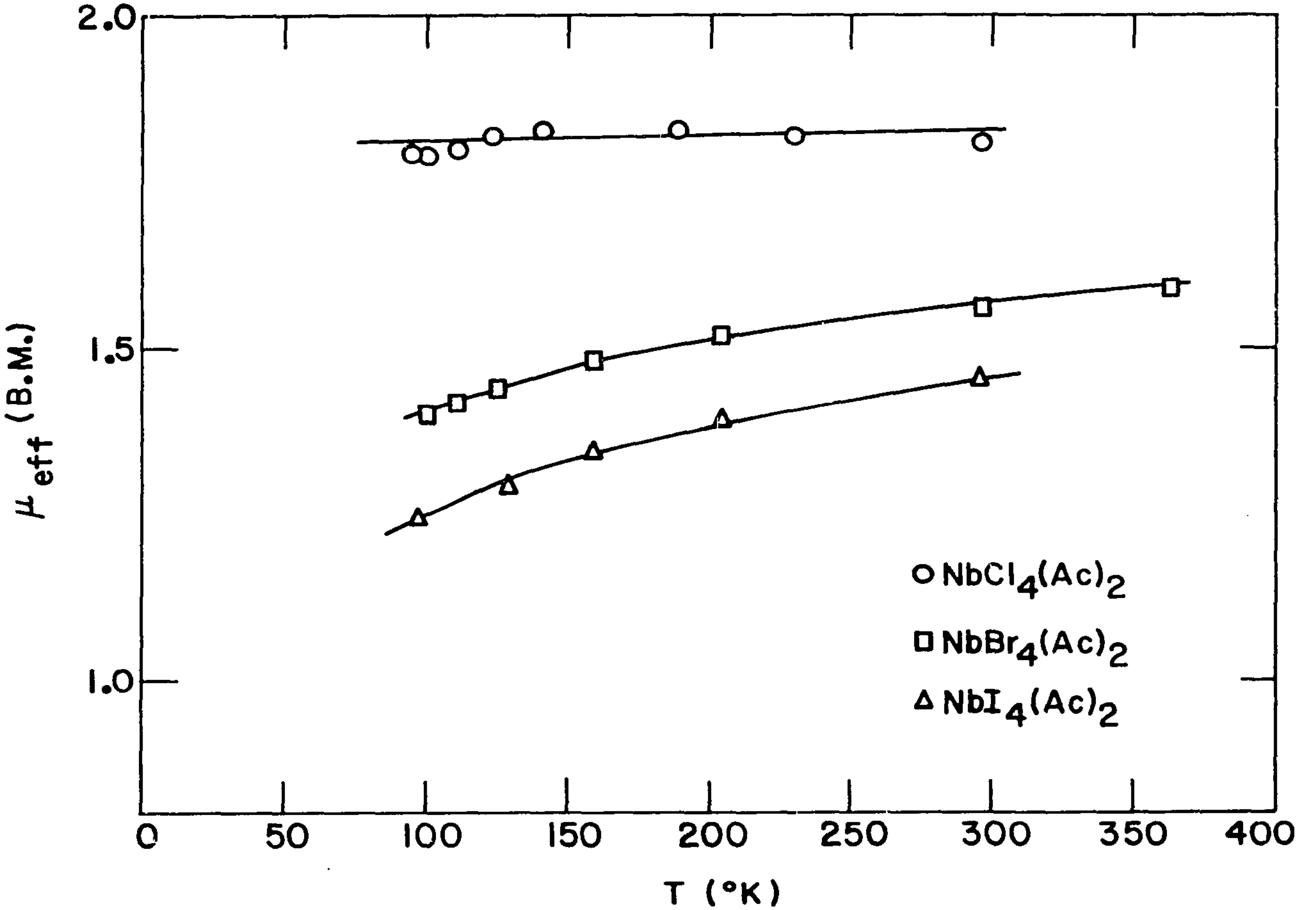
2.0
1.5
1.0
μ_{eff} (B.M.)
0
50
100
150
200
250
300
350
400
T (°K)
○ $NbCl_4(Ac)_2$
□ $NbBr_4(Ac)_2$
△ $NbI_4(Ac)_2$

it was possible to determine the magnitude and sign of Δ_2. Assuming that the spin-orbit coupling constant for the niobium(IV) ion in these complexes is ca. 300-700 cm^{-1}, as indicated by the magnetic studies of the A_2NbX_6 complexes, Δ_2 was found to decrease from a value of 4,000-5,000 cm^{-1} ($NbCl_4(Ac)_2$) to 600-1,000 cm^{-1} ($NbI_4(Ac)_2$). The magnitude of Δ_2 for the $NbCl_4(Ac)_2$ complex agrees well with that obtained for the total distortion of the t_{2g}* orbitals (4,650 cm^{-1}) from spectral measurements. Moreover, the magnitude and temperature variation of μ_{eff} in the compounds were definitely in accord with the singlet d_{xy}^* orbital lying lowest.

The magnitude and type of the ground state distortion proves that acetonitrile does not π-bond to any appreciable extent in the complexes. If this ligand did π-bond, the splitting of the t_{2g}* orbitals would be greatly reduced. If acetonitrile formed stronger π-bonds than the halogens the doublet d_{xz}*, d_{yz}* orbitals would be of lower energy (see Figure 27b), and the effective magnetic moments of the complexes would be much lower than the spin-only value and would vary drastically with temperature.

The above information is consistent with that obtained from measurements of the absorption spectra of the cis-$NbX_4(Ac)_2$ complexes. Differences in the degree of π-bonding of the halides in these compounds, and therefore the magnitude of the t_{2g}* splitting, will account for all of the magnetic properties. As indicated from the spectral data, magnetic measurements show that the degree of π-bond formation in the complexes decreases in the order Cl > Br > I > acetonitrile.

SUMMARY

Pure crystalline alkali metal hexahaloniobate(IV) and hexahalotantalate(IV) complexes, A_2MX_6 (A = K, Rb, Cs; M = Nb, Ta; X = Cl, Br, I), were synthesized by the reaction of stoichiometric amounts of AX and MX_4 in an evacuated sealed vessel at the melting point of the alkali metal halide. The compounds generally had melting points above the reaction temperature and were found to react with the atmosphere.

X-ray analysis of the powdered hexahalo complexes verified their purity and indicated that the compounds crystallized in a face centered cubic lattice (except the face centered tetragonal K_2NbBr_6). A detailed structural investigation of K_2NbCl_6 showed that these compounds have the antifluorite (K_2PtCl_6) structure with octahedral $MX_6^=$ ions at the corners and face centered positions of the unit cell and A^+ ions in the tetrahedral holes. The stability of this type of lattice was found to be a function of the cation/anion radius ratio.

The electronic absorption spectra of the A_2MX_6 complexes consisted of two low intensity peaks at longer wavelengths with additional high intensity peaks at shorter wavelengths. The spectra were not dependent on the alkali metal cation in

the lattice. The low intensity absorption bands were both assigned to the d-d transition $^2T_{2g} \rightarrow {}^2E_g$ between the t_{2g}^* and e_g^* molecular orbitals with the splitting ($\sim$5,000 $cm.^{-1}$) being caused by Jahn-Teller distortion of the excited ^2E_g state. The high intensity peaks were assigned to halide $\rightarrow$ t_{2g}^* and halide $\rightarrow$ e_g^* charge-transfer transitions. The positions of these charge-transfer peaks and the low magnitude of 10 Dq indicated a considerable degree of halide to metal p_π - d_π bonding in the A_2MX_6 complexes.

The magnetic susceptibilities of the hexahalo complexes yielded paramagnetic moments below the spin-only value of 1.73 B.M. The magnitude and temperature dependence of the effective magnetic moments of the niobium(IV) ion in these compounds agreed with the Kotani theory (24) for the condition Dq $\gg$ $\xi \cong$ kT. Spin-orbit coupling constants for niobium(IV) ranged from 300 $cm.^{-1}$ to 650 $cm.^{-1}$. The tantalum(IV) complexes had very low effective moments that did not vary appreciably with temperature. This behavior was consistent with that predicted by Kotani for Dq $\cong$ ξ $\gg$ kT ($\xi_{Ta(IV)}$ ~ 1,500 $cm.^{-1}$). More complete calculations using the theory of Moffitt and Liehr(52,53) indicated that the spin-orbit coupling constant for tantalum(IV) is closer to 1,000 $cm.^{-1}$

Because the effective magnetic moment of a given $MX_6^{=}$ ion was dependent on the cation in the lattice, antiferromagnetic lattice interactions, of low magnitude, were also indicated in the solid compounds. The derived spin-orbit coupling constants show that halide to metal π-bond formation decreases in the order chloride > bromide > iodide.

The reaction between the niobium(IV) halides and acetonitrile at room temperature yielded solid complexes of the composition NbX_4(acetonitrile)$_2$ (X = Cl, Br, I) after removal of excess nitrile. These compounds were observed to decompose at ca. 50° into their respective tetrahalides and acetonitrile. A solid of composition $NbCl_4$(acetonitrile)$_3$ was also found to be stable at acetonitrile pressures greater than 28 mm. Hg at 20°. Solids of this stoichiometry were not found in the $NbBr_4$- and NbI_4-acetonitrile systems. The $NbCl_4$(acetonitrile)$_2$ complex was observed to disproportionate as well as decompose at ca. 100° forming the volatile species $NbCl_5$(acetonitrile). Heating the other NbX_4(acetonitrile)$_2$ complexes to 100° also produced volatile species but these were not characterized.

Solution studies of the niobium(IV) halides in acetonitrile by conductance, absorption spectra and cryoscopic techniques proved that the soluble complexes existed as non-dissociated monomers. This information, coupled with that obtained from dipole moment and absorption spectra measurements of $NbBr_4$(acetonitrile)$_2$ in benzene, and reflectance measurements on the solid compounds, strongly indicated that the complexes have the composition NbX_4(acetonitrile)$_2$ in both benzene and acetonitrile. In addition, the complexes have a cis-octahedral coordination of ligands about the niobium(IV) ion in both the solid state and in solution.

The absorption spectra of the tetrahalobis(acetonitrile)-niobium(IV) complexes were consistent with those expected for complexes with an effective tetragonal symmetry. The two low intensity peaks in the visible region were assigned to d-d transitions from the lower $t_{2g}*$ orbitals to the split e_g* orbitals. The magnitude of the e_g* splitting was ca. 3,000-6,000 cm^{-1} depending on the complex. The spectroscopic data were consistent with the ligand field strengths acetonitrile > chloride > bromide > iodide. The splitting of the ground ($t_{2g}*$) orbitals was observed to be 4,650 cm^{-1} in $NbCl_4$(acetonitrile)$_2$. The magnitude of this ground state splitting plus infrared data showed that acetonitrile does not π-bond to an appreciable extent in the complexes. High intensity peaks

($\epsilon > 1{,}000$) at lower wavelengths in the spectra of the NbX_4-(acetonitrile)$_2$ complexes were assigned to ligand → metal charge-transfer transitions.

Magnetic moments of the tetrahalobis(acetonitrile)niobium(IV) complexes were closer to the spin-only value than the niobium(IV) hexahalo complexes and decreased in the order $NbCl_4$(acetonitrile)$_2$ > $NbBr_4$(acetonitrile)$_2$ > NbI_4(acetonitrile)$_2$. The magnitude and variation of μ_{eff} with temperature were fit to data compiled by Figgis (59) and the splitting of the ground state due to the asymmetric ligand component in the complexes was found to vary as : $NbCl_4$(acetonitrile)$_2$ (4,000-5,000 $cm.^{-1}$) > $NbBr_4$(acetonitrile)$_2$ (1,000-2,000 $cm.^{-1}$) > NbI_4(acetonitrile)$_2$ (600-1,000 $cm.^{-1}$). The magnetic data also indicated that the degree of ligand π-bond formation in the complexes decreasd in the order chloride > bromide > iodide > acetonitrile. Therefore acetonitrile is rather a unique ligand in that it forms a stronger σ-bond than the halides but a weaker π-bond, and thus provides the interesting case where the splitting of the ground state t_{2g}* orbitals is greater than the excited state e_g* orbitals.

BIBLIOGRAPHY

1. McCarley, R. E. and Torp, B. A. Inorg. Chem. 2, 540 (1963).

2. McCarley, R. E. and Boatman, J. C. Inorg. Chem. 2, 547 (1963).

3. Horner, S. M. and Tyree, S. Y. Inorg. Chem. 2, 568 (1963).

4. Edwards, A. J., Peacock, R. D. and Said, A. J. Chem. Soc. 1962, 4643 (1962).

5. Allen, E. A., Edwards, D. A. and Fowles, G. W. A. Chem. Ind. 1962, 1026 (1962).

6. Lewis, J., Machin, D. J., Newnham, I. E. and Nyholm, R. S. J. Chem. Soc. 1962, 2036 (1962).

7. Wentworth, R. A. D. and Brubaker, C. H. Inorg. Chem. 2, 551 (1963).

8. Wentworth, R. A. D. and Brubaker, C. H. Inorg. Chem. 3, 47 (1964).

9. Fowles, G. W. A. and Hoodless, R. A. J. Chem. Soc. 1963, 33 (1963).

10. Clark, R. J. H., Lewis, J., Machin, D. J. and Nyholm, R. S. J. Chem. Soc. 1963, 379 (1963).

11. Kennedy, C. D. and Peacock, R. D. J. Chem. Soc. 1963, 3392 (1963).

12. Brown, T. M. Preparation and reactions of some lower tungsten halides and halide complexes. Unpublished Ph.D. thesis. Ames, Iowa, Library, Iowa State University of Science and Technology. 1963.

13. Hargreaves, G. B. and Peacock, R. D. J. Chem. Soc. 1957, 4212 (1957).

14. Hargreaves, G. B. and Peacock, R. D. J. Chem. Soc. 1958, 3776 (1958).

15. Ballhausen, C. J. Introduction to ligand field theory. New York, New York, McGraw-Hill Book Co., Inc. 1962.

16. Dunn, T. M. Trans. Faraday Soc. 57, 1441 (1961).

17. Cotton, F. A. Chemical applications of group theory. New York, New York, Interscience Publishers, Inc. 1963.

18. Ballhausen, C. J. and Gray, H. B. Inorg. Chem. 1, 111 (1962).

19. Gray, H. B. and Hare, C. R. Inorg. Chem. 1, 363 (1962).

20. Wells, A. F. Structural inorganic chemistry. 3rd ed. London, England, Oxford University Press. 1962.

21. Korshunov, B. G. and Safonov, V. V. Russian Journal of Inorganic Chemistry 6, 385 (1961).

22. Korshunov, B. G., Safonov, V. V. and Shevtsova, Z. N. Russian Journal of Inorganic Chemistry 7, 1021 (1962).

23. Cozzi, V. and Vivarelli, S. Z. anorg. allgem. Chem. 279, 165 (1955).

24. Kotani, M. J. Phys. Soc. Japan 4, 293 (1949).

25. Bedon, H. D., Horner, S. M. and Tyree, S. Y. A molecular orbital treatment of the spectrum of TiF_6^{-3}. [To be published in Inorganic Chemistry. ca. 1964].

26. Emeléus, H. J. and Rao, G. S. J. Chem. Soc. 1958, 4245 (1958).

27. Gerrard, W., Lappert, M. F., Pyszora, H. and Wallis, J. W. J. Chem. Soc. 1960, 2182 (1960).

28. Brown, T. L. and Kubota, M. J. Am. Chem. Soc. 83, 4175 (1961).

29. Muetterties, E. L. J. Am. Chem. Soc. 82, 1082 (1960).

30. Lange, N. A., ed. Handbook of chemistry. 9th ed. Sandusky, Ohio, Handbook Publishers, Inc. 1956.

31. Jonassen, H. B., Cantor, S. and Tarsey, A. R. J. Am. Chem. Soc. 78, 271 (1956).

32. Telep, G. and Boltz, D. F. J. Anal. Chem. 24, 163 (1952).

33. U. S. National Bureau of Standards. Tables for conversion of x-ray diffraction angles to interplanar spacings. Washington, D. C., U. S. Government Printing Office. 1950.

34. Nelson, J. and Riley, D. Proc. Phys. Soc. (London) 57, 160 (1945).

35. Cullity, B. D. Elements of x-ray diffraction. Reading, Massachusetts, Addison-Wesley Publishing Co., Inc. 1956.

36. MacGillarry, C. H., Rieck, G. D. and Lonsdale, K., eds. International tables for x-ray crystallography. Vol. 3. Birmingham, England, Kynoch Press. 1962.

37. Hendricker, D. G. Aluminum hydride-trimethylamine. Unpublished M.S. thesis. Ames, Iowa, Library, Iowa State University of Science and Technology. 1963.

38. Corbett, J. D. and Seabaugh, P. J. Inorg. Nucl. Chem. 6, 207 (1958).

39. Schäfer, H. and Bayer, L. Z. anorg. allgem. Chem. 277, 140 (1954).

40. Moeller, T. Inorganic chemistry. New York, New York, John Wiley and Sons, Inc. 1952.

41. Kleinberg, J., Argersinger, W. L. and Griswold, E. Inorganic chemistry. Boston, Massachusetts, D. C. Heath and Co. 1960.

42. Dunn, T. M. The visible and ultra-violet spectra of complex compounds. In Lewis, J. and Wilkins, R. G., eds. Modern coordination chemistry. pp. 229-300. New York, New York, Interscience Publishers, Inc. 1960.

43. Jørgensen, C. K. Acta Chem. Scand. 10, 518 (1956).

44. Pauling L. and Wilson, E. B. Introduction to quantum mechanics. New York, New York, McGraw-Hill Book Co., Inc. 1935.

45. Cotton, F. A. and Wilkinson, G. Advanced inorganic chemistry. New York, New York, Interscience Publishers, Inc. 1962.

46. Bethe, H. Ann. Physik [5] 3, 133 (1929).

47. Jørgensen, C. K. Absorption spectra and chemical bonding in complexes. Reading, Massachusetts, Addison-Wesley Publishing Co., Inc. 1962.

48. Ito, Koji, Nakamura, D., Ito, Kazuo and Kubo, M. Inorg. Chem. 2, 690 (1963).

49. Orgel, L. E. An introduction to transition-metal chemistry: ligand-field theory. New York, New York, John Wiley and Sons., Inc. 1960.

50. Figgis, B. N. and Lewis, J. The magnetochemistry of complex compounds. In Lewis, J. and Wilkins, R. G., eds. Modern coordination chemistry. pp. 400-454. New York, New York, Interscience Publishers, Inc. 1960.

51. Kamimura, H., Koide, S., Sekiyama, H. and Sugano, S. J. Phys. Soc. Japan 15, 1264 (1960).

52. Moffitt, W., Goodman, G. L., Fred, M. and Weinstock, B. Mol. Phys. 2, 109 (1959).

53. Liehr, A. D. J. Phys. Chem. 64, 43 (1960).

54. Westland, A. D. and Bhiwandker, N. C. Can. J. Chem. 39, 2353 (1961).

55. Busey, R. H. and Sonder, E. J. Chem. Phys. 36, 93 (1962).

56. Owen, J. Proc. Roy. Soc. (London) A227, 183 (1955).

57. Duckworth, M. W., Fowles, G. W. A. and Hoodless, R. A. J. Chem. Soc. 1963, 5665 (1963).

58. Ulich, H., Hertel, E. and Nespital, W. Z. Phys. Chem. 17B, 21 (1932).

59. Figgis, B. N. Trans. Faraday Soc. 57, 198 (1961).

60. Griffith, J. S. The theory of transition metal ions. London, England, Cambridge University Press. 1961.

61. Selwood, P. W. Magnetochemistry. 2nd ed. New York, New York, Interscience Publishers, Inc. 1956.

ACKNOWLEDGEMENTS

The author is very grateful to Dr. Robert E. McCarley for his encouragement, criticism, and guidance through the course of this work.

Appreciation is extended to members of Metallurgy Group VI for their cooperation, comments, discussions, generous exchange of equipment and general interest.

Special thanks are extended to the following people: Mr. John D. Greiner for his many hours of assistance in the determination of the magnetic properties of the compounds prepared in the course of this work; Mr. Peter B. Fleming and Mr. Lawrence L. Franks for aid in the molecular weight studies; Mr. James C. Boatman for generously furnishing samples of the tantalum(IV) halides; Mr. Keith O. Berry and Mr. Gary A. Murray for special services rendered in preparing this thesis; and Miss Verna J. Thompson for typing services beyond the call of duty.

Finally the author would like to extend special thanks to his wife, Jeanette, and son, Steven, for their patience, understanding, and moral support throughout the course of this work.

APPENDIX

Table 13. X-ray diffraction data for the potassium hexachloroniobate(IV) complex

$\sin^2\theta$	d,Å	R.I.	hkℓ	~a,Å
0.01795	5.75	VS	111	10.0
0.02383	4.99	W	200	10.0
0.04781	3.52	S	220	10.0
0.06595	3.00	S	311	10.0
0.07168	2.88	VS	222	10.0
0.09549	2.49	S	400	10.0
0.11364	2.29	VW	331	10.0
0.11957	2.23	VW	420	10.0
0.14374	2.03	VW	422	10.0
0.16131	1.92	VVW	511,333	10.0
0.19121	1.76	S	440	10.0
0.20964	1.68	VVW	531	10.0
0.21608	1.66	VVW	600,442	10.0
0.25668	1.52	VVW	533	10.0
0.26357	1.50	W	622	10.0
0.28711	1.44	VW	444	10.0
0.30303	1.40	VVW	711	10.0
0.33557	1.33	VVW	642	10.0
0.35215	1.30	W	731	10.0
0.48133	1.11	VW	840	10.0

Table 14. X-ray diffraction data for the rubidium hexachloroniobate(IV) complex

$\sin^2 \theta$	d,Å	R.I.	hkℓ	~a,Å
0.01743	5.84	S	111	10.1
0.04648	3.57	VS	220	10.1
0.06392	3.05	M	311	10.1
0.06990	2.91	VS	222	10.1
0.09324	2.52	VS	400	10.1
0.11077	2.31	M	331	10.1
0.13967	2.06	S	422	10.1
0.15697	1.94	M	511,333	10.1
0.18622	1.79	VS	440	10.1
0.20385	1.71	W	531	10.1
0.23268	1.60	W	620	10.1
0.25591	1.52	W	622	10.1
0.27956	1.46	W	444	10.1
0.29680	1.41	VW	711,551	10.1
0.32596	1.35	W	642	10.1
0.34408	1.31	VW	731,553	10.1
0.37380	1.26	VW	800	10.1
0.42014	1.19	VW	660,822	10.1
0.43535	1.17	VW	751	10.1
0.44253	1.16	VW	662	10.1
0.46634	1.13	W	840	10.1

Table 15. X-ray diffraction data for the potassium hexabromoniobate(IV) complex

$\sin^2 \theta$	d-spacings, Å Observed	Calculated[a]	hkℓ	R.I.
0.01619	6.05	6.06	111	VVS
0.02024	5.41	5.42	002	S
0.02226	5.16	5.16	200	VS
0.04084	3.81[b]			VW
0.04473	3.64	3.65	220	VW
0.05497	3.29[b]			S
0.06067	3.13	3.13	311	S
0.06465	3.03	3.03	222	VVS
0.07579	2.80	2.80	312	S
0.08172	2.69	2.71	004	VS
0.08873	2.59	2.58	400	VVS
0.10396	2.39	2.38	331	W
0.10881	2.34[b]	2.33	042	W
0.11121	2.31	2.31	420	W
0.13148	2.12	2.12	422	W
0.13743	2.08	2.08	115	W
0.14411	2.03	2.02	333	VW
0.14930	1.99[b]	1.99	511	W
0.16427	1.90[b]			VW
0.17040	1.87	1.87	404	VVS
0.17808	1.83	1.83	440	S
0.18277	1.80	1.81	135,006	W
0.18847	1.77	1.77	1.53	W
0.19327	1.75	1.75,1.76	531,424	S
0.20866	1.69	1.71	026	S
0.22739	1.62[b]	1.62	335,226	S
0.24189	1.57	1.56	622	S
0.25927	1.51[b]	1.51,1.52	444,117	S
0.27083	1.48[b]	1.48	515,406	S
0.29759	1.41	1.40	624,317	W
0.31561	1.37	1.37	535	W
0.32620	1.35[b]	1.35	731,553	S

[a]Calculated from lattice constants a = 10.3Å, c = 10.8Å.

[b]Lines corresponding to d-spacings for KBr.

Table 15. (Continued)

$\sin^2\theta$	d-spacings, Å Observed	Calculated[a]	hkℓ	R.I.
0.35649	1.29	1.29,1.28	800,446	VW
0.37244	1.26[b]	1.26,1.27	802,733	W
0.37666	1.25	1.25	820	W
0.39792	1.22	1.22	822,660	W
0.40511	1.21	1.21	555,626	W
0.41592	1.19	1.19	662	W
0.43093	1.17	1.17	248	VW
0.43664	1.16[b]			W
0.45868	1.14	1.14	824	W

Table 16. X-ray diffraction data for the rubidium hexabromoniobate(IV) complex

$\sin^2 \theta$	d,Å	R.I.	hkℓ	~a,Å
0.01584	6.12	S	111	10.6
0.02114	5.30	VW	200	10.6
0.04224	3.75	W	220	10.6
0.05812	3.20	W	311	10.6
0.06328	3.06	VVS	222	10.6
0.08461	2.65	VS	400	10.6
0.10005	2.44	VVW	331	10.6
0.10557	2.37	VVW	420	10.6
0.12691	2.16	VVW	422	10.6
0.14227	2.04	VVW	511,333	10.6
0.16909	1.87	VS	440	10.6
0.18520	1.79	VVW	531	10.6
0.18983	1.77	VVW	600,442	10.6
0.23224	1.60	S	622	10.6
0.25333	1.53	S	444	10.6
0.26511	1.50	VVW	711,551	10.7
0.33903	1.32	VVW	800	10.6
0.40169	1.22	VW	662	10.6
0.41438	1.20	VW	840	10.7
0.50803	1.08	VVW	844	10.6

Table 17. X-ray diffraction data for the cesium hexaiodoniobate(IV) complex

$\sin^2 \theta$	d,Å	R.I.	hkℓ	~a,Å
0.01369	6.58	S	111	11.4
0.05379	3.32	VS	222	11.5
0.07168	2.88	S	400	11.5
0.12048	2.22	VVW	511,333	11.5
0.14300	2.04	S	440	11.5
0.19659	1.74	M	622	11.5
0.21436	1.66	M	444	11.5
0.28585	1.44	VW	800	11.5
0.33491	1.33	W	751	11.5
0.35716	1.29	W	840	11.5
0.42851	1.18	W	844	11.5
0.48150	1.11	VW	1022,666	11.5
0.57063	1.02	VVW	880	11.5
0.62519	0.974	VW	1062	11.5
0.64267	0.961	VW	1200,884	11.5
0.71431	0.911	VVW	1240	11.5
0.76953	0.878	VVW	1066	11.5

Table 18. X-ray diffraction data for the potassium hexachlorotantalate(IV) complex

$\sin^2 \theta$	d, Å	R.I.	hkℓ	~a, Å
0.01809	5.73	VVS	111	10.0
0.02388	4.98	S	200	10.0
0.04781	3.52	S	220	10.0
0.06586	3.00	S	311	10.0
0.07168	2.88	W	222	10.0
0.09570	2.49	S	400	10.0
0.11364	2.29	M	331	10.0
0.11980	2.26	M	420	10.0
0.14374	2.03	M	422	10.0
0.16156	1.92	M	511,333	10.0
0.19149	1.76	S	440	10.0
0.20936	1.68	W	531	10.0
0.21579	1.66	VW	600,442	10.0
0.23949	1.57	VW	620	10.0
0.25744	1.52	VVW	533	10.0
0.28726	1.44	VVW	444	10.0
0.30576	1.39	VVW	711,551	10.0
0.33540	1.33	VVW	642	10.0
0.35281	1.30	VVW	731,553	10.0
0.40648	1.21	VVW	820,644	10.0
0.47976	1.11	VVW	840	10.0

Table 19. X-ray diffraction data for the rubidium hexachlorotantalate(IV) complex

$\sin^2\theta$	d,Å	R.I.	hkℓ	~a,Å
0.01717	5.88	VVS	111	10.1
0.02304	5.07	VVW	200	10.1
0.04611	3.59	VVS	220	10.1
0.06396	3.05	VS	311	10.1
0.06927	2.93	S	222	10.1
0.09264	2.53	VVS	400	10.1
0.11055	2.32	M	331	10.1
0.11619	2.26	W	420	10.1
0.13948	2.06	VS	422	10.1
0.16015	1.92	S	511,333	10.1
0.18602	1.77	VVS	440	10.1
0.20343	1.71	S	531	10.1
0.20922	1.68	VVW	600,442	10.1
0.23224	1.60	M	620	10.1
0.24970	1.54	W	533	10.1
0.25576	1.52	W	622	10.1
0.27941	1.46	M	444	10.1
0.29632	1.42	M	711,551	10.1
0.32555	1.35	S	642	10.1
0.34267	1.32	M	731,553	10.1
0.37143	1.26	VVW	800	10.1
0.41782	1.19	W	660,822	10.1
0.43577	1.17	W	751	10.1
0.46477	1.13	S	840	10.1
0.48115	1.11	W	911	10.1
0.51153	1.08	VW	664	10.1
0.52947	1.06	VW	931	10.1
0.55799	1.03	W	844	10.1
0.57546	1.02	VVW	933,755	10.1
0.60413	0.991	W	1020	10.1
0.62198	0.977	VVW	773	10.1
0.66872	0.942	VVW	953	10.1
0.69873	0.921	VVW	1042	10.1
0.74468	0.893	VVW	880	10.1
0.76215	0.882	VVW	1131	10.1
0.79121	0.866	VVW	1060	10.1
0.83831	0.841	VW	1200,884	10.1
0.88537	0.819	VVW	1064	10.1

Table 20. X-ray diffraction data for the rubidium hexabromo-tantalate(IV) complex

$\sin^2 \theta$	d,Å	R.I.	hkℓ	~a,Å
0.01580	6.13	VS	111	10.6
0.02109	5.30	S	200	10.6
0.04224	3.75	S	220	10.6
0.05804	3.20	VS	311	10.6
0.06345	3.06	VVS	222	10.6
0.08461	2.65	VVS	400	10.6
0.10026	2.43	S	331	10.6
0.10557	2.37	S	420	10.6
0.12657	2.17	S	442	10.6
0.14252	2.04	S	511,333	10.6
0.16922	1.87	VVS	440	10.6
0.18480	1.79	S	531	10.6
0.18983	1.77	M	600,442	10.6
0.21093	1.68	W	620	10.6
0.22665	1.62	W	533	10.6
0.23224	1.60	VS	622	10.6
0.25318	1.53	VS	444	10.6
0.26897	1.49	S	711,551	10.6
0.27425	1.47	VVW	640	10.6
0.29520	1.42	M	642	10.6
0.31124	1.38	M	731,553	10.6
0.33755	1.33	M	800	10.6
0.35882	1.29	W	820	10.6
0.37938	1.25	VW	660,822	10.6
0.39519	1.23	W	751	10.6
0.40117	1.22	W	662	10.6
0.42247	1.19	VS	840	10.6
0.43682	1.17	VVW	911	10.6
0.44426	1.16	VVW	842	10.6
0.48011	1.11	VVW	931	10.6
0.50629	1.08	VS	844	10.6
0.52269	1.07	VVW	933,755	10.6
0.54932	1.04	VVW	1020	10.6
0.56388	1.03	VVW	773	10.6
0.67527	0.937	VW	880	10.6
0.75901	0.884	VW	1200,884	10.6

Table 21. Magnetic data for the potassium hexachloroniobate(IV) complex

$\chi_M \times 10^6$ (emu/mole)	$\chi_M^{corr.} \times 10^6$ (emu/mole)[a]	T (^oK)	μ_{eff} (B.M.)
526	718	346	1.41
552	744	298	1.34
629	821	236	1.25
700	892	191	1.17
778	970	159	1.12
807	999	143	1.07
879	1071	125	1.04
910	1102	115	1.01
930	1122	111	1.00

[a]Calculated for $\chi_{dia.} = -192 \times 10^{-6}$ emu/mole (61).

Table 22. Magnetic data for the rubidium hexachloroniobate(IV) complex

$\chi_M \times 10^6$ (emu/mole)	$\chi_M^{corr.} \times 10^6$ (emu/mole)[a]	T (^oK)	μ_{eff} (B.M.)
616	821	293	1.39
769	974	203	1.26
881	1086	158	1.18
998	1203	126	1.11
1057	1262	112	1.07
1106	1311	99	1.03

[a]Calculated for $\chi_{dia.} = -205 \times 10^{-6}$ emu/mole (61).

Table 23. Magnetic data for the potassium hexabromoniobate(IV) complex

$\chi_M \times 10^6$ (emu/mole)[a]	$\chi_M^{corr.} \times 10^6$ (emu/mole)[b]	T (^oK)	μ_{eff} (B.M.)
705	957	296	1.51
769	1021	237	1.40
802	1054	205	1.32
840	1092	174	1.24
908	1160	144	1.16
963	1215	122	1.09

[a]Values corrected for the diamagnetism of 35.7% KBr in the sample.

[b]Calculated for $\chi_{dia.} = -252 \times 10^{-6}$ emu/mole (61).

Table 24. Magnetic data for the rubidium hexabromoniobate(IV) complex

$\chi_M \times 10^6$ (emu/mole)	$\chi_M^{corr.} \times 10^6$ (emu/mole)[a]	T (^oK)	μ_{eff} (B.M.)
319	584	361	1.30
341	606	294	1.20
370	635	221	1.07
391	656	181	0.98
399	664	171	0.96
407	672	156	0.92
418	683	142	0.88
435	700	125	0.84
446	711	112	0.80
458	723	105	0.78
467	732	100	0.77

[a]Calculated for $\chi_{dia.} = -265 \times 10^{-6}$ emu/mole (61).

Table 25. Magnetic data for the cesium hexaiodoniobate(IV) complex

$\chi_M \times 10^6$ (emu/mole)	$\chi_M^{corr.} \times 10^6$ (emu/mole)[a]	T (^oK)	μ_{eff} (B.M.)
136	519	294	1.11
155	538	205	0.94
162	545	160	0.84
177	560	127	0.76
193	576	97	0.67

[a]Calculated for $\chi_{dia.} = -383 \times 10^{-6}$ emu/mole (61).

Table 26. Magnetic data for the rubidium hexachlorotantalate(IV) complex

$\chi_M \times 10^6$ (emu/mole)	$\chi_M^{corr.} \times 10^6$ (emu/mole)[a]	T (^oK)	μ_{eff} (B.M.)
5	215	362	0.79
17	227	295	0.74
28	238	204	0.62
32	242	135	0.51
52	262	112	0.49
42	252	91	0.43

[a]Calculated for $\chi_{dia.} = -210 \times 10^{-6}$ emu/mole (61).

Table 27. Magnetic data for the rubidium hexabromotantalate(IV) complex

$\chi_M \times 10^6$ (emu/mole)	$\chi_M^{corr.} \times 10^6$ (emu/mole)[a]	T (^oK)	μ_{eff} (B.M.)
-34	236	296	0.75
-28	242	178	0.59
-23	247	142	0.53
+ 4	274	93	0.45

[a]Calculated for $\chi_{dia.} = -270 \times 10^{-6}$ emu/mole (61).

Table 28. Magnetic data for tetrachlorobis(acetonitrile)-niobium(IV)

$\chi_M \times 10^6$ (emu/mole)	$\chi_M^{corr.} \times 10^6$ (emu/mole)[a]	T (^oK)	μ_{eff} (B.M.)
1208	1373	296	1.81
1634	1799	229	1.82
2041	2206	188	1.83
2776	2941	141	1.83
3199	3364	123	1.82
3449	3614	111	1.80
3815	3980	100	1.79
3981	4146	96	1.79

[a]Calculated for $\chi_{dia.} = -156 \times 10^{-6}$ emu/mole (61).

Table 29. Magnetic data for tetrabromobis(acetonitrile)-niobium(IV)

$\chi_M \times 10^6$ (emu/mole)	$\chi_M^{corr.} \times 10^6$ (emu/mole)[a]	T (^oK)	μ_{eff} (B.M.)
657	862	363	1.59
820	1025	296	1.56
1206	1411	203	1.52
1509	1714	158	1.48
1863	2068	124	1.44
2039	2244	111	1.42
2236	2441	100	1.40

[a]Calculated for $\chi_{dia.} = -205 \times 10^{-6}$ emu/mole (61).

Table 30. Magnetic data for the tetraiodobis(acetonitrile)-niobium(IV) complex

$\chi_M \times 10^6$ (emu/mole)	$\chi_M^{corr.} \times 10^6$ (emu/mole)[a]	T (^oK)	μ_{eff} (B.M.)
618	887	294	1.45
918	1187	203	1.39
1145	1414	158	1.34
1359	1628	128	1.29
1682	1951	97	1.24

[a]Calculated for $\chi_{dia.} = -269 \times 10^{-6}$ emu/mole (61).